The Structures and Energetics of Strongly-Bound Gaseous Clusters of Protonated Biomolecules with Alcohols

by

Kris R. Eldridge

A thesis
presented to the University of Waterloo
in fulfilment of the
thesis requirement for the degree of
Master of Science
in
Chemistry

Waterloo, Ontario, Canada, 2008

I hereby declare that I am the sole author of this thesis. This is a true copy of the thesis, including any required final revisions, as accepted by my examiners.

I understand that my thesis may be made electronically available to the public.

Abstract

A growing interest in the strengths of several interactions that play important structural roles in biochemical systems has been building over the past couple decades. The binding energies and entropies of formation of the clusters of several protonated amino acids and nucleic acid bases with methanol have been measured using High Pressure Mass Spectrometry. The results generally show that binding energy decreases when the proton affinity difference between the alcohol and amino acid is increased. The structures and energies of various alcohol stabilized conformers of these protonated biomolecules were computed using *ab initio* calculations at the MP2(Full)/6-311++g(2d,2p) level of theory. The enthalpies of formation of the lowest energy conformers of the proton-bound clusters between the alcohols and amino acids or peptides match very closely with the experimental values, indicating that protonation and subsequent methanol attachment occurs primarily at the terminal amine functionality. The methanol stabilized protonated nucleic acid bases have energies that match closely with a more entropically favourable conformation of the cluster, hence yielding less negative enthalpy changes experimentally. The effect of alcohol size on binding energy was also monitored through measurements of enthalpies and entropies of formation for the clusters of protonated diglycine with several alcohols. The binding energy between protonated diglycine and benzene was also measured, yielding a measurable cation-π interaction of over 20 kcal mol^{-1}, a comparable value to typical strong hydrogen bonds.

Acknowledgments

This is by far the most challenging section to write. It is difficult for me to communicate my appreciation on a piece of paper, for everyone who has helped and supported me over the past two years, in addition to the four years culminating up to the beginning of my time as a graduate student.

First, I would like to acknowledge those who have worked closest with me over the past couple years, my group members: Ronghu, Rick, Rob, Jon and Matt Fuzz. It's truly been a pleasure working, learning, teaching, and being the life of numerous conferences with all of you. You guys have helped make research a fun and rewarding experience, and I hope that I've given back even just a fraction of the knowledge I've gained from you. It's also been nice meeting several people who have come in and out of the group in the relatively short time I've been here; Nathan, Opal, Sabrina, Matt W. and Cveta, as well as Scotty W, who didn't work in our lab, but still managed to pop in and out. Most of all, I would like to thank Chad "Chazz" Atkins, a great friend and roommate who kept me sane not only in the office while he was here, but also throughout the entire time we've known each other since our first year of University. In addition, I would also like to thank Mike Burt, who came here from Memorial University last year. It was a fun and productive experience working with him.

Other friends I've made at university either from living in residence or in my undergraduate/graduate program should be acknowledged as well. I won't name names to avoid leaving anyone out, but they know who they are! We've had a lot of good times over the past 6 years, and I look forward to many more in the future. Thanks guys.

Of course, one of the biggest acknowledgements that can't be communicated on a piece of paper nearly as much as I'd like it to be goes to my family. First, my two big sisters, Julie and Shannon, who since as long as I can remember have thought it novel simply that I existed. Second, Peter and Cheryll, my aunt and uncle (but not in that order). In addition to wanting their dogs, I've always wanted Peter's knowledge of science, and Cheryll's ability to make the tastiest soup ever served on the planet. Thanks for all the meals! Third, my grandparents, who were really fun people to visit early in my life, and incredible sources of inspiration later in theirs. Although not a person, I have to acknowledge my dog Cotton, man's best friend, who tried her hardest to stick around to see me graduate, and lived nearly 120 dog years, almost enough time to see it happen. Lastly, my parents, Ron and Patricia Eldridge. All they had to do was feed me and provide some shelter until I was an adult, but they did so much more, and never thought twice about it, even getting upset when I refused their help. Thanks for all the financial and emotional support you've given me over the last 25 years, it's been more than appreciated.

One of the only ways to learn is to face a question you can't initially answer. I'd like to thank my advisory committee, Dr. Bill Power and Dr. Jean Duhamel for providing me with some of those questions. Most of all though, I'd like to thank my supervisor Terry McMahon. There was no question after a few weeks into my fourth year honours project with Terry that I wanted to stay on another couple years to complete this thesis. Terry has been one of the busiest, hardest working people I've met in my past six years at the University of Waterloo, yet he still made time to meet with me if I had a question or problem, have all of us over to his house, and occasionally share in a few drinks and good conversations. The experience I've gained with him isn't even limited to the work presented in this thesis, as even at the moment of writing this, he is still providing me with new, exciting research opportunities, that are impossible to turn down. Terry, I can't thank you enough.

Table of Contents

List of Tables

List of Illustrations

Chapter 1
Introduction

This thesis focuses on the characterization and evaluation of interactions that play important roles in the structure of biological molecules, including many folding modes in protein secondary structure. These interactions include but are not limited to, hydrogen bonding and ionic hydrogen bonding, salt bridge interactions and cation-π interactions. All three of these interactions can be studied to some degree in the gas phase to yield absolute interaction energies, since indirect third party interactions are not present as with bulk solutions. The interacting systems can be scaled down to smaller molecules so that they can be studied in the gas phase.

1.1 Non-Covalent Ion-Molecule Electrostatics

As outlined by Legon and Millen,[1] in their work using microwave spectroscopy to study hydrogen bonded clusters of donors of the form HX (X = F, Cl, CN, Br) with acceptors, B, there are only a few simple rules relating the structure, energy, and bond lengths of hydrogen bonds in the gas phase. The structure of the hydrogen bond can be explained based on electrostatics, and generalized for a large number of hydrogen bonded clusters. The first rule is that the hydrogen bond donor is always oriented along the axis of the lone pair of electrons on the acceptor. This is consistent with valence bond theory and the valence shell electron repulsion theory. This is equally true when the acceptor has one, two or three lone pairs of electrons, provided those lone pairs are equivalent, or in other words, in the same environment with respect to the symmetry of the acceptor molecule. The second rule regarding structure concerns acceptors which do not possess typical moieties that would accept a hydrogen bond, but instead, have a π-overlap, such as ethylene. In this case, since an end-to-end overlap of donor with acceptor is not favourable, the acceptor aligns perpendicular to the direction of π-overlap. The explanation for this orientation is

that a strong quadrupole moment exists in the presence of the π bond, and the dipole on the donor aligns itself with the oppositely charged pole of the quadrupole of the acceptor. An illustration of the difference in structure between the H-F interactions with water, and ethylene is shown in Fig. 1.1. This HF--ethylene interaction is termed a π-hydrogen bond.

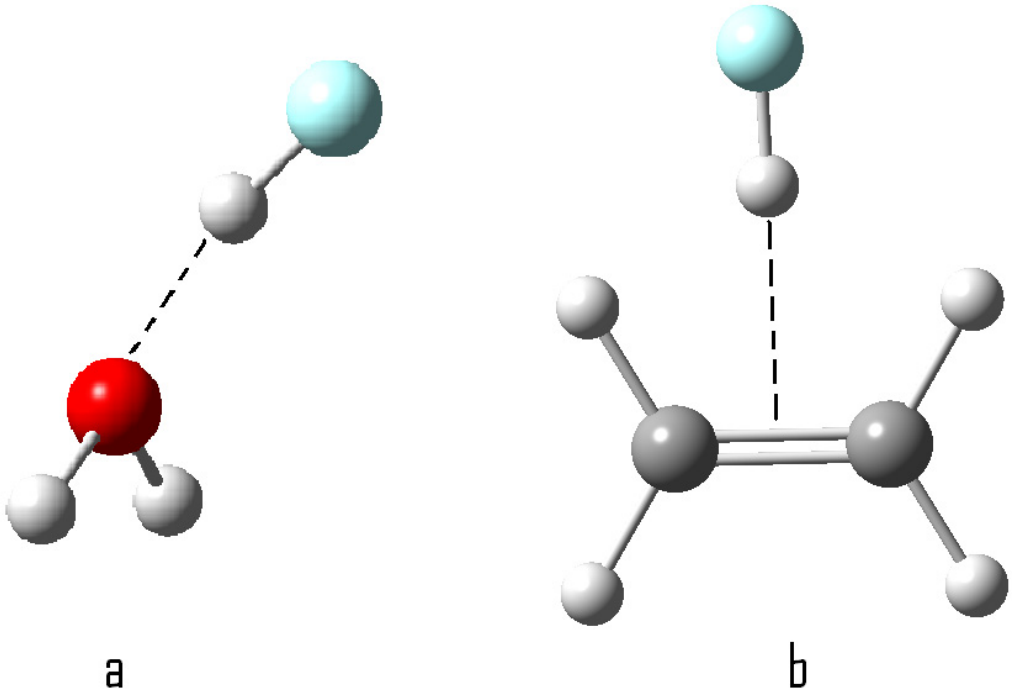

Fig. 1.1: Comparing the directionality of the hydrogen bond using HF as a donor to a. water and b. ethene

The strength of the gas phase hydrogen bond will increase with increasing nucleophilicity of the acceptor, and increasing electrophilicity of the donor. For example, a survey of data reveals that for the donor HF, the hydrogen bond formed with water is roughly five times stronger than the hydrogen bond with carbon monoxide.[2,3] When the donor is changed to HCl,[4,5] both hydrogen bond strengths are roughly halved, simply because the H-F bond is much more strongly polarized than the H-Cl bond due to the electronegativity of the fluorine atom. Hydrogen bond strengths in the gas

phase can range from very weak to near ionic bond strengths, depending on the origin of the interaction.

More specifically, every reaction that has been studied for this thesis can be classified as being an ion-molecule reaction that produces an ionic cluster. The strongest interaction within such a cluster is an ionic hydrogen bond. This presents an interesting interaction, since there must be an electrostatic attraction initiated by the ion, coupled with polarization of the neutral species. Generally, non-polar molecules interact more weakly with an ion, so only highly polar and functional molecules are of interest in such clusters. The radial dependence of the ion-molecule interaction is the best quantitative piece of information related to the bond energy. Therefore a breakdown of the actual radial dependence of the charge-dipole interaction is convenient at this time.

The attractive force between two approaching oppositely charged ions separated by internuclear distance r, is described by a Coulombic force, F(r), given by Eq. 1.1

$$F(r) - \frac{e^2 Z_+ Z_-}{4\pi\varepsilon_o r^2} \tag{1.1}$$

Where Z_+ and Z_- are the effective charges on the cation and anion respectively, e is the electron charge, and ε_o is the permittivity of vacuum. The potential between the two ions, u(r), will therefore be the force multiplied by the distance separating them, as shown in Eq. 1.2,

$$u(r) = \frac{e^2 Z_+ Z_-}{4\pi\varepsilon_o r} \tag{1.2}$$

Two neutral particles approaching one another interact either via electrostatic or induction forces. The possible combinations of polarization interactions are dispersion forces, governed by

induced dipole-induced dipole attraction, as well as van der Waals interactions including induced dipole-permanent dipole and permanent dipole-dipole interactions. All three of these weak interactions can be modelled by a Lennard-Jones potential, u(r), which is expressed as Eq. 1.3,

$$u(r) = 4\epsilon\left[\left(\frac{\sigma}{r}\right)^{12} - \left(\frac{\sigma}{r}\right)^{6}\right] \qquad (1.3)$$

and hence the ion-molecule interaction is dominated by the electrostatic contribution, which will still be large even at long internuclear distances. The radial dependence of the ion-molecule interaction can be estimated by taking the average of the exponent orders on the radius for both classes of interaction, which are -1 and -6, to give the average of -3.5. Although this is simply an estimate with no substantial empirical data to back it up, it is interesting to note the similarity between this estimate, and the radial dependence of a charge-induced dipole interaction of -4. A common interaction in clusters of the type of interest here are ionic hydrogen bonds, whereby from the radial analysis above, are significantly stronger than typical hydrogen bonds, where the radial dependence is closer to that of van der Waals interactions. Some charge-dipole interactions including F-H--F^- have been measured in the gas phase as being stronger than some weak ionic bonds.

Ionic hydrogen bonds are not solely conceptual interactions studied in the gas phase. They are in fact widely known to be present in protein systems. The amino acids lysine and arginine for example have isoelectric points of 9.7 and 10.8 respectively. Therefore in solution of pH 7, the side chains of these residues are protonated, becoming ammonium groups which then act as strong hydrogen bond donors to the nearby residues of aspartic acid (Asp) and glutamic acid (Glu), which contain carboxylic acid groups, thought to be deprotonated in aqueous solution, having isoelectric points of 2.8 and 3.2 respectively. Proteins also bind group 1 and group 2 cations that serve as essential nutrients. These cations play a role in forming protein secondary structure such as helix

and β-turns. Protonation of the nucleobases making up DNA and RNA will contribute to the helical structure of nucleic acids. Internal salts of amino acids, called zwitterions, are also stabilized by ion-solvent interactions in aqueous solution.

This introduces the next category of ion-molecule interactions of interest here, called salt-bridge interactions. In solution and in the solid state, the zwitterionic amino acid is the dominant form. This is because charge-dipole and charge-charge interactions stabilize the zwitterion in solution and in the solid state respectively. In the gas phase, high-order clusters, in which an amino acid is stabilized by a number of solvent molecules, should be necessary to stabilize the zwitterion.

Since the zwitterion is the dominant form of most amino acids while in solution, it is convenient to study the structure of the ion-solvent interaction in the solution itself. IR spectroscopy is a useful structural tool, and one of its applications used extensively in the Waterloo group to study ionic amino acids and peptides that originated in solution is Infrared Multiple Photon Dissociation (IRMPD).[6,7] IRMPD spectra can be collected with the use of a free electron laser (FEL). FELs use a high energy electron beam to amplify an optical wave. The electrons oscillate in a direction perpendicular to the propagation of the electron beam while passing through a tuneable magnetic field called an undulator. The oscillating electron beam is coupled with the optical wave to increase its amplification. The undulator provides a much higher degree of spectral intensity than the optical wave, so that the frequency of the emitted laser radiation is proportional to the oscillating frequency of the electrons. The resonance wavelength, λ_R, emitted by the laser, is given by Eq. 1.4,

$$\lambda_R = \frac{\lambda_o}{2\gamma^2\left(1 + \frac{K^2}{2}\right)} \qquad (1.4)$$

Where λ_o is the magnetic wavelength of the undulator, and K is a deflection parameter proportional to the magnetic field of the undulator. Therefore, by tuning the undulator or the electron beam energy, the wavelength of the FEL can be varied continuously. The frequency range of the laser is limited by the energies that can be reached by the electron accelerator, and short wavelengths give very weak optical gain. Although the UV range is generally obtainable, the IR frequencies provide reliable gain over their complete range, and FELs often operate in this region.

The FEL used here is the CLIO facility in Orsay France,[6] operating at the mid-infrared, an important region of the spectrum, since it provides wavelengths in the fingerprint range. Its current spectral range is between 3 and 100 μm, operating with two identical yet independently adjustable undulators at accelerator energies between 10 to 50 MeV. Among the spectra that have been recorded at this facility by our group are those providing evidence of the proline zwitterion stabilized by methylammonium ion in the gas phase.[8]

The third class of non-covalent interaction of interest in this thesis is the quadrupole-ion interaction. This can be an attractive or a repulsive interaction between an aromatic molecule and an ion. Classically, it has been thought of and described as either an electrostatic interaction, or the result of an ion-induced polarization, or a nearly equal combination of both.[9] Since a quadrupole-ion interaction is mostly electrostatic, one would expect that an ion with some charge should orient itself along the oppositely charged pole of the quadrupole moment. For example, benzene is a cyclic aromatic molecule with a negative quadrupole moment aligned perpendicular to the plane of the ring. It would be expected, and has been confirmed, that a cation such as Na^+ should coordinate perpendicular to the benzene ring in order to create an attractive interaction with the benzene quadrupole moment.[10] This is specifically referred to as a cation-π interaction. If this is true, then the opposite must be true for the orientation of an anion with respect to benzene. The anion

should be positioned along the edge of the benzene molecule in order to interact favourably with the positive end of the quadrupole. Since the cation-π interaction was one of the underlying foci of this thesis, it is appropriate to investigate previous work which characterized this interaction and unveiled it as an important interaction in biomolecular structure.

The cation-π interaction between small molecules has been the focus of biochemistry for many years. To get a full picture of the nature of the interaction, other interactions involving quadrupole moments will now be briefly discussed. The weakest in this category is the CH/π interaction, which has been observed between hydrocarbon C-H bonds and aromatic rings,[11-18] and has been thought to play a role in crystal structure and molecular assemblies of biological molecules. The CH/π interaction is only a weak attraction in saturated hydrocarbons, typically being only 1.0-1.1 kcal mol^{-1}. Under these conditions, the origin of the interaction is a dispersion force, or induced polarization of the C-H bond by the quadrupole moment of the aromatic molecule. Since the interaction is so weak, the directionality is also weak. Methane will point a C-H bond directly towards the plane of a benzene molecule, but a slight offset in the binding angle does not increase the energy of the cluster significantly. To further stabilize the interaction in polycyclic aromatics, the cluster will adopt a polydentate structure. Methane is bidentate with naphthalene, and tridentate with pyrene.[19] The CH/π interaction is enhanced, or "activated" in alkynes and halogen-substituted hydrocarbons, increasing to 2-3 kcal mol^{-1} and 5-6 kcal mol^{-1} respectively. In these cases, the C-H hydrogen atom becomes more acidic. *Ab initio* calculations[19-21] show a small increase in the electrostatic component, but more importantly, the dispersion force increases substantially. A highly polarized bond terminated by a labile proton (N-H and O-H) can form a π-hydrogen bond with an aromatic ring. The magnitude of this interaction according to recent experiments is weaker than the CH/π interaction formed with the halogen-substituted hydrocarbons, but has a larger electrostatic component, approaching that of a hydrogen bond, and

therefore more directionality than any CH/π interaction.[22] Experiments measuring the potential well-depth of the benzene-water and benzene-ammonia clusters produced values of 2.44 ±0.09 and 1.84 ±0.12 kcal/mol respectively.[23,24]

Although they were not of specific interest in any work to be presented here, arene-arene interactions serve a useful role in a greater qualitative and quantitative understanding of the effect of aromatic substitution on the magnitude of quadrupole moments. Benzene has a negative quadrupole moment perpendicular to the ring because the C-H bonds on the outside of the ring push negative charge towards the centre. A previous report on the magnitude of the benzene quadrupole moment lists a value of -2.83×10^{-39} Cm^{-2}.[9] Hexafluorobenzene, using an opposite reasoning, has a positive quadrupole moment, $+3.17 \times 10^{-39}$ Cm^{-2} perpendicular to the ring plane.[9] These two molecules would therefore have an attractive interaction if placed together face-to-face. If two benzene molecules were placed together face-to-face, the negative quadrupole moments would repel each other, until they were oriented in an edge-to-face configuration. However, if this rotation were hindered, then the rotational energy barrier between the face-to-face orientation and the edge-to-face orientation could be monitored as a function of quadrupole moment magnitude, through stepwise substitutions.[25] Stepwise addition of fluorine atoms for example practically shows a linear increase in the rotational barrier due to a stronger arene-arene interaction forming with the shift in electron density from the centre of the ring to the edge of the ring.

Dougherty has been an important contributor in our current understanding of cation-π interactions taking place within proteins. To aid in tracking cation-π pairings in proteins, he and his research group have developed a computer program called CAPTURE[26] (Cation-π Trends Using Realistic Electrostatics) to calculate the distance between cationic side chains of arginine and lysine with aromatic rings. Implemented into CAPTURE is a subset of an OPLS (Optimized Potentials for

Liquid Simulations) force field to calculate the electrostatic and van der Waals components of the OPLS energy. Simultaneously, the Hartree-Fock binding energies of model systems of each cation-π pair (the Lys-Phe pair can be represented by the ammonium ion and benzene for example) were calculated. The *ab initio* binding energies gave good correlation with the electrostatic component, but not the total energy of the OPLS calculation, emphasizing the importance of electrostatic treatment of the interaction. As a consequence, Dougherty has also traced electrostatic potential surfaces of benzene, phenol and indole to explain why tryptophan (which possesses an indole ring) so prominently forms cation-π interactions despite being an infrequent residue in proteins.[27] He explained it based on the larger and more intense area of negative electrostatic potential in the indole rings relative to benzene and phenol, which from an electrostatic view, are similar to each other.[28]

1.2 HPMS and its Caveats

High Pressure Mass Spectrometry (HPMS) is an outstanding method for measuring enthalpies, entropies and free energies of ionic cluster formation exactly, for a number of reasons. First, the gas phase introduces a nearly ideal environment for obtaining intrinsic binding energies, because unwanted third party interactions are not present. Secondly, the high pressure environment generates on the order of 100 collisions every microsecond, ensuring the ions are thermalized and come to chemical equilibrium on a very short timescale.

The requirements of obtaining reliable thermochemical data using HPMS are that the reactant and product ions are both observable in significantly high abundance that their relative concentrations are within one order of magnitude from each other, and that both species are in chemical equilibrium. The high pressure conditions ensure sufficient collisional stability, so that the kinetic energies of the ions have a Maxwell-Boltzmann distribution. In other words, the conditions

of the experiment ensure the ions are in thermal equilibrium. There are however several caveats in HPMS beyond the control of the user which hinder one or more of these conditions which have been outlined previously,[29] and those pertaining importance to the experiments conducted for this thesis will be summarized.

Samples with low volatility

Biological molecules of the type used in this thesis introduce a limited temperature range within which equilibrium constants can be measured. The maximum temperature is defined by a threshold temperature at which the ionic or neutral species dissociate by breaking covalent bonds due to thermal excitation. The lower temperature limit depends on the vapour pressure of the molecule. Most often, these molecules have very low vapour pressures, and the ion source temperature must exceed 100^{o}C to ensure sufficient concentrations in the gas phase.

To avoid these temperature limitations, a relatively new ionization technique, called electrospray ionization has been developed that does not require large molecules to initially be in the gas phase. Electrospray ionization (ESI) is a popular tool for producing hydrated gaseous amino acids and peptides[30-35] and solvated metal ion-amino acid clusters.[36,37] The main advantage of ESI is that instead of producing ions through medium to high energy collisions with electrons or heavy atoms, they are produced in solution, therefore even high order clusters can be studied. The successful mating of an ESI source to a high pressure source has been described in detail previously.[30] Typically, a solution containing the analyte and a polar solvent such as water or methanol is pumped at constant flow rate into an electrospray capillary fitted with a needle set to an appropriate potential. The solution is sprayed towards a curtain plate, which itself is set at a different potential than the ESI capillary, and allows sample inlet through a curtain gas to a pressure reducing capillary set at the same potential as the high pressure reaction chamber. A deflection

electrode at the base of the pressure reducing capillary is supplied with short electrical pulses to push the emerging charged sample into the reaction chamber, where it reacts with a reagent gas, supplied by a reactant gas inlet. This setup is not without potential problems. One problem that could arise is that the injection potential supplied to the deflection electrode may penetrate into the reaction chamber, and perturb the measured equilibrium constant by supplying excess kinetic energy to the ions. However, tests conducted by Wincel showed that between voltages of 25 and 50 V, the equilibrium constant was in fact unperturbed. When a similar test was conducted by modifying the reaction chamber field strength, it was discovered that ion intensities peaked at 33 V/cm, rationalized as a time discrimination at high potentials of larger ions having longer residence times during transport into the reaction chamber. However, by successfully combining ESI and HPMS, the temperature range can be allowed to extend as low as near room temperature.

Non-Equilibria Steady States

The presence of a steady state when chemical equilibrium is not present is a phenomenon that can be observed for a number of reasons. For example, consider the proton transfer reaction from AH^+ to B, where A and B represent two arbitrary bases, represented by Eq. 1.5

$$AH^+ + B \leftrightarrows BH^+ + A \qquad (1.5)$$

If B is unstable, protonation may induce a change in structure, giving an unreactive protonated isomer, $B'H^+$ in a steady state represented by Eqs. (1.6a) and (1.6b),

$$AH^+ + B \rightarrow B'H^+ + A \qquad (1.6a)$$

$$B'H^+ + A \rightarrow B' + AH^+ \qquad (1.6b)$$

where both AH^+ and $B'H^+$ are in a steady state, and show an apparent but false equilibrium. An apparent equilibrium constant, K' (Eq. 1.7) can be introduced

$$K' = \frac{k_a}{k_b} \quad (1.7)$$

with k_a and k_b being the rate constants for the reactions in Eqs. 1.6a and 1.6b respectively. K' is not typically equal to the actual equilibrium constant from Eq. 1.5. This is an important artifact, especially for example if one is interested in measuring the free energy or enthalpy change for the stepwise addition of solvent molecules to a base, because if the first solvent molecule induces a change in the structure of the base, yielding an unreactive species and resulting in a steady state, then the overall equilibrium constant will not be equal to the product of the equilibrium constant for each addition, also meaning the overall free energy change and enthalpy changes will not be the sum of the free energy and enthalpy changes for each stepwise addition.

Obviously, one of the most common causes for the observation of non-equilibrium steady states is isomerisation induced by chemical ionization, charge transfer, or cluster formation which is microscopically irreversible. For example, protonation of ethylene oxide in the gas phase will promote ring opening, and a polyethylene oxide oligomer can actually be formed. The ring opening of furan has also been monitored during a charge transfer reaction with the molecular ion of fluorobenzene.[29] The probable ring-opening of furan from the N_2^+ and N_4^+ charge transfer sources resulted in the production of an unreactive $C_4H_4O^+$ isomer, contributing a gross error to the equilibrium concentration of the $C_4H_4O^+$ at equilibrium. Impurities in the reaction mixture can also lead to reactions that produce unreactive isomers.

Mass Coincidence

The third of these pitfalls is mass coincidence, a problem that affects all areas of mass spectrometry. The magnetic sector of a mass spectrometer does not discriminate between two ions of identical mass and charge. This often is a problem when impurities are introduced into the ion

source either by thermal dissociation or cluster formation with products of chemical ionization ($C_2H_5^+$, $C_3H_7^+$, $C_4H_9^+$), among other ways. Most often, the impurity exists at low concentrations, and does not change the signal of the mass it coincides with initially to a significant degree so that equilibrium can still be measured accurately at low reaction times. Near the end of the ion lifetime, the impurity signal grows so that the overall signal trails off, and the reaction state appears to diverge from equilibrium. If mass coincidence is a suspected phenomenon, it can be detected by cleaning out the sample, and replacing it with a deuterated sample to monitor the ion abundance of the ion of common mass.

It is the aim of this thesis to demonstrate that beyond these few minor shortcomings, high pressure mass spectrometry is an appropriate and effective tool in which to measure cluster energetics and to derive structural information regarding those clusters.

Chapter 2
Experimental and Theoretical

2.1 Experimental

The instrument used to produce ions and record relative abundances of those ions over their lifespan is a pulsed electron beam high pressure mass spectrometer (HPMS), mated with a home-built high pressure ion source, the general design of which is consistent with other High Pressure Mass Spectrometers used at Waterloo, and which has been described elsewhere.[1-4] A schematic of the instrument is shown in Fig. 2.1. The instrument was built from a commercial model VG ZAB-2F analytical mass spectrometer. The analytical portion of the instrument is double-focusing, meaning that it can separate masses using a magnetic sector featuring a 1.8 Tesla magnet, and further separate fragments according to kinetic energy by use of an electric sector. This section can also be described as having a reverse geometry (BE), in which the magnetic sector comes before an electric sector. While the instrument possesses these two field regions, there are three field-free regions in which ions may travel and react according to Boltzmann statistics. These regions are present in between the ion focusing optics and the magnetic sector, between the magnetic sector and the electrostatic sector (see Fig. 2.1), and between the electrostatic sector and the electron multiplier detector. All three field-free regions are maintained at high vacuum pressure by diffusion pumps supported by roughing pumps. The low pressure chamber which houses the high pressure ion source and thermocouples is pumped by a 2500 Ls^{-1} diffusion pump. Our high pressure ion source is illustrated in cross-section in Fig. 2.2.

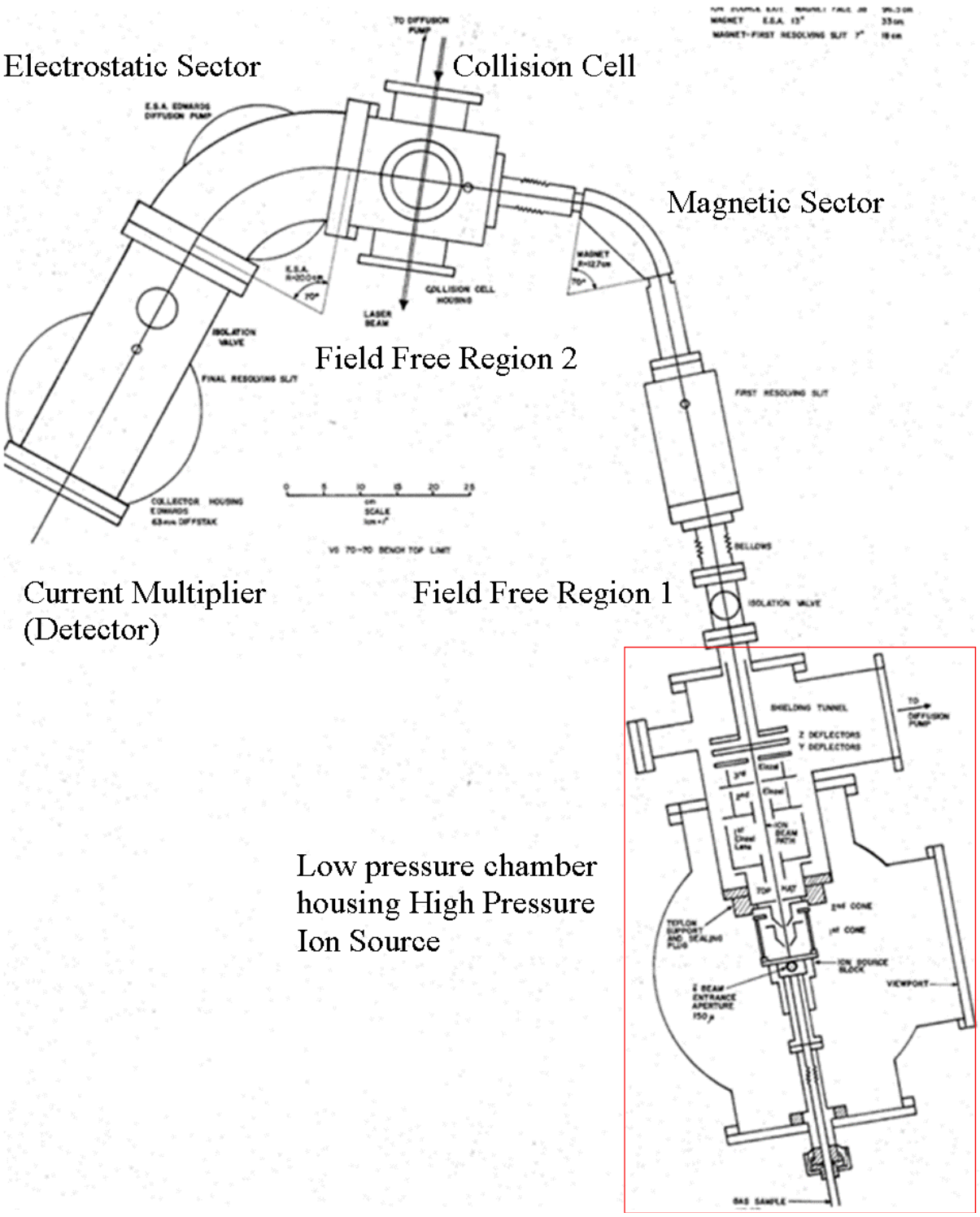

Fig. 2.1: Complete schematic of the VG ZAB-2F mass spectrometer mated to a home-built high pressure ion source

The typical experimental setup begins with a 2.54 L heated reservoir maintained at 80°C, in which a mixture of solvent gas and a bath gas/chemical ionizing agent exist in the gaseous phase. The total pressure inside the reservoir is monitored via a pressure transducer, and given as a digital read-out on a display. The partial pressure of a solvent introduced as a liquid is estimated using an ideal gas assumption based on the volume and density of liquid introduced. The relative composition of the mixtures are typically 0.1% to 5% solvent, with the rest being a chemical ionizing (CI) agent. Most often methane is used as the CI agent in the experiments detailed here throughout. In addition to these two components, a small amount of carbon tetrachloride (CCl_4) is often used, as it is a good electron scavenger, and can thus lengthen the residence times of ions in the source, facilitating experimental measurements and making them more reliable. The gas mixture is bled into the ion source under constant flow rate by a solenoid flow control valve, to any pressure ranging from 5 to 15 Torr. The constant pressure is maintained in a feed-back loop by a Baratron absolute pressure monometre.

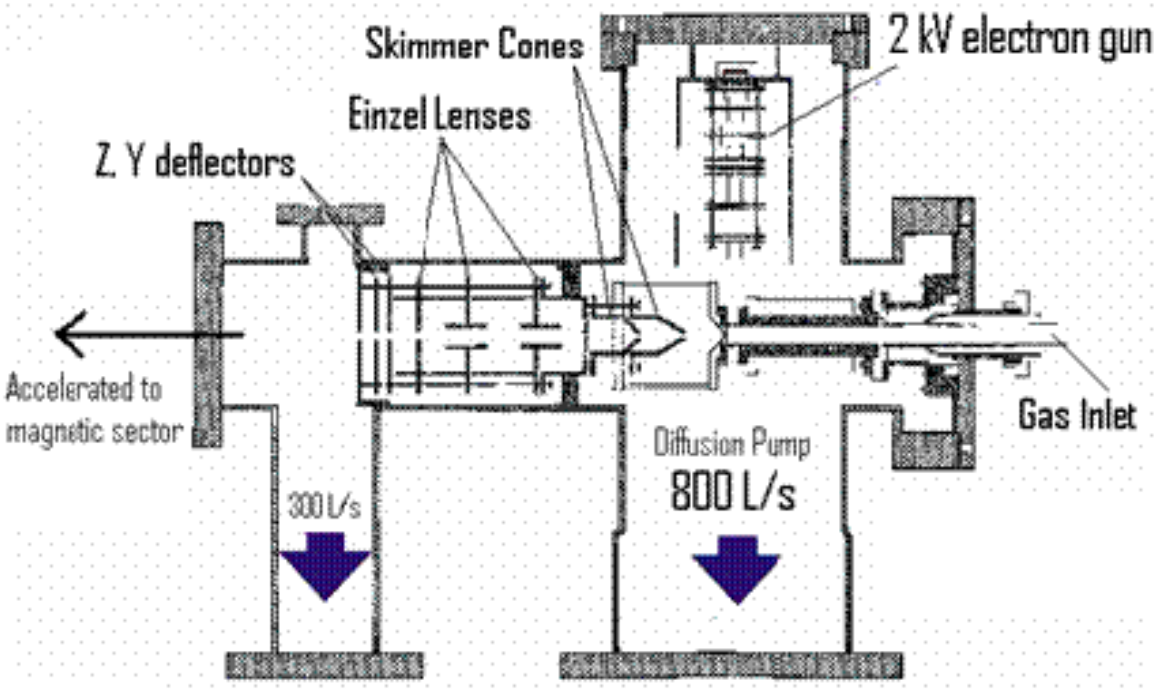

Fig. 2.2: Cross-Section of high pressure ion source and ion optics showing two differentially pumped regions.

The ion source is designed to allow high pressure relative to more conventional forms of mass spectrometry. It is a cylindrical tube, roughly 1 mL in volume, insulated by a copper block, consisting of two heaters, each insulating one half the circumference of the ion source and maintaining the temperature of the source in the range of room temperature safely up to 350^{o}C. The temperature is measured and maintained constant (within ±1^{o}C) by a pair of iron/constantan thermocouples which feed-back current through the heaters. The source is floated at a potential of +4 kV.

A beam of electrons at 2 keV is produced from an isolated electron gun assembly positioned directly above a 200 μm electron entrance aperture to the source. The electron entrance aperture, in addition to the ion exit aperture are the only two openings between the high pressure source and the low pressure housing. The filament in the electron gun assembly is made of a tungsten-iridium alloy, and subjected to a voltage of +2 kV. The electrons are accelerated through a potential of 2 kV, focused by a series of Einzel lenses and guided by directional deflector electrodes up to a potential of +4 kV, and penetrate into the ion source through the electron aperture, to initiate a chemical ionization sequence with methane. To initiate a time dependence of the ion abundances, a pulsed electron beam is used as opposed to a continuous beam. The pulse length in the experiments described here was approximately 50 μs, at a repetition rate of 20 Hz. The collision of a high energy electron with the gas mixture in the ion source initiates an electron impact reaction with CH_4, to produce the $CH_4^{\bullet +}$ radical cation and CH_3^+, Eqs. 2.1 and 2.2

$$CH_4 + e^- \rightarrow CH_4^{\bullet +} + 2e^- \quad (2.1)$$

$$CH_4 + e^- \rightarrow CH_3^+ + H^{\bullet} + 2e^- \quad (2.2)$$

At low pressures, both $CH_4^{\bullet+}$ and CH_3^+ are thermodynamically stable, but under the experimental conditions, both species quickly react further with CH_4, producing the protonated methane cation, CH_5^+, and the protonated ethylene cation, $C_2H_5^+$, shown by the simultaneous reactions depicted in Eqs. 2.3 and 2.4

$$CH_4^{\bullet+} + CH_4 \rightarrow CH_5^+ + CH_3^{\bullet} \quad (2.3)$$

$$CH_3^+ + CH_4 \rightarrow C_2H_5^+ + H_2 \quad (2.4)$$

Like all other components, the base that we wish to ionize must also be put in the gas phase. Since the biomolecular samples studied in these experiments are all in the solid state under standard conditions, the solid samples were placed directly inside the ion source, held in a glass tube cut from a disposable pipette covered at the bottom by Teflon. The glass tube was placed directly underneath the electron entrance aperture, and the solid sample allowed to sublimate by heating the ion source to temperatures between 80^{o}C and 200^{o}C, at which the experiments were performed. This method was believed to be a good strategy for obtaining suffiently high vapour pressure of the analytes, which were normally involatile. The ionized products from Eqs. 2.3 and 2.4 are very strongly acidic, and protonate the gaseous base. The number of collisions inside the ion source is on the order of $1x10^8$ per second, ensuring all ions are thermalized, and the ion energies follow a Boltzmann distribution.

The resulting ions leave the source through a 200 μm exit aperture, proceeding to be focused by the ion optics. The first stage in the ion optics is a pair of skimmer cones. The ions which pass through the cones enter a region supported by a 300 Ls^{-1} diffusion pump. These ions are focused by a set of three Einzel lenses, and directed by two ion deflectors, each covering perpendicular components in 2-D space. The accelerated ions that successfully pass through the ion

optics then enter the first field free region of the instrument, and continue to move towards the mass analyzer with a potential, V. The mass analyzer is surrounded by a variable field magnet, which is curved at an angle of 55^{o} from the original path direction. If set to a fixed field strength, the magnet permits the selection of particular ions based on their momentum. For an ion with charge, ze, to pass through the magnetic sector, it requires a kinetic energy related to its velocity, v, to be equal to the potential energy it was given to accelerate past the ion optics. This is summarized for an ion with mass m in Eq. 2.5, and rearranged for the velocity in Eq. 2.6

$$\frac{1}{2}mv^2 = zeV \tag{2.5}$$

$$v = \sqrt{\frac{2zeV}{m}} \tag{2.6}$$

A particle travelling along a trajectory of the circumference of a circle with radius r must have a centripetal force equal to the force exerted by the magnetic field, B, in order not to collide with the wall. This yields Eq. 2.7, and solving again for the velocity term yields Eq. 2.8

$$\frac{mv^2}{r} = zevB \tag{2.7}$$

$$v = \frac{zeBr}{m} \tag{2.8}$$

Equating Eqs. 2.6 and 2.8 for the velocity of the ion and rearranging to solve for the mass to charge ratio, m/z gives Eq. 2.9

$$\frac{m}{z} = \frac{eB^2r^2}{2V}$$

(2.9)

Thus the resolution is partially controlled by the curvature of the magnetic sector. For larger curvature angles, the radius will be lower, and large changes in the magnetic field would be necessary to increase the m/z ratio. This is helpful since the magnetic field strength is controlled by hand via an analog dial.

The second field free region of the instrument is differentially pumped by two diffusion pumps, maintaining pressures as low as $1x10^{-8}$ mbar. As previously mentioned, the ZAB-2F mass spectrometer also possesses a second analyzer, which separates ion fragments based on their kinetic energies by means of an electric field. This portion of the instrument could be used to run a Collision Induced Dissociation (CID) experiment, which would yield general structural information about the ions. Simply put, this is accomplished by introducing an inert collision gas, such as helium, and allowing it to collide with the mass selected precursor ions, breaking the collision-sensitive bonds and giving fragment ions, whose abundance will be inversely proportional to the strength of the bond that was broken to result in that fragment. These fragments are separated by scanning the electrostatic field. The electrostatic analyser was rarely used for structure identification during the course of these experiments.

The ions are detected by means of a channeltron current multiplier, which is connected directly to a digital oscilloscope. The time-dependent ion abundances generated by the pulsed electron beam are recorded digitally by a multi-channel scalar data acquisition card fit inside a computer, which also uses the pulsed electron beam gate to initiate recording. The length of each channel depends on the lifetime of the ions before collision with the walls of the source. Typically, 1000 channels, with each channel being 15 to 30 μs in length were used, giving experimental time

scales ranging from 15 to 30 ms. An example of a time-intensity profile for protonated glycine and its cluster with methanol is shown in Fig. 2.3. From this, one can see that both ions occupy the same residence times in the source. Based on a hard sphere collision model, the rate of diffusion of an ion with molar mass, M into the walls of the source, at temperature, T, will be proportional to the root-mean-square speed of the ion, u_{rms}, given by Eq. 2.10. In the high pressure source, the ions are thermalized, so that the ratio of the diffusion times of two ions, $t_{diff,1}$ and $t_{diff,2}$ will be given by Graham's Law, Eq. 2.11

$$u_{rms} = \sqrt{\frac{3RT}{M}} \tag{2.10}$$

$$\frac{t_{diff,1}}{t_{diff,2}} = \frac{u_{rms,2}}{u_{rms,1}} = \sqrt{\frac{M_1}{M_2}} \tag{2.11}$$

This means that if the lifetime of an ion was only dependent on its rate of diffusion, the two ions with different masses must have different residence times. The fact that protonated glycine and its methanol cluster have the same residence times indicates that the cluster becomes collisionally destabilized in the source, and dissociates into protonated glycine and neutral methanol. Fig. 2.3 is qualitative evidence that the protonated ion and the cluster ion reach chemical equilibrium inside the ion source.

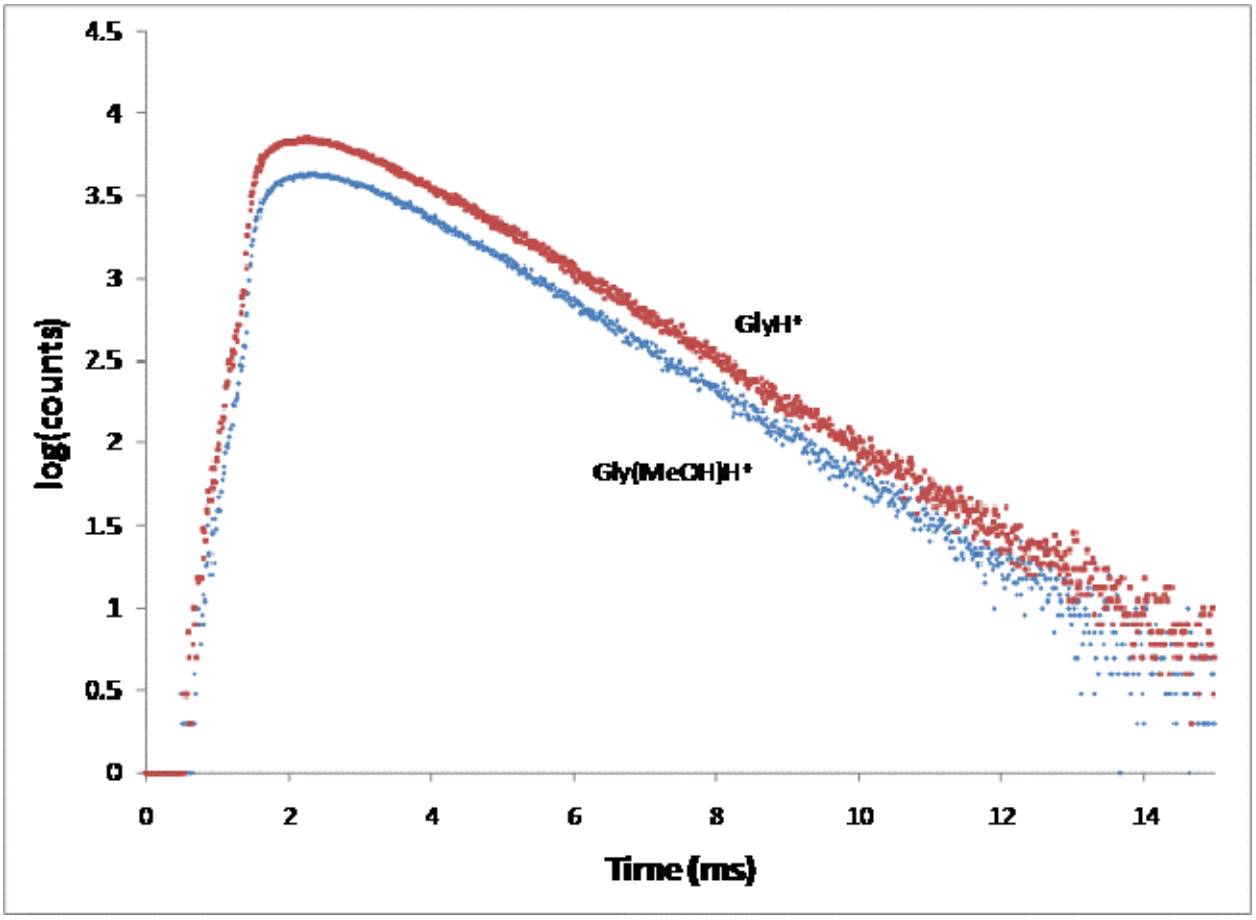

Fig. 2.3: Time-dependent intensity profile for the gas phase reaction $GlyH^+ + MeOH \leftrightarrows Gly(MeOH)H^+$ at 152°C. The relative ion intensities depends on both temperature and concentration of methanol introduced into the ion source.

The reaction in Fig. 2.3 depicts a specific gas phase ion-molecule reaction at a specific temperature. It can be represented more generally by Eq. 2.12, where species AH^+ is a protonated base, and B a neutral prototypical solvent molecule. Under equilibrium conditions, the equilibrium constant for the reaction can be written as Eq. 2.13

$$AH^+ + B \leftrightarrows (AB)H^+ \qquad (2.12)$$

$$K = \frac{a_{(AB)H^+}}{a_{AH^+} a_B} \tag{2.13}$$

where the activities of the three components are their pressures with reference to a pressure of P^o = 1 atm or 1 bar. For the determination of equilibrium constants throughout this thesis, P^o = 1 atm was used. At equilibrium, the pressure of an ion will be directly proportional to its ion intensity as determined from data acquisition of the appropriate signal, isolated by mass in the magnetic sector, Eqs. 2.14 and 2.15 below.

$$P_{AH^+} = c[I_{AH^+}] \tag{2.14}$$

$$P_{(AB)H^+} = k[I_{(AB)H^+}] \tag{2.15}$$

where the proportionality factors, c and k, are assumed to be equal since the major process occurring in the gas phase is the simultaneous association of ion and molecule, and dissociation of the cluster. Substituting the definitions for activities and the relationship between ion pressure and signal intensity into the expression for the equilibrium constant yields Eq. 2.16,

$$K = \frac{I_{(AB)H^+} P^o}{I_{AH^+} P_B} \tag{2.16}$$

The partial pressure of the neutral compound would be determined by assuming it behaves as an ideal gas at these pressures. Therefore, by measuring the ion intensities of the two ions when they have reached a state of chemical equilibrium, an equilibrium constant at a temperature, T, can be

calculated. The gas phase association equilibrium constant is related to the standard Gibbs free energy of association at equilibrium through the Eq. 2.17

$$K = e^{-\frac{\Delta G^O}{RT}} \tag{2.17}$$

and the standard free energy of association at equilibrium is related to the enthalpy and entropy of association by Eq. 2.18

$$\Delta G^o = \Delta H^o - T\Delta S^o \tag{2.18}$$

When Eqn. 2.17 is substituted into Eq. 2.18, the van't Hoff equation, Eq. 2.19 is formed,

$$lnK = -\frac{\Delta G^O}{RT} = -\frac{\Delta H^O}{R}\frac{1}{T} + \frac{\Delta S^O}{R} \tag{2.19}$$

Therefore, measuring K at various temperatures and plotting lnK vs. T^{-1} will yield ΔH^o, from the slope and ΔS^o, from the intercept, as well as ΔG^o for the association reaction of the cation with the neutral solvent molecule. To determine at what time after the initial pulse the reaction reaches equilibrium, the time-intensity profiles of both the protonated cation and its cluster with the neutral compound following the example given in Fig. 2.3 are normalized, giving Fig. 2.4. For example, the normalized intensity of AH^+ at some point in time is related to its absolute intensity through Eq. 2.20

$$I_{AH^+}^{norm} = \frac{I_{AH^+}}{I_{AH^+} + I_{(AB)H^+}} \tag{2.20}$$

The normalized intensity for the $(AB)H^+$ cluster follows an analogous expression to Eq. 2.20, with $I_{(AB)H+}$ replaced in the numerator. Therefore, summing up both normalized intensities must give unity. Also note that as the result of a common denominator in both expressions, the ratio of the normalized intensities of AH^+ and $A\text{-}H^+\text{--}B$ must be equal to the ratio of their absolute intensities. From the normalized time-intensity plot, one can see that the relative abundance of both species is time independent, just 4 ms after the electron pulse initiates the reaction. This qualitative diagram also indicates that the steady state behaviour of one ion is directly related to that of the other ion. What this means is that the chemical equilibrium between the two ions is the only major reaction dynamic resulting in their steady states. Side reactions with impurities or the products of the electron impact with methane do not affect this equilibrium.

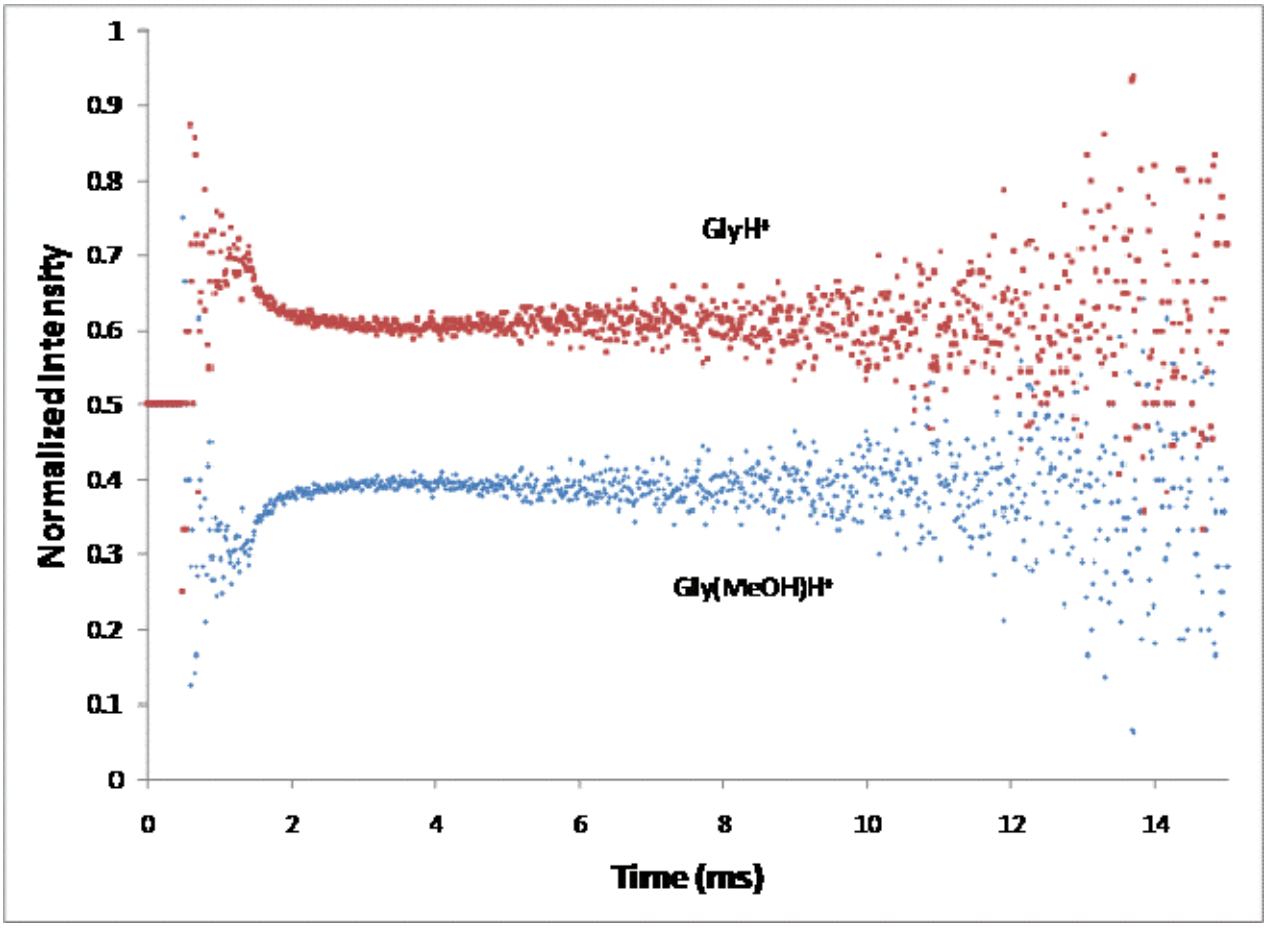

Fig. 2.4: "Normalized" time-intensity profile for the same reaction and temperature as Fig. 2.3.

2.2 Geometry Optimization and Energy Calculations

To elucidate the most probable geometries of the various conformers in the system of clusters investigated, computation in the form of *ab initio* calculations are performed using the Gaussian 03 suite of programs.[5] The SHARCNET computing facility at the University of Waterloo was utilized for the bulk of the calculations in this thesis. Before calculating the energy, a structure goes through a geometry optimization, to determine the minimum energy conformation. A geometry optimization begins by making an initial "guess" of the local minimum geometry via redundant internal coordinates by specifying initial bond lengths, bond angles and dihedral angles in the form of a Z-matrix,[6] or by specifying Cartesian coordinates of every atom with respect to another atom and an arbitrary axis orientation. The initial "guess" specifies a starting point for the wavefunction. The molecular wavefunction itself can be expressed as a Slater determinant, made up of individual molecular orbitals, ψ_i, which are in turn customarily in the form of a linear combination of atomic orbitals (LCAO-MO), so that the i^{th} molecular orbital would be expressed by Eq. 2.21 with coefficients c_{ki} and atomic orbitals, ϕ_k.

$$\psi_i = \sum_{k=1}^{N} c_{ki}\,\phi_k \qquad (2.21)$$

For a LCAO-MO composed of N atomic orbitals, the N coefficients could be solved for using the variational method, and diagonalizing an N by N Hamiltonian, or, more conventionally by a self-consistent field calculation (SCF), using the Roothaan equations. To simplify the mathematics of the calculation, Gaussian determines the symmetry point group of the wavefunction from the initial geometry input, and uses that symmetry to simplify the calculation of the electronic integrals. Larger molecules such as amino acids, peptides and nucleic acids generally have low symmetry as C_1

point groups, and geometry optimization can be quite time consuming and resource demanding. The next step in the optimization is to analyze the basis set, and assign Gaussian functions to each atomic orbital, and then evaluate the one-electron, two-electron repulsion, kinetic energy and potential energy integrals of the Hamiltonian. If the difference in the value of the energy from two consecutive cycles is less than a prestated error, typically 10^{-6} Hartrees, the calculation ends, if not, the geometry is altered and the integrals are re-evaluated based on the new coordinates until the error requirement is met.

The atomic orbitals making up the LCAO-MO are represented by split-valence basis sets, built from Slater orbitals (STO), and are expressed as Gaussian functions to simplify the mathemetics involved in integrating the secular determinants. Split valence basis sets assign a particular number of Gaussian functions to the inner shell orbitals and outer shell orbitals with different values of the orbital exponents, ζ_i. For example, the 6-311+g(d,p) basis set often used here for geometry optimization of amino acids and peptide clusters is called a triple-zeta split valence basis set. In this case the inner-shell orbitals would each be represented as a linear combination of six Gaussian functions, while the valence shell orbitals would be represented as a linear combination of three Slater orbitals, the first being the sum of three Gaussian functions, and the last two containing a single Gaussian function. This basis set representation is also an augmented basis set, because of the extra functions added at the end. The '+' sign assigns a diffuse function to period 2 and greater atoms, to take into consideration the different radial dependence of p,d, and f orbitals that form σ, versus π, versus δ overlap. This diffuse orbital exponent enhances all systems, but most of all lowers the energies of anions relative to neutrals and cations[7,8] likely because the orbitals of anions must be larger. A second diffuse function would be applied to the s orbitals on the hydrogenic atoms if '++' were used, but this second diffuse function only tends to significantly affect the results of the hydride ion.[7] The g(d,p) portion could also be written as a double asterisk (**) and assigns

polarization functions by means of the addition of low-lying d orbitals on non-hydrogenic atoms, and low lying p orbitals on hydrogen and helium atoms. Polarization functions exist to characterize the distortion of atomic orbitals as two atoms approach one another. Generally, the convergence to a stationary point is more specific the higher the basis set.[9]

The geometry optimizations conducted for this thesis were all performed using the B3LYP functional method, a hybrid of the Hartree-Fock Hamiltonian and Density Functional Theory, and is hence semi-empirical. Vibrational frequencies were also calculated in order to yield thermochemical data. The frequencies are calculated based on a harmonic oscillator approximation, and are not scaled. This harmonic approximation is one source of error in the calculated entropies of various species, especially with the degree of asymmetry within the molecules and ionic clusters being optimized. After the frequency calculation, a thermal energy correction and a zero-point vibrational correction is made to 298 K, to take into account the translational and internal energy of the structure at room temperature.

In a bonding orbital, two electrons of opposite spin must interact. Therefore, although an energy can be extracted from the optimization output, to more accurately calculate the energy of a molecular structure, the optimized geometries are put through a single-point energy calculation using a Moeller-Plesset perturbation model, abbreviated as MP2. An MP2 calculation is purely theoretical and allows for a higher degree of electron correlation, giving more reliable values for energy, especially when weak electrostatic interactions play a role. For each single-point energy calculation, the 6-311++g(2d,2p) basis set was used. This means that diffuse functions were also placed on hydrogen atoms, and two polarization functions were used on each atom.

Chapter 3

The Structures and Energies of the Methanol Stabilized Protonated Amino Acids

3.1 Introduction

The twenty naturally occurring amino acids, with the exception of glycine, all contain a unique side chain on the α-carbon which contributes largely to both the solvation of the individual molecule, as well as the secondary structure of a protein, through electrostatic interactions such as cation-π interactions,[1-4] as well as hydrogen bonding[5], salt-bridge interactions, and hydrophobic interactions. Since proteins play important biochemical roles in living organisms, it is of interest to understand the solvation behavior of amino acids in various solvents. In general, there are two forms that an amino acid may adopt. The first, and most dominant, form in aqueous solution is the zwitterion form, where the basic site is protonated, while the acidic site is deprotonated, forming a charge-separated species. The second is the canonical form, in which the acidic and basic sites of the molecule are charge neutral. In the gas phase, the isolated amino acid has only been found to exist in its canonical form.[6-10] However, by binding the amino acid to one or several prototypical solvent molecules or ions of sufficiently high gas-phase basicity, it is possible to stabilize the zwitterionic form through various charge-transfer or proton-transfer mechanisms.[7,8,11-25] Much of the experimental work that revolves around amino acid zwitterion stability involves the solvation of the neutral amino acid by one or more group 1[13,16,20] or group 2 [15] cations, to form salt-bridges. For example, Jockush et al. used blackbody infrared radiative dissociation (BIRD) to show that the arginine zwitterion stability increases with increasing group 1 cation size.

Many studies have attempted to model the behaviour of glycine and other amino acids in aqueous solution, by binding several water molecules to glycine[11,14,19,26] and alanine[18] among other amino acids[27] in the gas phase. These studies however are either computational, or examine the

clusters of water with the deprotonated forms of the amino acids, which only provides a lower limit to the solvation energy. To experimentally measure more reliable binding energies for such clusters, the method of chemical ionization (CI) may be employed to study cationic clusters. The protonation [6,28] and dissociation [29] of various amino acids is already well understood, and such ions have been produced and studied experimentally using multiple techniques, such as Collision Induced Dissociation (CID),[6,29-31] Fast Atom Bombardment,[6] Electrospray Ionization,[22,27,31] Fourier Transform Mass Spectrometry (FTMS) [13,15,16,24,32] and Pulsed High Pressure Mass Spectrometry (HPMS).[21,33] HPMS is a very useful tool for studying such sensitive reactions, because at high pressures, the ions can quickly come to chemical and thermal equilibrium to yield accurate and absolute energies.

Wu et al. recently reported on the 1:1 cluster of ammonia with protonated glycine.[21] They found that proton transfer from the glycine carboxyl group to ammonia is not energetically demanding, and the zwitterion is practically energy degenerate with the lowest energy charge-solvated form. This can be rationalized based on the proton affinity difference between ammonia and glycine, as it is relatively small, which accounts for a low potential energy barrier between the canonical form, and the zwitterion form. Based on these considerations, in the 1:1 cluster of a less basic solvent such as methanol with protonated glycine, it might be expected that the glycine zwitterion would not be so readily accessible.

This chapter explores the use of pulsed High Pressure Mass Spectrometry (HPMS) to perform equilibrium measurements and obtain the net binding energies and relative entropies of the clusters of one methanol molecule bound to the protonated amino acids glycine, alanine, valine, leucine, isoleucine, and proline. The intention here revolves around the effectiveness of HPMS to measure absolute enthalpy and entropy changes for association reactions which form strongly bound ionic clusters.[33,34] Our choice of using methanol as a solvent as opposed to water is based on an inconveniently large proton affinity difference between glycine and water (ΔPA = 46.9 kcal mol^{-1}).

Even the 1:1 glycine-water proton-bound adduct will not be bound strongly enough to observe appreciable amounts in the gas phase. This prediction is supported experimentally, in which the binding energy of protonated diglycine with water was measured as being only 17 kcal mol^{-1}, and various other complexes of protonated peptides with water have shown even lower binding energies.[35] The goal here is to model the complexation of one water molecule by the protonated adduct of various aliphatic amino acids (Gly, Ala, Val, Leu, Ile, Pro), with methanol. Of course, the main concern in attempting to make conclusions based on such an approximation is that of the effect of methyl substitution on solvent coordination and binding energy. Grimsund and Kebarle have used HPMS to study the effect of methyl substitution on the hydrogen ion, and found that for clusters of $H^+(H_2O)_n$ and $H^+(CH_3OH)_n$ up to n=8, the overall binding energies were comparable.[36] This study will establish a foundation of a much larger investigation towards understanding how the zwitterion structure of aliphatic amino acids is stabilized by various gaseous solvents.

3.2 Experimental and Computational Results

3.2.1 **Protonation of the Gas Phase Amino Acids Gly, Ala, Val**

Previous work has revealed two dominant forms of neutral glycine; a transoid form, in which the amino end group and hydroxyl moieties are not in close contact, and a cisoid form in which the O-H moiety donates an intramolecular hydrogen bond to the lone pair of electrons on the amino nitrogen atom.[14] Based on this, it was assumed that in the protonation of glycine and the other amino acids studied, that the cisoid structure would be destabilized in the process. From the transoid conformation, there are potentially three proton accepting sites if the amino acid has a side chain with only alkyl substituents. These are the amine nitrogen, which holds one lone pair of non-bonding electrons, the carbonyl oxygen atom, and the hydroxyl oxygen atom, each possessing two

pairs of non-bonding electrons. Although one would intuitively estimate that the nitrogen atom be the preferred site for the first proton, confirmation of the lowest energy tautomer for the first protonation of each amino acid must be established quantitatively and qualitatively through computational methods. Fig. 3.1 shows the three conformers that have been optimized for protonated glycine ($GlyH^+$), protonated alanine ($AlaH^+$) and protonated valine ($ValH^+$). The relative energies calculated at the MP2(full)/6-311++g(2d,2p)//B3LYP/6-311+g(d,p) level are shown in Table 3.1. The lowest energy conformer of each protonated amino acid involves protonation at the amine group, and the resulting ammonium group forms an intramolecular hydrogen bond with the nearby carbonyl group of the acid moiety. This hydrogen bond strength is unaffected by the character of the side chain as the bond length remains at 1.91 Å throughout all three amino acids. This is an interesting observation because the proton affinity of the amino acids increases with increasing side chain size. From this, one would predict that with increasing side chain size, the $GlyH^+$ ammonium group should form weaker hydrogen bonds with the carbonyl oxygen atom as the ammonium group becomes less acidic (the conjugate becomes more basic). GH02, AH02 and VH02 are simply rotamers of GH01, AH01 and VH01 respectively, and are slightly higher energy conformers since in each case a strong hydrogen bond must be broken and is replaced by one or two weaker hydrogen bonds with the weakly basic hydroxyl oxygen atom. Attempts to optimize the conformer in which the proton resides on the hydroxyl group of glycine resulted in reversion to GH02. Identical results were obtained for the conformers of alanine and valine. When the carbonyl oxygen atom is protonated as opposed to the amino group (GH03, through VH03), the energy of the conformer increases dramatically. This is likely because no intramolecular hydrogen bond exists in the conformer, and the carbonyl oxygen atom is much more weakly basic than the amino nitrogen atom. Therefore, based on a fitting of relative free energies to a Boltzmann distribution, only the two lowest energy conformers for each amino acid should be present with a significant abundance

in practice. Fig. 3.2 shows the transition state between GH01 and GH02 which reveals that rotation of the carboxyl group by 180^{o} is subject to an energy barrier of 7.3 kcal mol^{-1}, since the strong intramolecular N-H—O hydrogen bond (between ammonium and carbonyl moieties) must be broken. Note that in addition to the carboxyl rotation, the ammonium group adopts a staggered conformation with the hydrogen atoms on the a-carbon, as the loss of the intramolecular hydrogen bond allows steric hindrance to control the conformation along the N-H covalent bond. Therefore, from a kinetic standpoint, the energies and entropies of the conformers for the proton-bound clusters of all amino acids studied here with methanol were calculated with reference to the lowest energy conformer for the protonated amino acid, i.e. those analogous to GH01.

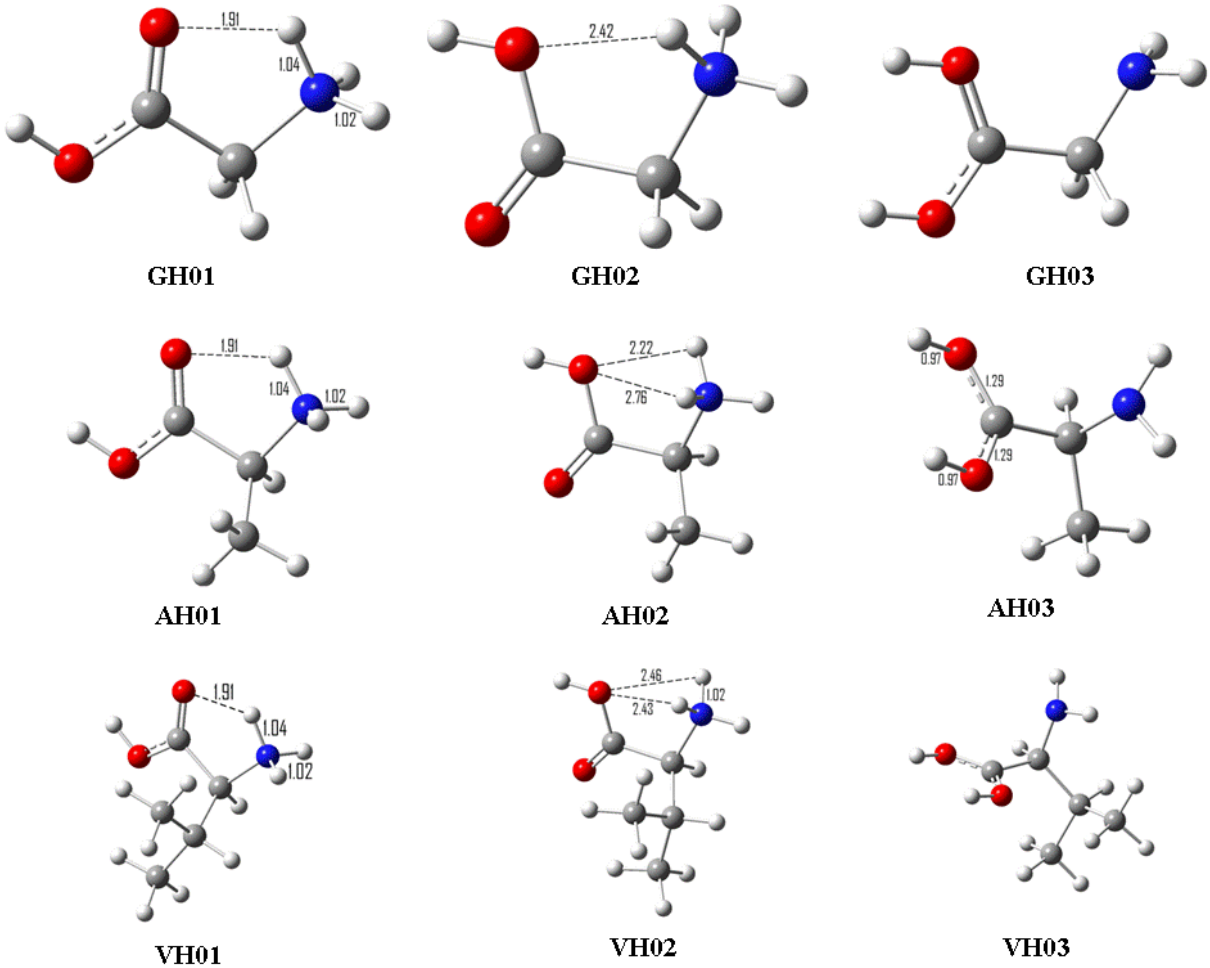

Fig. 3.1: Structures of the most stable conformers of protonated Gly, Ala and Val optimized at the B3LYP/6-311+g(d,p) level of theory

Table 3.1: Relative enthalpies and entropies of the structures shown in Fig. 3.1. Energies were calculated as single-point energies based on the geometries obtained from the optimation. Energies are calculated at the MP2(Full)/6-311++g(2d,2p) level of theory and include thermal energy and zero-point energy corrections.

	ΔH° (kcalmol^{-1})	ΔS° (calmol^{-1}K^{-1})
GH01	0.0	0.0
GH02	4.6	2.5
GH03	29.9	3.5
AH01	0.0	0.0
AH02	3.9	1.1
AH03	30.7	-0.3
VH01	0.0	0.0
VH02	3.5	1.8
VH03	32.8	0.7

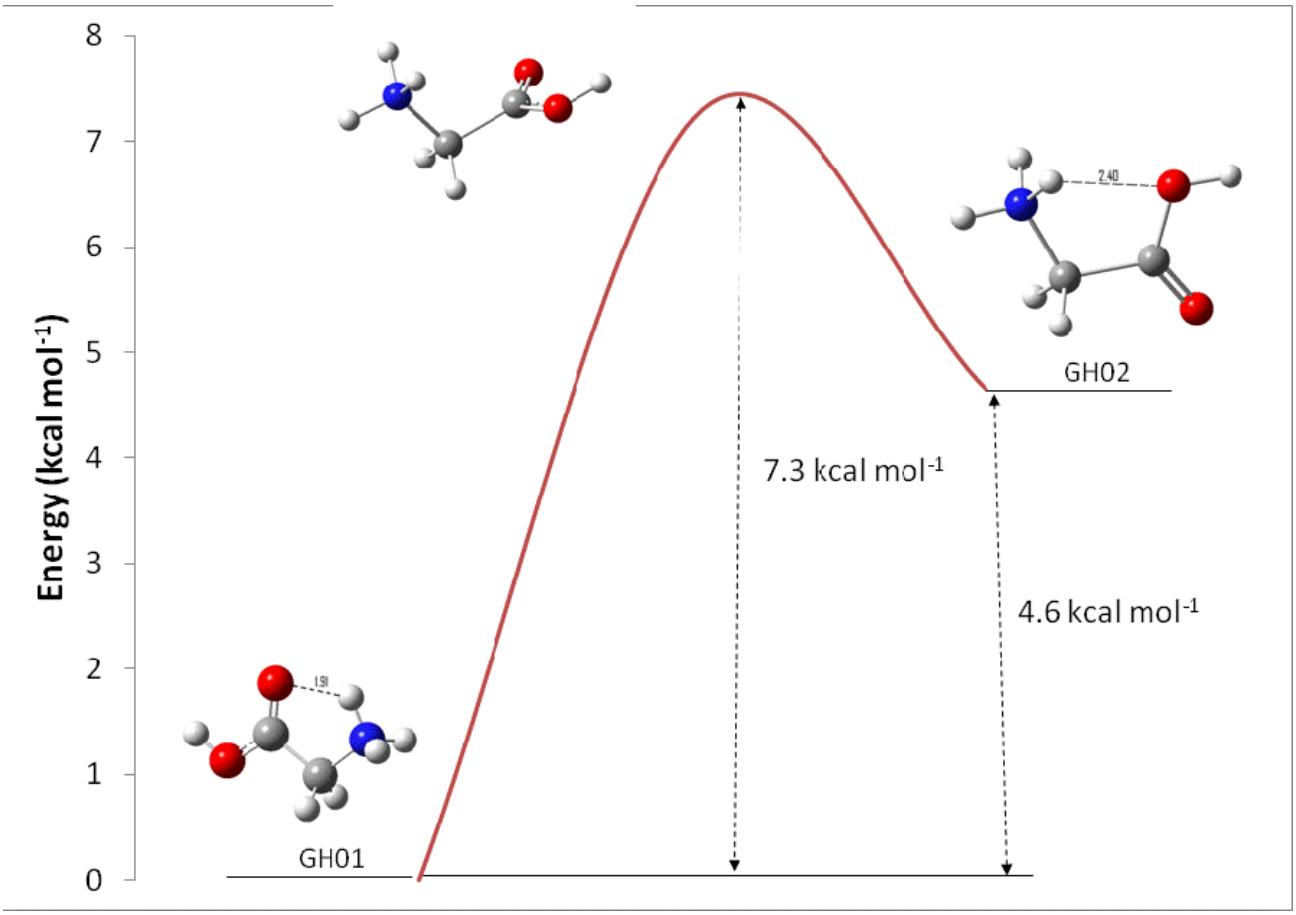

Fig. 3.2: The isomerization pathway of protonated glycine between its most stable form, GH01, where the carbonyl oxygen forms an ionic hydrogen bond with an ammonium group proton, and its second most stable form, GH02 in which the hydroxyl oxygen acts as the hydrogen bond acceptor.

3.2.2 **Experimental Results**

The six independent cluster reactions of six protonated amino acids with methanol are shown in Eqs. 3.1 through 3.6

$$GlyH^+ + MeOH \leftrightarrows Gly\text{-}H^+\text{--}MeOH \quad (3.1)$$

$$AlaH^+ + MeOH \leftrightarrows Ala\text{-}H^+\text{--}MeOH \quad (3.2)$$

$$ValH^+ + MeOH \leftrightarrows Val\text{-}H^+\text{--}MeOH \quad (3.3)$$

$$LeuH^+ + MeOH \leftrightarrows Leu\text{-}H^+\text{--}MeOH \quad (3.4)$$

$$IleH^+ + MeOH \leftrightarrows Ile\text{-}H^+\text{--}MeOH \quad (3.5)$$

$$ProH^+ + MeOH \leftrightarrows Pro\text{-}H^+\text{--}MeOH \quad (3.6)$$

where Gly is glycine, Ala, alanine, Val, valine, Leu, leucine, Ile, isoleucine, and Pro is proline, which falls in a different class of amino acid than the first five due to its pyrrolidine ring, rendering it a secondary amino acid. The enthalpies and entropies of each reaction were extracted from the series of van't Hoff plots in Fig. 3.3. These values for all six association reactions are summarized in Table 3.2.

The Gly-H^+--MeOH cluster ion has an enthalpy and entropy of binding of -22.0 kcal mol^{-1} and -33.5 cal mol^{-1} K^{-1} respectively. According to Table 3.2, it is the strongest bound cluster in the series of amino acid-methanol proton-bound clusters investigated, since the binding energy is the negative of the enthalpy change. The experimental enthalpy is 1.4 kcal mol^{-1} higher than the calculated enthalpy for the most stable conformer of Gly-H^+--MeOH at MP2(Full)/6-311++g(2d,2p), GM01 falling just outside the experimental error of ±1 kcal mol^{-1}. The entropy is 2.7 cal mol^{-1} K^{-1} greater than the computed entropy, which can be considered to be excellent agreement.

The second most strongly bound cluster ion is Ala-H^+--MeOH, having an experimental enthalpy and entropy of binding of -19.9 kcal mol^{-1} and -31.0 cal mol^{-1} K^{-1}. The enthalpy falls only 0.2 kcal mol^{-1} lower than the computed enthalpy of the most stable conformer of Ala-H^+--MeOH, AM01, and the entropy is only 1.2 cal mol^{-1} K^{-1} lower than the computed entropy. Both values are well within experimental error. The van't Hoff plot for the Ala-H^+--MeOH cluster was also measured over a slightly larger temperature range than that for the Gly-H^+--MeOH cluster, since alanine showed greater stability at slightly higher temperatures.

The cluster of Val-H^+--MeOH gave an experimental enthalpy of binding of -19.7 kcal mol^{-1} and an entropy of -33.0 cal mol^{-1} K^{-1}. VM01, the most stable computed conformer of Val-H^+--MeOH has an enthalpy and entropy of -19.3 kcal mol^{-1} and -33.0 cal $mol^{-1}K^{-1}$ respectively. Again, the measured values fall very well within the experimental error.

The experimental enthalpy and entropy for the association of the Leu-H^+--MeOH cluster are -19.0 kcal mol^{-1} and -29.0 cal mol^{-1} K^{-1} respectively. When these values are compared to their respective values for LM01, experiment agrees to within 0.2 kcal mol^{-1} and 0.6 cal mol^{-1} K^{-1} with the calculated values, giving excellent agreement.

Finally, for the cluster Ile-H^+-MeOH, the experimental enthalpy and entropy are-18.8 kcal mol^{-1} and -29.8 cal mol^{-1} K^{-1} respectively. The experimental enthalpy and entropy of association fall well within experimenal error when compared to the respective values for IM01, being only 0.2 kcal mol^{-1} lower and 0.7 cal mol^{-1} K^{-1} higher than the calculated values respectively. It is apparent from both the experimental results and the computed values that in the series of proton-bound clusters of amino acids with methanol, where the amino acid contains only an alkyl chain as its α-substituent, that the binding energy of the cluster decreases with increased size of the alkyl chain. This conclusion will now be examined in more detail.

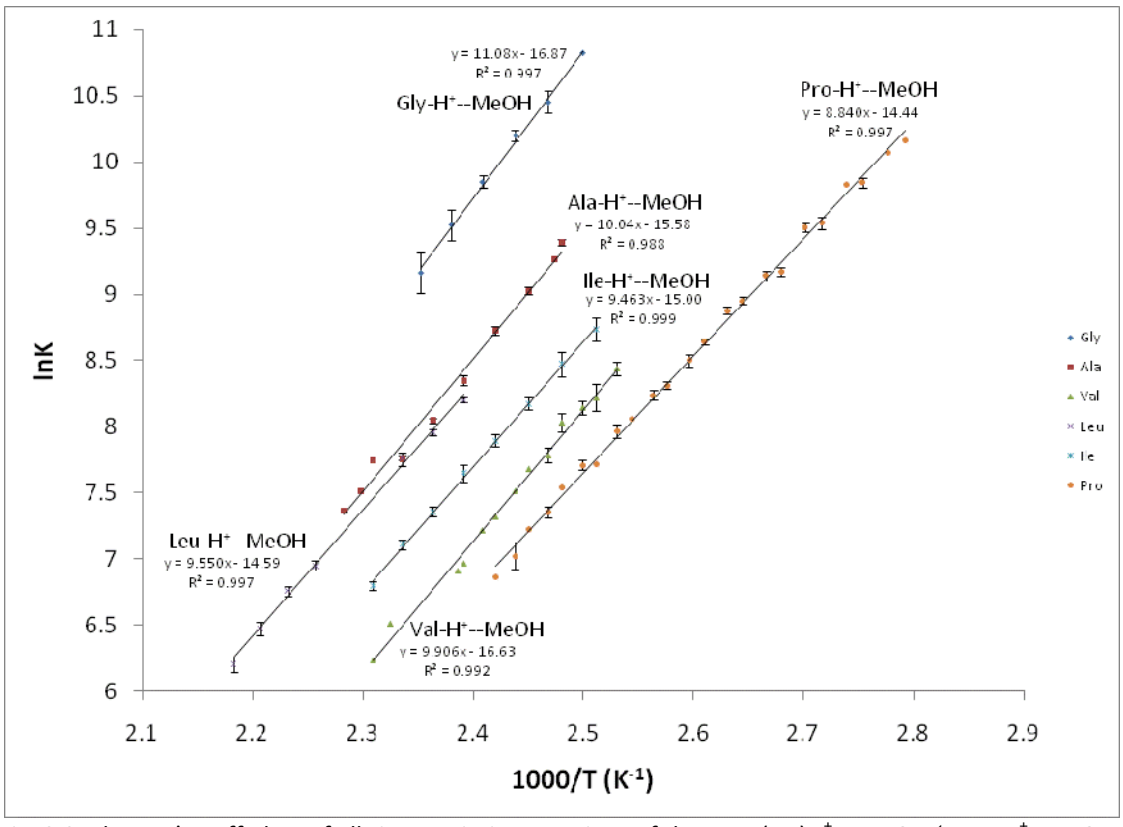

Fig. 3.3: The van't Hoff plots of all six association reactions of the type $(AA)H^+ + MeOH \leftrightarrows AA\text{-}H^+\text{--}MeOH$.

Table 3.2: Measured ΔH^o and ΔS^o of each amino acid-methanol cluster obtained through High Pressure Mass Spectrometry

	ΔH^o (kcalmol^{-1})	ΔS^o (calmol^{-1}K^{-1})
Gly(MeOH)H$^+$	-22 ±1 kcal/mol	-33.5 ±3 cal/molK
Ala(MeOH)H$^+$	-19.9	-31.0
Val(MeOH)H$^+$	-19.7	-33.0
Leu(MeOH)H$^+$	-19.0	-29.0
Ile(MeOH)H$^+$	-18.8	-29.8
Pro(MeOH)H$^+$	-17.6	-28.7

Table 3.3: Computed ΔH^o and ΔS^o of the lowest energy adducts of each cluster reaction at MP2(Full)/6-311++g(2d,2p)

	ΔH^o (kcalmol^{-1})	ΔS^o (calmol^{-1}K^{-1})
Gly(MeOH)H$^+$	-20.6	-30.8
Ala(MeOH)H$^+$	-20.1	-32.2
Val(MeOH)H$^+$	-19.3	-30.2
Leu(MeOH)H$^+$	-19.2	-29.6
Ile(MeOH)H$^+$	-19.0	-29.1
Pro(MeOH)H$^+$	-17.8	-28.0

Since the clusters studied here are proton-bound clusters, the binding energies must depend on the competitive proton accepting nature of the two bases that form the cluster. The proton affinity of a gas phase molecule, B, which can be written as PA(B), is the energy required to remove a proton from the protonated ion, BH^+. It is therefore analogous to the electron affinity of a gaseous atom, and can be represented by the reaction in Eq. 3.7,

$$BH^+_{(g)} \leftrightarrows B + H^+ \qquad \Delta H = PA(B) \qquad (3.7)$$

From this definition, the proton affinity is always a positive value. According to the NIST database, the proton affinities of Gly, Ala, Val, Leu and Ile are 211.9, 215.5, 217.6, 218.6 and 219.3 kcal mol^{-1} respectively, while the proton affinity of methanol is 180.3 kcal mol^{-1}. This means that within the cluster, the proton should reside closer to the amino acid than to methanol, and proton transfer to methanol is unlikely, since the energy barrier of proton transfer from the amino acid to methanol must be at least 30 kcal mol^{-1}. Putting this amount of internal energy into the cluster would result in dissociation before proton transfer could take place. One would therefore expect that with less competition for the proton, that is, the smaller the proton affinity difference between two bases, the higher the binding energy in the proton-bound cluster should be. Since all clusters include methanol, only the proton affinities of the amino acids should affect the relative binding energies of the clusters. A plot of binding energy versus proton affinity for these five clusters is shown in Fig. 3.4. It can be seen from the plot that there is an evident linear dependence between binding energy and proton affinity difference in this case.

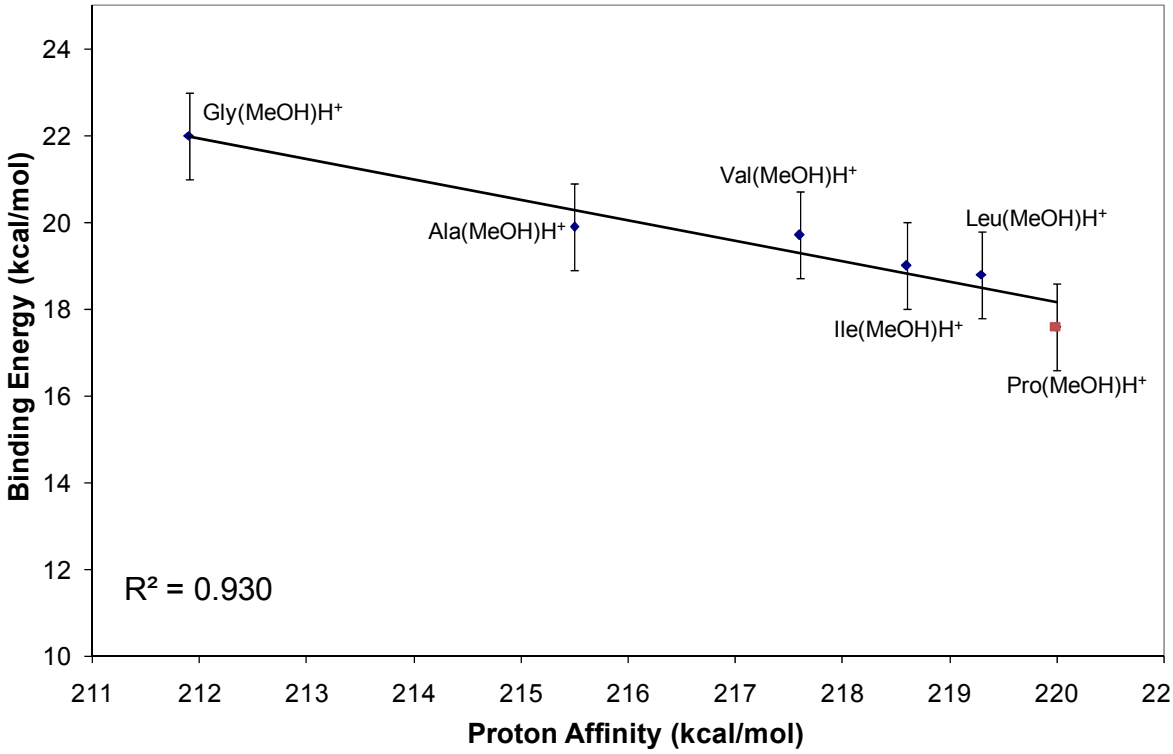

Fig. 3.4: The HPMS measured binding energies for the clusters produced in reactions 3.1 through 3.6 plotted against the proton affinities of the amino acids.

The straight line obtained in Fig. 3.4 is evidence of two things. First, the coordination, or at least the regioselectivity of one methanol molecule to each protonated amino acid is the same, or there would exist no relationship between binding energy and proton affinity. This also provides evidence to support the theory that protonation always occurs at the amino funcitionality, since correlation of binding energy with amino acid proton affinity suggests analogous conformations of each cluster in the series. This is not to suggest that conformational or geometric isomerization can not take place within the cluster. The entropy change upon cluster formation from the initial state of separated protonated amino acid and methanol is always negative, primarily because the total degrees of translational freedom are reduced by half. There is however a slight increase in the internal degrees of freedom, namely rotational and vibrational. If a cluster is tightly bound, then it does not gain as much rotational freedom as a cluster which is more loosely bound, and the

resulting entropy change will be greater. If the entropy change is sufficiently unfavourably large, an isomerization may ensue to minimize the free energy of complexation. Therefore, it is now convenient to define another property of gaseous atoms or molecules, referred to as the gas phase basicity. Gas phase basicity is simply the free energy change of the process described by Eq. 3.7, and is hence the free energy analog to proton affinity. The free energy of formation of each proton-bound amino acid-methanol cluster versus the gas phase basicities of each amino acid is plotted in Fig. 3.5. Again, a relatively good linear relationship is shown to exist between the free energy of the cluster and gas phase basicity of the amino acids. This is not a surprising result, since the population of a particular conformer of a cluster is free energy controlled, and one would expect that the experimentally measured enthalpy and entropy should be related to the most abundant conformer.

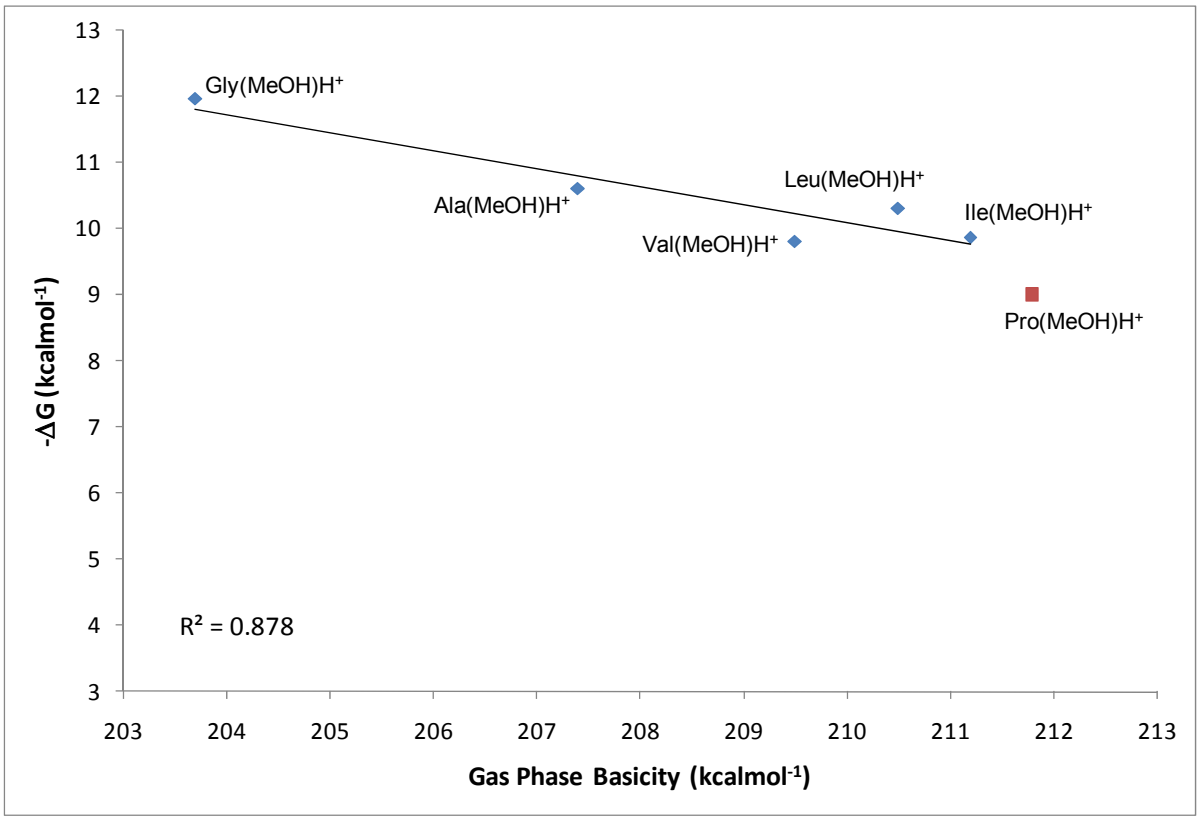

Fig. 3.5: $-\Delta G^{o}$ of association at 440K for the clusters produced in reactions 3.1, 3.2, 3.3, 3.4, 3.5 and 3.6 plotted against the gas phase basicity of the amino acids.

3.2.3 **Computation of the Structures and Energies of AA-H^+--MeOH type Clusters**

3.2.3.1 **The Potential Energy Surface for the Isomerization of Gly(MeOH)H^+**

All conformers of favourable free energies are thermodynamically accessible, but to deduce a reasonable isomerization pathway between kinetically accessible conformers, the calculation of transition states between various local minimum structures was necessary. The one dimensional conformational isomerization potential energy surface for the complexation of methanol to protonated glycine was calculated after several attempts to determinine a reasonable pathway. Coordination of methanol onto protonated glycine is initiated at the ammonium group, where the positive charge is mainly localized. Therefore, methanol acts as the hydrogen bond acceptor, donating electron density from the hydroxyl oxygen to the glycine ammonium group. Note that in GM02 (see Fig. 3.9), the intramolecular hydrogen bond between the ammonium group and the carbonyl oxygen atom is weakened in glycine from its non-solvated form, indicating that the formation of the new hydrogen bond has a polarization effect on the N-H bonds. This is important to note because it means that the measured enthalpy change will be somewhat underestimated relative to the actual hydrogen bond strength due to perturbation of the intramolecular hydrogen bond within protonated glycine. From GM02, the cluster is allowed to go through several rotamers separated by low energy transition states, since rotation along the resulting O-H-N hydrogen bond is unhindered. These rotamers may also be the result of a changing H-N-C-C dihedral angle, as is the case going from GM03 to GM01. Upon calculation of various minima in which methanol was coordinated to the hydroxyl group of glycine, it was found that the energy at the B3LYP/6-311+g(d,p) and MP2(Full)/6-311++g(2d,2p) levels of theory for these conformers was only 2 kcal mol^{-1} higher in energy than for the conformers where methanol is coordinated to the ammonium group. The small energy difference between the two coordination modes arises from the ability of protonated glycine to form an intramolecular hydrogen bond between its ammonium group and its

carbonyl oxygen. For example, from Fig. 3.6, GM02 and GM04 are examples of similar $GlyH^+$ conformations. The only difference is the position of the methanol molecule. The intramolecular N-H-O hydrogen bond in GM02, where methanol is coordinated to the ammonium group is 2.02 Å, whereas in GM04, where methanol attaches to the hydroxyl group, the N-H-O intramolecular hydrogen bond length is only 1.87 Å. Therefore, coordination of methanol to the ammonium group weakens the intramolecular hydrogen bond. This phenomenon provided motivation for an attempt to find a feasible pathway across the glycine molecule to accommodate both coordination modes.

Before describing the most feasible pathway, an alternative pathway that was investigated and proved unlikely will be discussed. This involved proton transfer from glycine to methanol, from the ammonium group to the methanol oxygen atom, and is shown in Fig. 3.6. Note that the energies plotted in this diagram are the zero-point energies obtained at 0 K through the geometry optimization at the B3LYP/6-311+g(d,p) level of theory. The energies of each conformer calculated at the MP2(Full)/6-311++g(2d,2p) level of theory with vibrational and thermal corrections to 298 K are summarized in Table 3.4. The energy required for the proton transfer between GM04 and GM05 is directly related to the proton affinity difference between glycine and methanol, and lies roughly 15-16 kcal mol^{-1} above the energy of GM04, increasing the energy of the cluster above its dissociation energy. This step is followed by rotation of protonated methanol about the hydrogen bond formed with the carboxyl group. Protonated methanol acts as a hydrogen bond donor to both the carbonyl oxygen atom, and hydroxyl oxygen atom in GM05. A low energy transition state that suggests there is a relatively fast tautomerization within the cluster as a proton is transferred from protonated methanol to the carbonyl group of glycine in GM06, followed by a shift in positive charge towards the amino group, as the proton on the glycine hydroxyl group is itself easily transferred to the amino group. The failure in this mechanism arises because the hydrogen bond originally formed between the glycine ammonium group and the methanol oxygen atom is

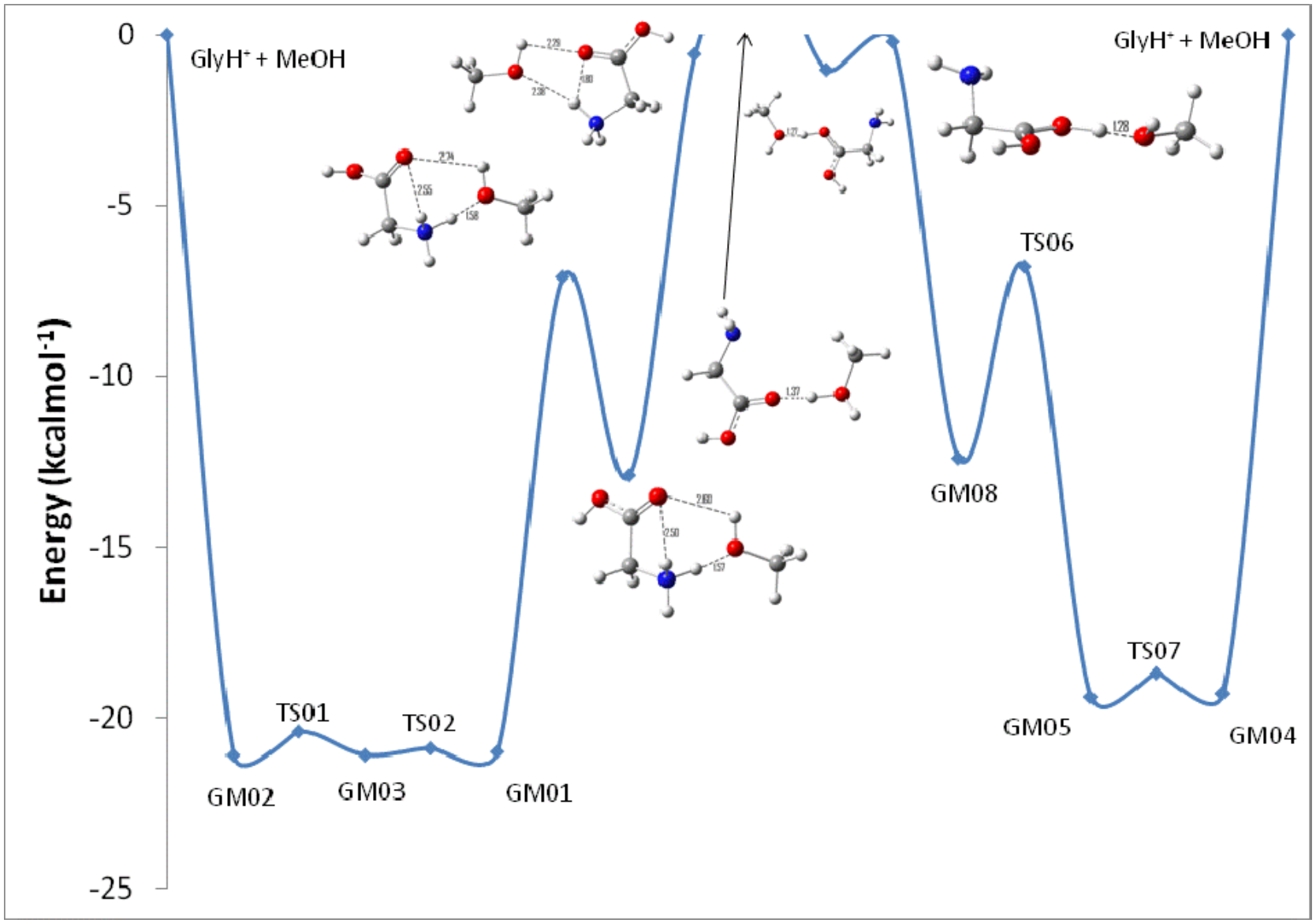

Fig. 3.6: The first attempted isomerization pathway of the Gly-H^+--MeOH cluster

broken, and no other attractive interaction compensates for it. The cluster gains so much internal energy that it dissociates.

Seeing that the rotational isomers are each separated by low energy barriers, a mechanism based on rotation about the intermolecular hydrogen bonds was attempted. The 1-dimensional potential energy surface for this mechanism is plotted in Fig. 3.7, and the structure of each local minimum and transition state is shown in Fig. 3.9. The energies in Fig. 3.7 follow the same calculation as those in the previous potential energy surface. The mechanism is initially identical to that shown in Fig. 3.6, where methanol freely rotates about the O-H-N hydrogen bond it forms with the glycine ammonium group. Instead of proton transfer from the ammonium group to methanol, there is hydrogen bond formation between the hydroxyl group proton and the methanol oxygen. The formation of this hydrogen bond stabilizes the cluster sufficiently to allow for the strong hydrogen bond at the ammonium group to weaken, as the bond length increases by approximately 0.2 Å with the secondary hydrogen bond in turn shortening by 0.2 Å as the cluster passes through the transition state TS04, in which hydrogen bond formation of the former compliments the hydrogen bond breaking of the latter. Although TS04 is 15.5 kcal mol^{-1} higher in energy than GM06, its energy is below the cluster dissociation threshold, meaning, given enough internal energy, the cluster can isomerize from GM06 to GM07 without dissociating. Once this major barrier is overcome, the cluster geometry again may pass through a series of rotamers. The most difficult rotation is that going from GM08 to GM05 through the transition state TS06, because this rotation is somewhat hindered by the methanol methyl group.

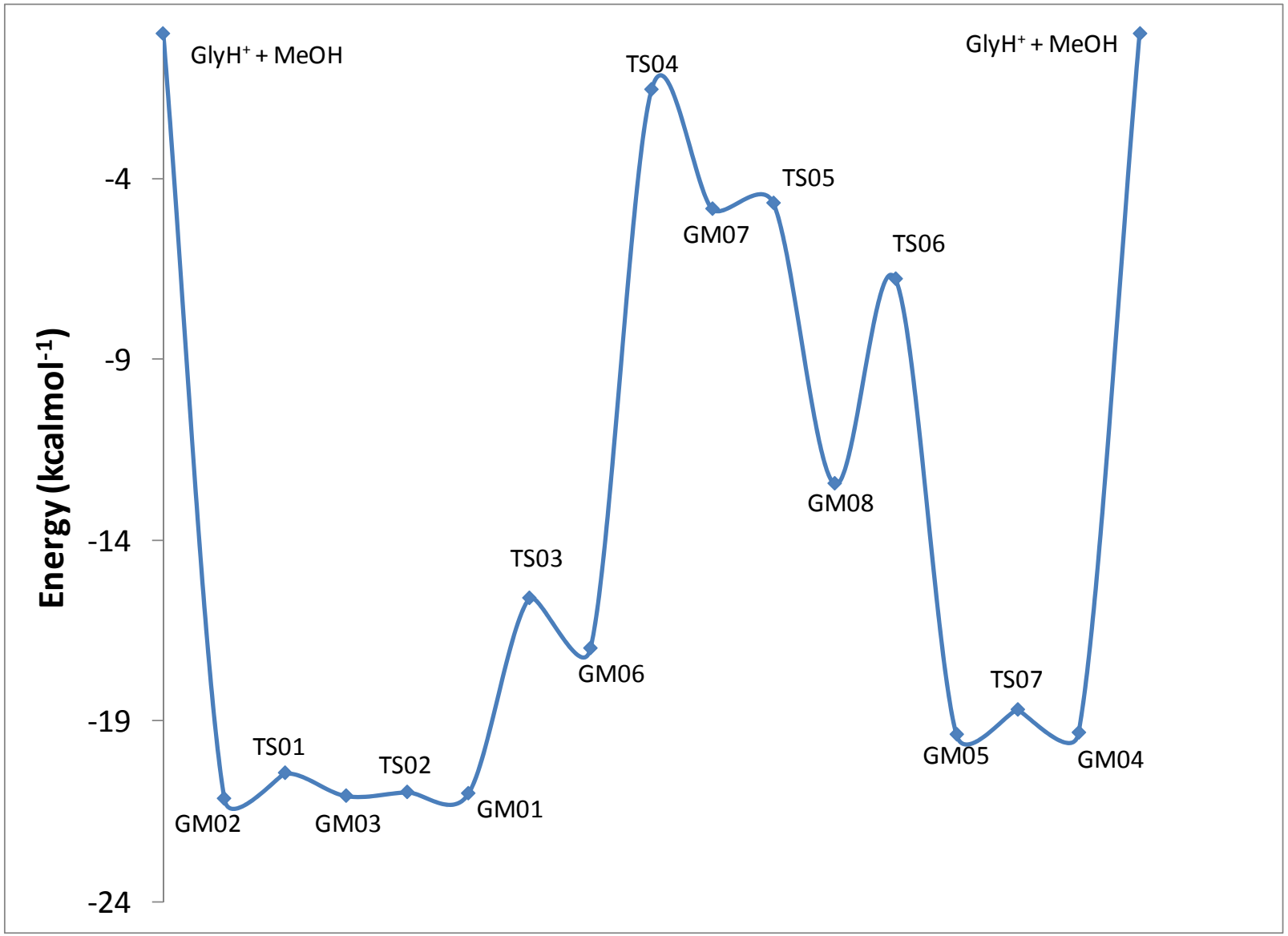

Fig. 3.7: The potential energy surface of the Gly(MeOH)H^+ conformers calculated at B3LYP/6-311+g(d,p) and 0 K.

The relative energies change somewhat when calculated at MP2(Full)/6-311++g(2d,2p), as shown in Fig. 3.8. The energies of the transition states generally decrease in energy, while those of the minima increase slightly. This effect arises mainly because the B3LYP functional ignores electron correlation, and thus is not suitable for calculating energies of weak interactions of generally greater than 2.15 Å separation. The energies of strongly bound species are underestimated, and those of weakly bound species are overestimated.

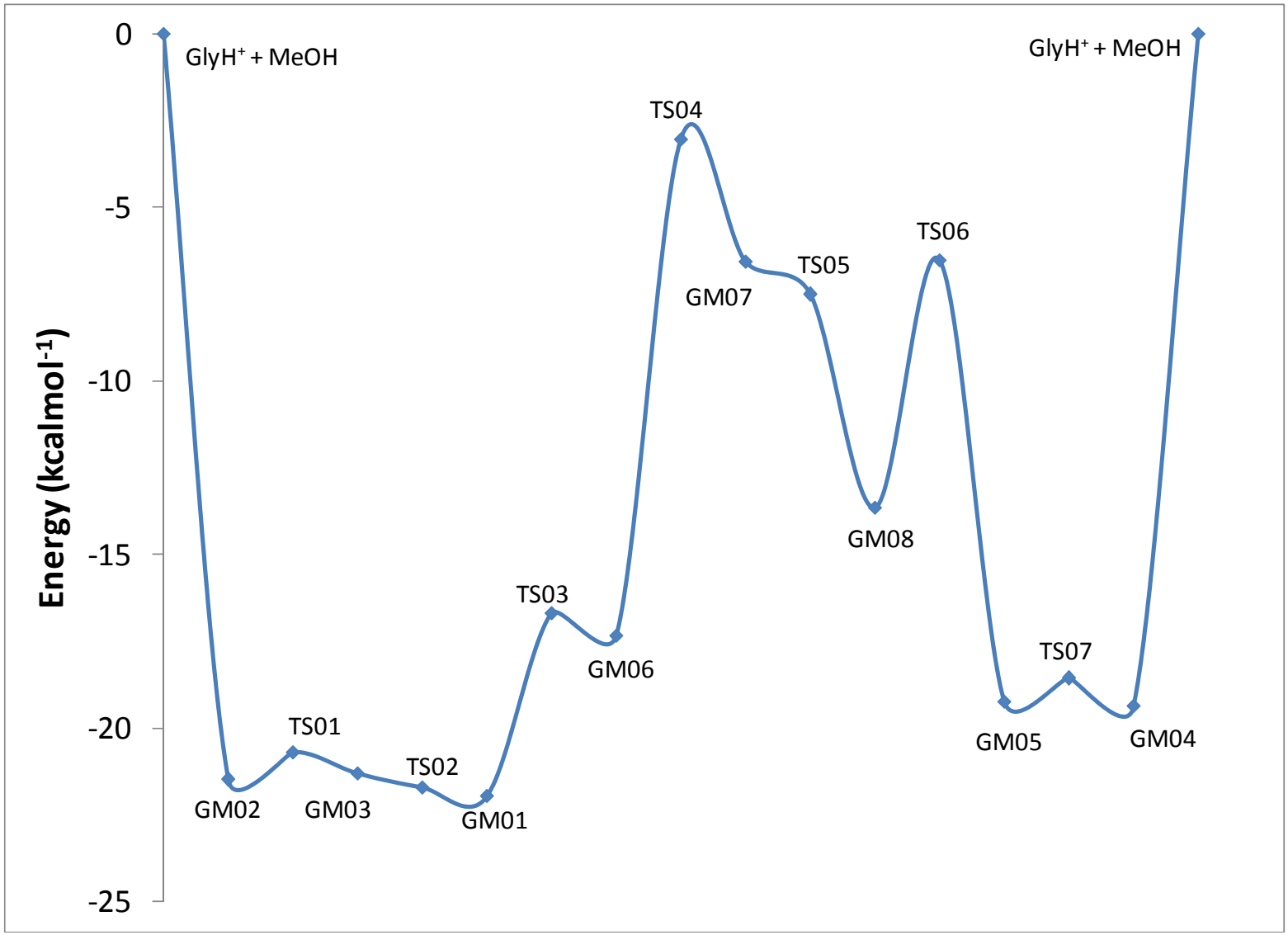

Fig. 3.8: The potential energy surface of the Gly(MeOH)H+ conformers calculated at MP2(Full)/6-311++g(2d,2p)//B3LYP/6-311+g(d,p) and 0 K.

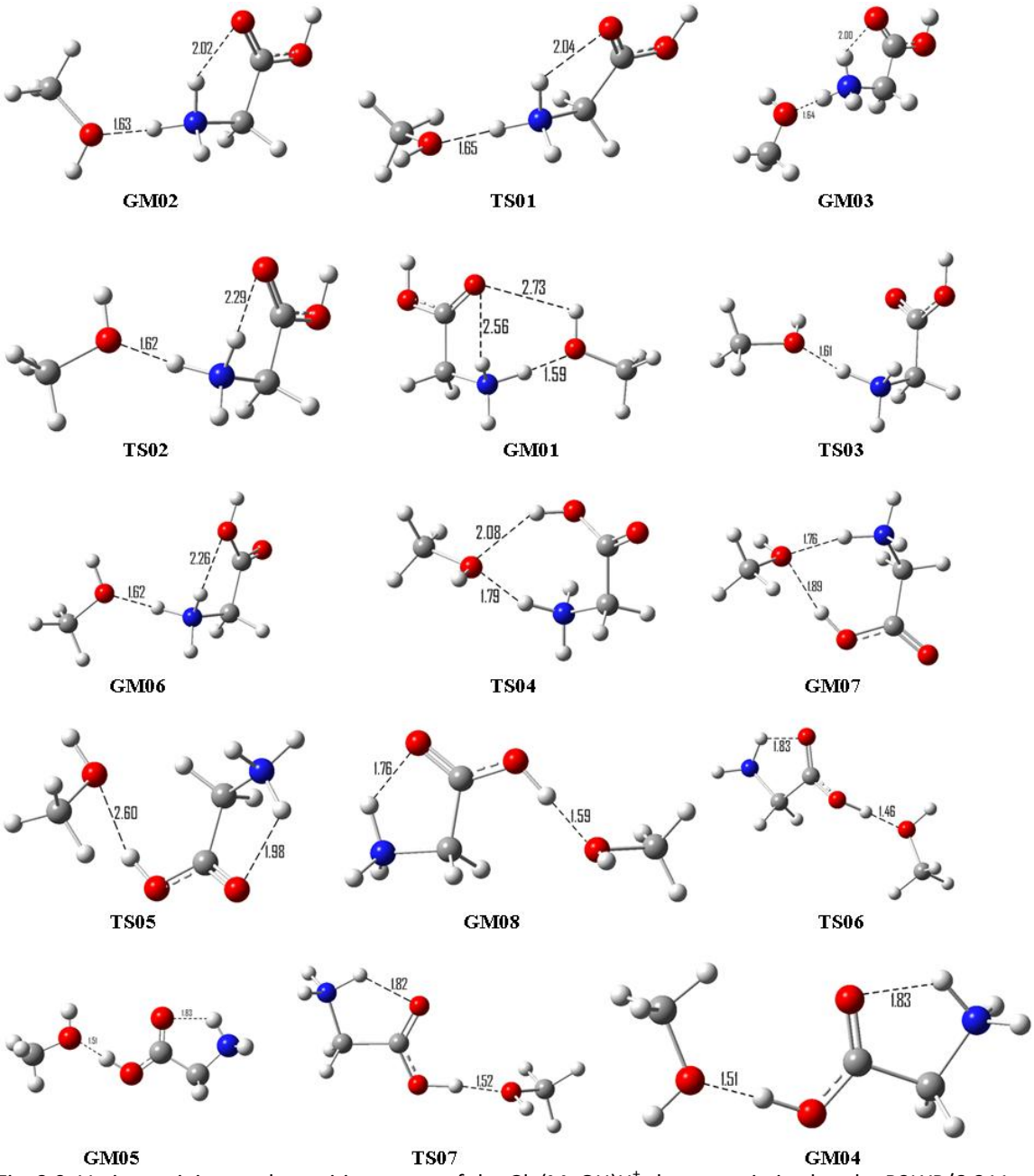

Fig. 3.9: Various minima and transition states of the Gly(MeOH)H^+ cluster optimized at the B3LYP/6-311+g(d,p) level.

Table 3.4: A summary of the energies of the stationary points presented in Fig. 3.7 and 3.8, calculated at the MP2(Full)/6-311++g(2d,2p)//B3LYP/6-311+g(d,p) level of theory.

	B3LYP (kcalmol^{-1})	MP2 (kcalmol^{-1})	ΔS (calmol^{-1}K^{-1})
GM02	-21.1	-21.5	-26.1
TS01	-20.4	-20.7	-33.7
GM03	-21.1	-21.3	-28.6
TS02	-20.9	-21.7	-35.7
GM01	-21.0	-22.0	-30.8
TS03	-15.6	-16.7	-35.7
GM06	-17.0	-17.3	-27.2
TS04	-1.5	-3.0	-35.1
GM07	-4.8	-6.6	-30.7
TS05	-4.7	-7.5	-33.9
GM08	-12.4	-13.7	-31.5
TS06	-6.8	-6.5	-35.3
GM05	-19.4	-19.2	-29.0
TS07	-18.7	-18.6	-35.2
GM04	-19.3	-19.4	-29.7

3.2.3.2 **The Structures and energies of the lowest energy conformers of the Gly-H$^+$--MeOH Cluster Ion**

The potential energy surface shown in Fig. 3.7 proves that the lowest energy conformers of the Gly-H$^+$--MeOH cluster are kinetically accessible. The structures and energies of the lowest energy conformers will now be summarized. Various conformers and several transition states of the Gly-H$^+$--MeOH cluster are shown in Fig. 3.9, and their computed energies are shown in Table 3.4. The relative abundance of each conformer is calculated as the probability of the formation of each cluster based on a free energy dependent Boltzmann distribution of those conformers. The lowest energy conformer, **GM01** in the reaction of protonated glycine with methanol involves coordination of the methanol molecule at the ammonium group of GlyH$^+$. At the MP2/6-311++g(2d,2p) level of theory at room temperature, the enthalpy of association to achieve this conformation is -20.6 kcal mol^{-1}. Here, methanol acts as an electron pair donor, stabilizing the positive charge on the GlyH$^+$

ammonium group, and forming a strong ionic hydrogen bond. At the same time, methanol acts as a hydrogen bond donor as it forms a weaker hydrogen bond with the oxygen atom on the glycine carboxyl group. Although this has an enthalpically stabilizing effect, it hinders the internal rotation of the cluster, and results in a relatively large decrease in entropy upon association, -30.8 cal mol^{-1} K^{-1}. The rotamers of **GM01**, in which rotation of the methanol molecule takes place about the intermolecular hydrogen bond are **GM02** and **GM03**, and are easily accessible, being within 1 kcal mol^{-1} of energy from **GM01**. In both of these conformers, methanol only forms one intermolecular ionic hydrogen bond with the ammonium group. As a consequence, the enthalpy of association is lower in both cases, but the decrease in entropy is also lower, both of which are attributed to the gain in rotational freedom in the cluster.

When methanol is coordinated to the carboxyl group, the binding energy of the cluster decreases by 2.2-2.3 kcal mol^{-1} as illustrated by **GM04** and **GM05**. Although the glycine carboxyl group is the most acidic site in its neutral form, here it is less acidic than the ammonium group, and is therefore a weaker hydrogen bond donor in comparison. In turn, this allows the ammonium group to form a stronger intramolecular ionic hydrogen bond with the carbonyl oxygen atom, which further stabilizes the cluster. The potential energy surface for the conformers of Gly-H^+--MeOH was calculated using the B3LYP as well as the MP2(Full) methods. They are presented here in Figs. 3.7 and 3.8 respectively with no thermal energy or vibrational corrections. It becomes evident from these diagrams that isomerization from the methanol molecule being coordinated to the ammonium group to coordination with the carboxyl group is kinetically inaccessible. Likely, what exists in practice is an exclusive mixture of ammonium coordinated conformers.

Table 3.5: A comparison of the ΔH^o for reaction 3.1 between B3LYP and MP2(Full) methods for the six lowest energy conformers. % abundance is calculated assuming a Boltzmann distribution of energies, all of which were calculated using the MP2(Full) method. Values include a vibrational correction, and thermal energy correction.

	B3LYP (kcalmol^{-1})	MP2 (kcalmol^{-1})	ΔS (calmol^{-1}K^{-1})	% abundance
GM01	-19.6	-20.6	-30.8	18.3
GM02	-19.8	-20.1	-26.1	27.5
GM03	-19.7	-19.9	-28.6	27.2
GM04	-18.3	-18.4	-29.7	11.8
GM05	-18.4	-18.3	-29.0	13.7
GM06	-15.6	-15.9	-27.2	1.5

3.2.3.3 **The Structures and energies of the lowest energy conformers of the Ala(MeOH)H$^+$ Cluster Ion**

Alanine, like all amino acids except glycine, has a side chain group on its β-carbon (central carbon) atom, and thus loses the level of symmetry that glycine possesses. The low-lying conformers of the Ala(MeOH)H$^+$ clusters in Fig. 3.10 are somewhat analogous to those of the Gly(MeOH)H$^+$ clusters, but the asymmetry in alanine due to its side chain methyl group seemingly doubles the number of possible conformers. The ΔH^o and ΔS^o for the formation reactions of the eight most stable conformers of Ala-H$^+$--MeOH are displayed in Table 3.6. The side chain methyl group increases the pK_a of alanine with respect to glycine, and therefore its conjugate acid is a weaker acid than GlyH$^+$. The conformers of AlaH$^+$ bound to methanol have relatively weaker binding energies than their Gly-H$^+$--MeOH analogues. Following the previous discussion, the clusters of Ala-H$^+$--MeOH need no detailed discussion. Again however, it is apparent that there are some discrepencies between the binding energies calculated at the B3LYP level and those at the MP2 level of theory which yield some surprising results. The most stable structure at the MP2 level (**AM01**) involves the formation of two hydrogen bonds between methanol and protonated alanine, analogous to **GM01**. This structure has an enthalpy of association of -20.1 kcal mol^{-1}. Here,

methanol binds to the same side of the ammonium group as the methyl group on alanine. The structure **AM03** is similar, but has methanol binding on the opposite side of the ammonium group, and has a net binding energy of 19.9 kcal mol^{-1}. The methyl group does not appear to play a hindering role towards methanol coordination on its side of the molecule. This could be the result of a weak polarization in the methanol methyl group, which leads to a favourable van der Waals interaction with the side chain methyl group of $AlaH^+$. However, Table 3.6 shows that the loss of entropy to form **AM01** is 2.8 cal mol^{-1} K^{-1} greater than the loss of entropy in **AM03**, which can be attributed in part to a loss of internal rotation of the two methyl groups, due to their proximity, as well as the increased intermolecular hydrogen bond strength in **AM01**. At the average experimental temperature, **AM03**,which is the entropically more favourable structure of the two, will be present in the highest abundance of all the conformers.

The same phenomenon is observed in the conformers, **AM02** and **AM04**. Both conformers include only one intermolecular hydrogen bond between the $AlaH^+$ ammonium group and the methanol methyl group, while the methanol hydroxyl group is oriented away from the $GlyH^+$ carboxyl group. The preference here is for the methanol molecule to bind on the same side of $AlaH^+$ as the methyl group, since **AM02** has a binding energy which is 0.4 kcal mol^{-1} higher than that of **AM04** at the MP2/6-311++g(2d,2p) level of theory. This selectivity may be explained based on the same arguments used above. However, a somewhat contradictory trend seen here is in the computed entropy change at the B3LYP/6-311+g(d,p) level of theory. **AM04** loses 2.8 cal mol^{-1} K^{-1} more entropy than **AM02** upon association. This is difficult to explain, but may be attributed to errors which arise from differences in the degree of electron correlation between the MP2 and hybrid DFT methods. **AM05** and **AM06** are analogous conformers to **AM04** and **AM02** respectively, where the methanol molecule simply rotates approximately 180^o about the hydrogen bond that is formed with the $AlaH^+$ ammonium group. Both conformers have a lower enthalpy of formation than

their **AM04** and **AM02** counterparts, by as much as 1.1 kcal mol^{-1}, as well as less negative entropies of formation. This is because **AM05** and **AM06** have slightly looser geometries than **AM04** and **AM02**, and hence have greater internal rotational and vibrational freedom, while at the same time the hydrogen bonds that bind the complexes together lengthen, and thus their binding energies weaken.

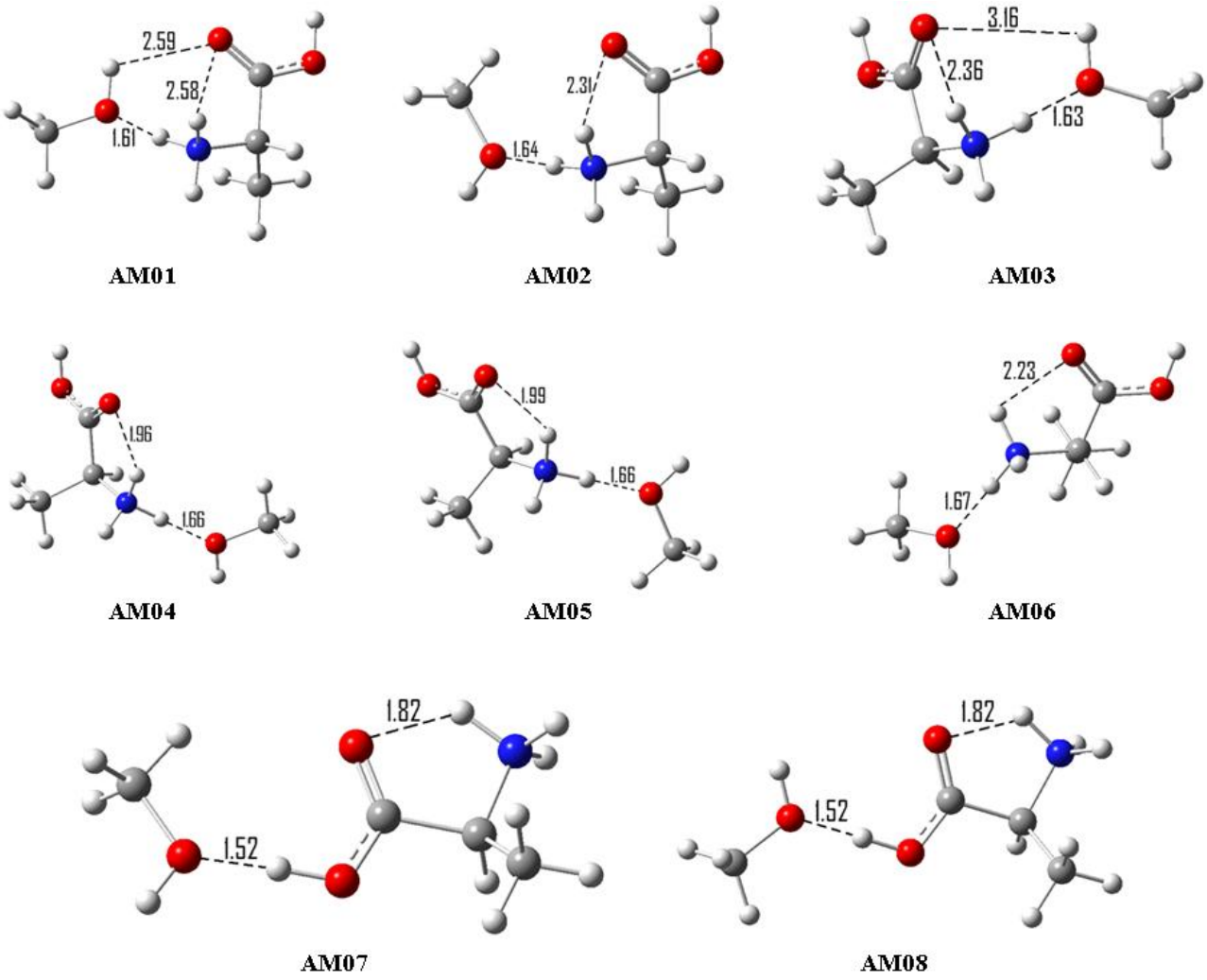

Fig. 3.10: The lowest energy conformers of the Ala(MeOH)H^+ cluster.

Table 3.6: A comparison of the ΔH^{o} for reaction 3.2 between B3LYP and MP2(Full) methods for the eight lowest energy conformers. % abundance is calculated assuming a Boltzmann distribution of energies, all of which were calculated using the MP2(Full) method.

	B3LYP (kcalmol^{-1})	MP2 (kcalmol^{-1})	ΔS (calmol^{-1}K^{-1})	%abundance
AM01	-18.4	-20.1	-32.2	10.5
AM02	-18.2	-20.0	-31.8	11.1
AM03	-18.6	-19.9	-29.4	32.7
AM04	-19.1	-19.6	-34.6	1.8
AM05	-18.4	-18.9	-29.2	11.4
AM06	-17.8	-18.9	-27.7	23.7
AM07	-17.7	-17.9	-30.3	2.0
AM08	-17.8	-17.7	-27.4	6.9

3.2.3.4 **The Structures and energies of the lowest energy conformers of the Val(MeOH)H^{+} Cluster Ion**

The most strongly bound computed adducts of protonated valine with methanol are illustrated in Fig. 3.11 and their enthalpies and entropies of association are listed in Table 3.7 at the B3LYP/6-311+g(d,p) and MP2/6-311++g(2d,2p) levels of theory. Due to the bulky valine isopropyl side chain, the free energies and thus the relative abundance of the various conformers become more dependant on the entropy of association. The most abundant conformers, **VM05** (33.3% abundance), and **VM04** (24.9% abundance) are not the most enthalpically stable conformers, but do respectively have the smallest ΔS^{o} of formation, being -27.4 cal mol^{-1} K^{-1} and -28.2 cal mol^{-1} K^{-1} respectively. The structures of these conformers show that the methanol forms a single strong ionic hydrogen bond with the ValH^{+} ammonium group and consequently, the entire molecule is able to rotate and vibrate freely about this hydrogen bond, with minimal hindrance from the isopropyl valine side chain.

VM01 and **VM02** are structurally very similar to **VM04** and **VM05**, differing by slight dihedral rotations of the ammonium group of protonated valine. Although these clusters are the most

strongly bound at 19.3 kcal mol^{-1}, their entropies of association are quite large relative to those of **VM04** and **VM05**, while their combined abundance is only 29.9% of a mixture of conformers at 420 K. **VM01** and **VM02** bind methanol slightly more strongly than **VM04** and **VM05**. The hydrogen bond lengths are roughly 1.62 Å versus 1.65 Å. Therefore, methanol stabilizes the ammonium group to a greater degree in **VM01** and **VM02**, translating to a weaker intramolecular hydrogen bond between the ammonium group and carboxyl group of $ValH^+$. The decreased intramolecular binding energy allows enough rotational freedom within the clusters that the decrease in entropy of both conformers is still comparable to the rest in the series.

The decrease in ΔG^o for formation of clusters such as **VM03** and **VM06** results from the position of methanol relative to the valine side chain. In both conformations, methanol is doubly coordinated to $ValH^+$, which minimizes the allowed internal energy of the cluster, and results in a relatively large entropy change upon cluster formation. Consequently, despite being strongly bound clusters, their free energy changes are limited by an unfavourable loss of entropy.

VM07 and **VM08** are two rotamers which have the methanol oxygen bound to the $ValH^+$ hydroxyl hydrogen atom. The carboxyl group acts as a weak hydrogen bond donor, yielding a slightly more weakly bound conformation than the conformers which were proton-bound at the ammonium group.

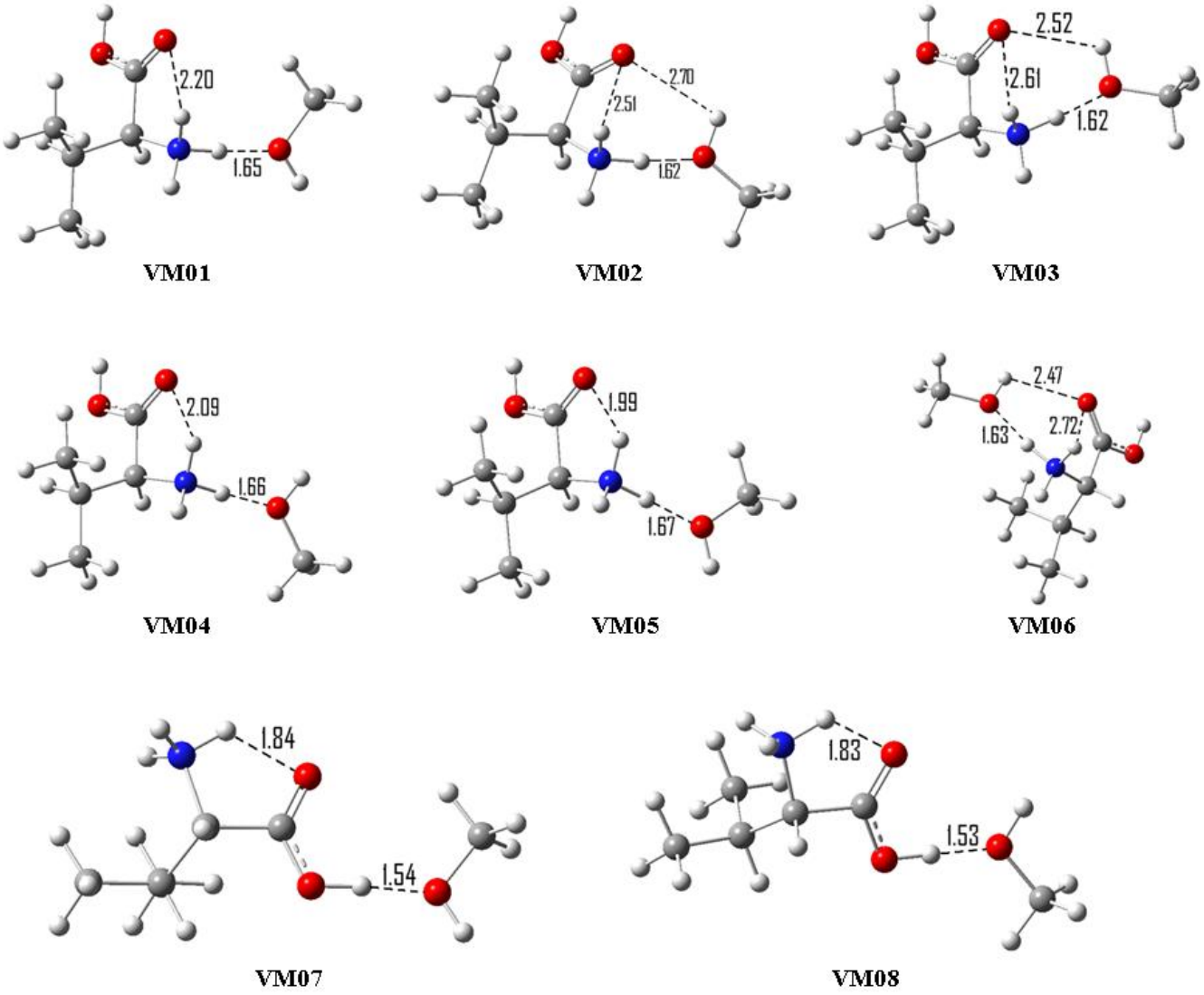

Fig. 3.11: The lowest energy conformers of the Val(MeOH)H^+ cluster.

Table 3.7: A comparison of the ΔH^o for reaction 3.3 between B3LYP and MP2(Full) methods for the eight lowest energy conformers. % abundance is calculated assuming a Boltzmann distribution of energies, all of which were calculated using the MP2(Full) method.

	B3LYP (kcalmol^{-1})	MP2 (kcalmol^{-1})	ΔS (calmol^{-1}K^{-1})	%abundance
VM01	-17.7	-19.3	-30.2	18.7
VM02	-17.7	-19.3	-31.1	11.2
VM03	-16.4	-19.1	-32.3	5.1
VM04	-17.6	-18.7	-28.2	24.9
VM05	-17.6	-18.6	-27.4	33.3
VM06	-16.6	-18.5	-31.9	3.2
VM07	-17.1	-17.4	-30.5	1.8
VM08	-17.1	-17.3	-30.1	1.8

3.2.3.5 **The Structures and energies of the lowest energy conformers of the Leu(MeOH)H+ and Ile(MeOH)H^+ Cluster Ions**

The structures of the Leu(MeOH)H^+ and Ile(MeOH)H^+ conformers are shown in Figs. 3.12 and 3.13 respectively. Their energies are reported in Tables 3.8 and 3.9 respectively. Both the Leu(MeOH)H^+ and Ile-H^+--MeOH series of conformers have markedly similar structures, while calculations of their enthalpy and entropy of association again show that the most preferable free energy conformers at 420 K are the entropically favourable structures, **LM01** and **IM02** respectively. Their structures are similar in that they include only one intermolecular ionic hydrogen bond between the methanol oxygen and the ammonium group. We observe a looser structure in these cases, as methanol binds on the opposite side of the molecule from the bulky tert- and iso-butyl groups of side chains of the amino acids in order to maintain a high degree of internal rotation. Although **LM01** and **IM01** are the most strongly bound clusters in each series, and are structurally the same, **IM01** is entropically less favourable than **LM01**, suggesting that the side chain plays a more rotationally hindering role with respect to the ammonium group in IleH^+ than in LeuH^+.

When compared to the lowest energy conformers in the previously discussed clusters (**GM01**, **AM01**, **VM01** and **VM02**), **LM01** and **IM01** have methanol binding in a looser geometry. At this point, side chain size begins to play an important factor in binding energy, as both side chains appear to decrease the nucleophilicity of the amino acid carbonyl oxygen atom. The cluster becomes more stable if methanol only forms a hydrogen bond to the ammonium group, leaving the carbonyl group isolated.

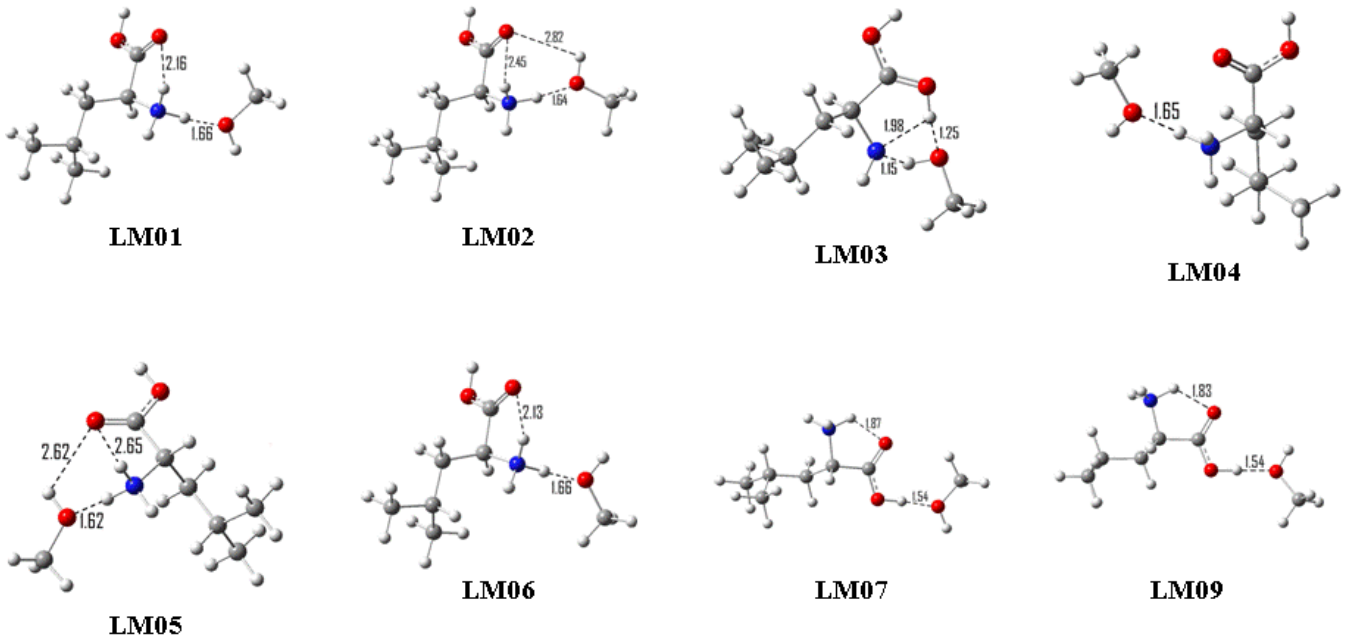

Fig. 3.12: The lowest energy conformers of the Leu(MeOH)H^+ cluster.

Table 3.8: A comparison of the ΔH^o for reaction 3.4 between B3LYP and MP2(Full) methods for the eight lowest energy conformers. % abundance is calculated assuming a Boltzmann distribution of energies, all of which were calculated using the MP2(Full) method.

	B3LYP ($kcalmol^{-1}$)	MP2 ($kcalmol^{-1}$)	ΔS ($calmol^{-1}K^{-1}$)	% abundance
LM01	-17.8	-19.2	-27.5	49.7
LM02	-17.6	-19.2	-29.6	17.5
LM03	-17.2	-19.1	-32.9	3.0
LM04	-17.0	-19.1	-31.4	6.5
LM05	-17.2	-19.0	-33.0	2.7
LM06	-17.7	-18.7	-28.6	16.9
LM07	-16.9	-17.1	-30.3	1.0
LM08	-17.0	-17.0	-28.1	2.8

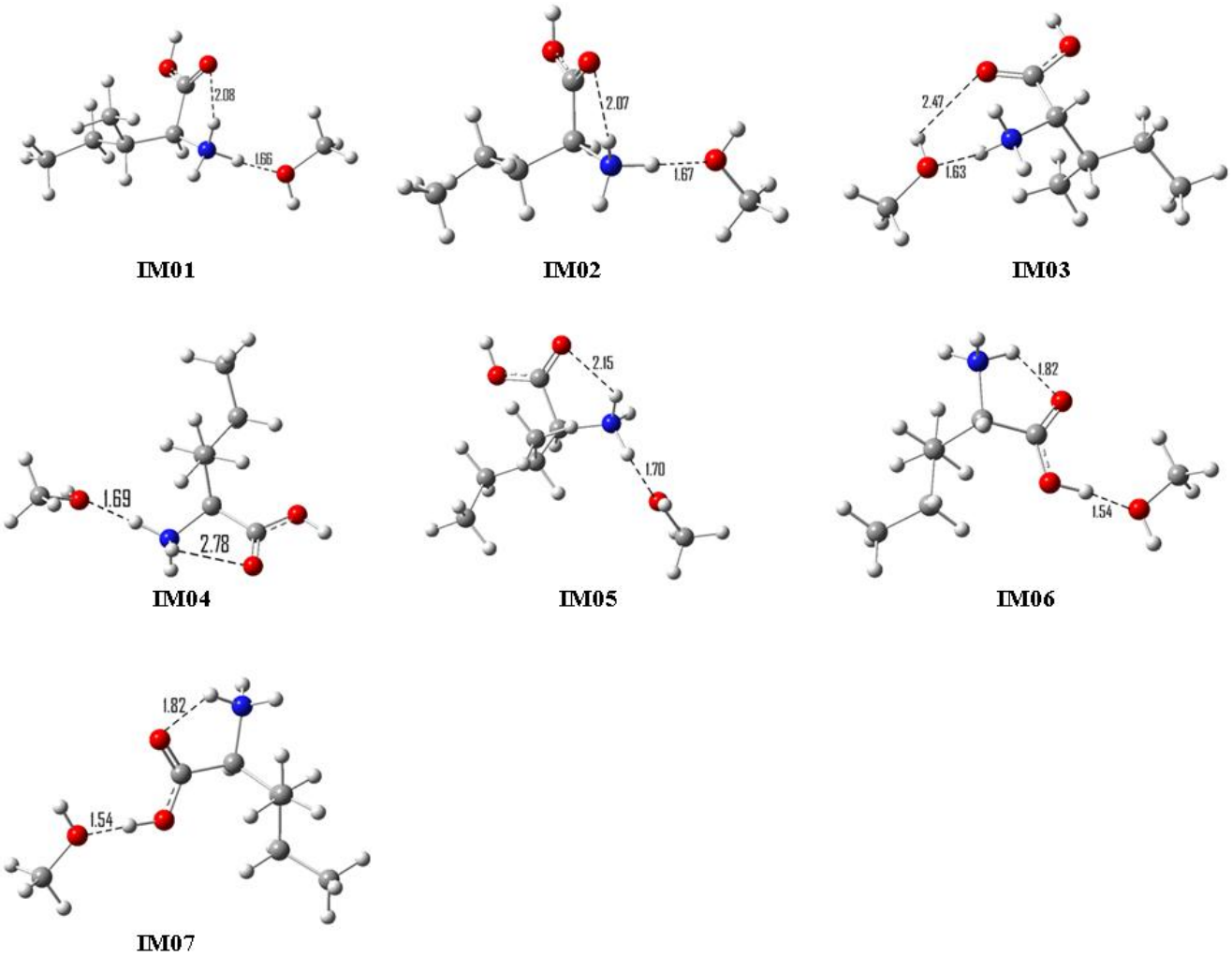

Fig. 3.13: The lowest energy conformers of the Ile(MeOH)H^+ cluster.

Table 3.9: A comparison of the ΔH^o for reaction 3.5 between B3LYP and MP2(Full) methods for the seven lowest energy conformers. % abundance is calculated assuming a Boltzmann distribution of energies, all of which were calculated using the MP2(Full) method.

	B3LYP (kcalmol^{-1})	MP2 (kcalmol^{-1})	ΔS (calmol^{-1}K^{-1})	% abundance
IM01	-17.8	-19.0	-29.1	26.1
IM02	-17.7	-18.7	-27.9	33.2
IM03	-16.6	-18.4	-32.5	2.4
IM04	-17.0	-18.0	-27.4	19.1
IM05	-16.5	-18.0	-29.4	6.8
IM06	-16.9	-17.3	-30.4	1.8
IM07	-16.5	-17.2	-26.6	10.6

3.2.3.6 **Conformations of Neutral and Protonated Proline, and of the Proton-Bound Cluster Pro(MeOH)H^+**

The low-lying conformations of neutral proline have been calculated and discussed by other authors.[37,38] Lee et al. calculated four low energy conformers at the B3LYP/6-311++G** level of theory, and each conformer can be distinguished from the others based on two criteria: ring conformation, and carboxyl group orientation. These conformers are presented in Fig. 3.14, and their relative energies calculated at the MP2/6-311++g(2d,2p)//B3LYP/6-311+g(d,p) level of theory are listed in Table 3.10. The structural optimization yielded virtually the same geometries and hydrogen bond lengths for each conformer, but the relative enthalpies differ in the third and fourth lowest lying conformers. The diffuse functions employed by Lee et al. on their hydrogen atoms in their geometry optimization appear to treat interactions greater than 2.25 Å more appropriately. This is a surprising result, since the second diffuse function traditionally has only an influence for anions and hydrides.[39]

The protonated version of proline is predicted to follow a slightly different structural trend. The extra proton binds directly to the amine nitrogen atom of the pyrrolidine ring, occupying the lone pair of electrons which were previously donated in the formation of an intramolecular ionic hydrogen bond with the hydroxyl group (**P01**). This forces a conformation change, as the secondary ammonium group must stabilize itself through the donation of an ionic hydrogen bond to the carbonyl group (**PH01**). It can be predicted that this added internal stability will translate into a slightly weaker intermolecular hydrogen bond with methanol, relative to that in which the internal interaction is not present.

For clusters of Pro-H^+--MeOH, as shown in Fig. 3.15, the proline pyrrolidine ring may carry ring strain, and the cluster is expected to adopt a conformation which favours a lower entropy over a strong binding energy, hence the inclusion of proline in this study. In fact, the lowest energy

conformer is not analogous to those seen for the other amino acid adducts, such as **GMO1**, because the secondary amino group may not freely rotate, as is the case for the primary amino acids. **PM07**, the analogous conformer to **GM01**, suffers a great loss in entropy, leading to an insignificant abundance at 420 K of 0.2% of the eight most strongly bound conformers. Out of these, the most enthalpically favourable conformer, **PM01**, involves methanol coordinated at the secondary ammonium group, and is further stabilized by an additional intramolecular hydrogen bond between the second ammonium hydrogen atom and the carbonyl oxygen. Rotation of the methanol molecule to produce **PM02** costs 0.2 kcal mol^{-1}. Rotation of the proline carboxyl group by 180^{o} to allow the ammonium group to bind to the hydroxyl oxygen is less favourable than **PM01** by 3.2 kcal mol^{-1}, and is not shown in Fig. 3.15. When methanol is bound to the carboxyl group (**PM06** and **PM07**) the binding energy of the complex drops by 1.2 kcal mol^{-1}, a loss which is comparable with the analogous configurations of the previous amino acid adducts.

Comparison of **PM01** and **PM04** indicates that methanol coordination to the ammonium group appears to neither stabilize nor destabilize the S-conformation of the pyrrolidine ring relative to the U-conformation. The energy difference between the two ring conformations before and after complexation with methanol remains as 0.4 kcal mol^{-1} as shown in Tables 3.11 and 3.12. This indicates that at this binding site, methanol does not interfere with the stabilizing intramolecular hydrogen bond between the carbonyl group and the secondary ammonium group. Conversely, the U-conformation is only slightly destabilized upon coordination of methanol to the carbonyl group (**PM03** and **PM05**), as methanol does not withdraw electron density from the carboxyl group, and hence does not affect the intramolecular hydrogen bond which stabilizes the U-conformation.

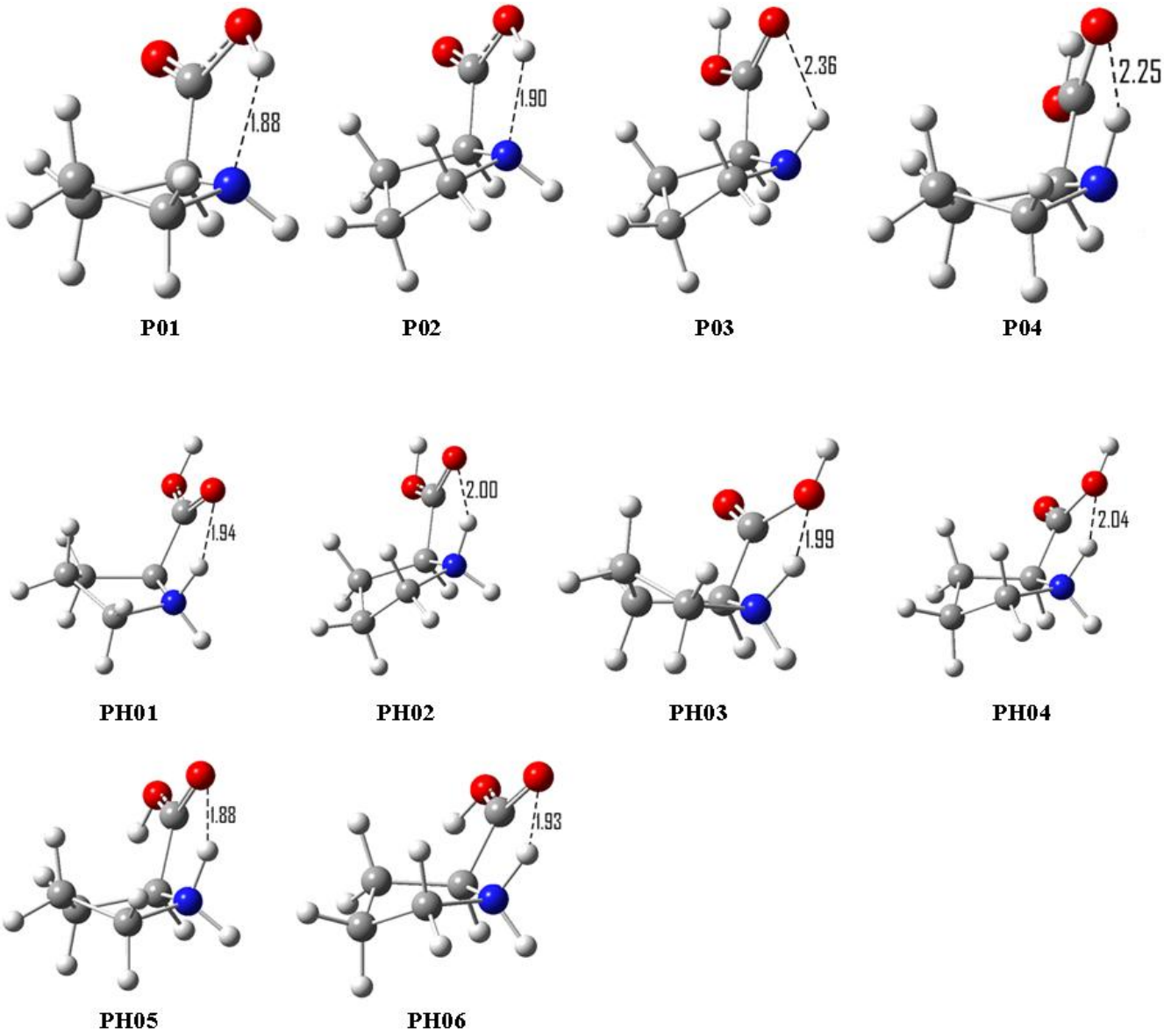

Fig. 3.14: Four conformations of neutral proline, and 6 conformations of protonated proline, all optimized at the B3LYP/6-311+g(d,p) level of theory.

Table 3.10: Calculated relative energies of four conformations of neutral proline

	B3LYP ($kcalmol^{-1}$)	MP2 ($kcalmol^{-1}$)
P01	0	0
P02	0.5	0.8
P03	1.7	1.8
P04	1.9	1.9

Table 3.11: Calculated relative energies of six conformations of protonated proline

	B3LYP (kcalmol^{-1})	MP2 (kcalmol^{-1})
PH01	0	0
PH02	0.3	0.7
PH03	4.6	5.1
PH04	4.6	5.5
PH05	8.2	7.5
PH06	8.5	8.3

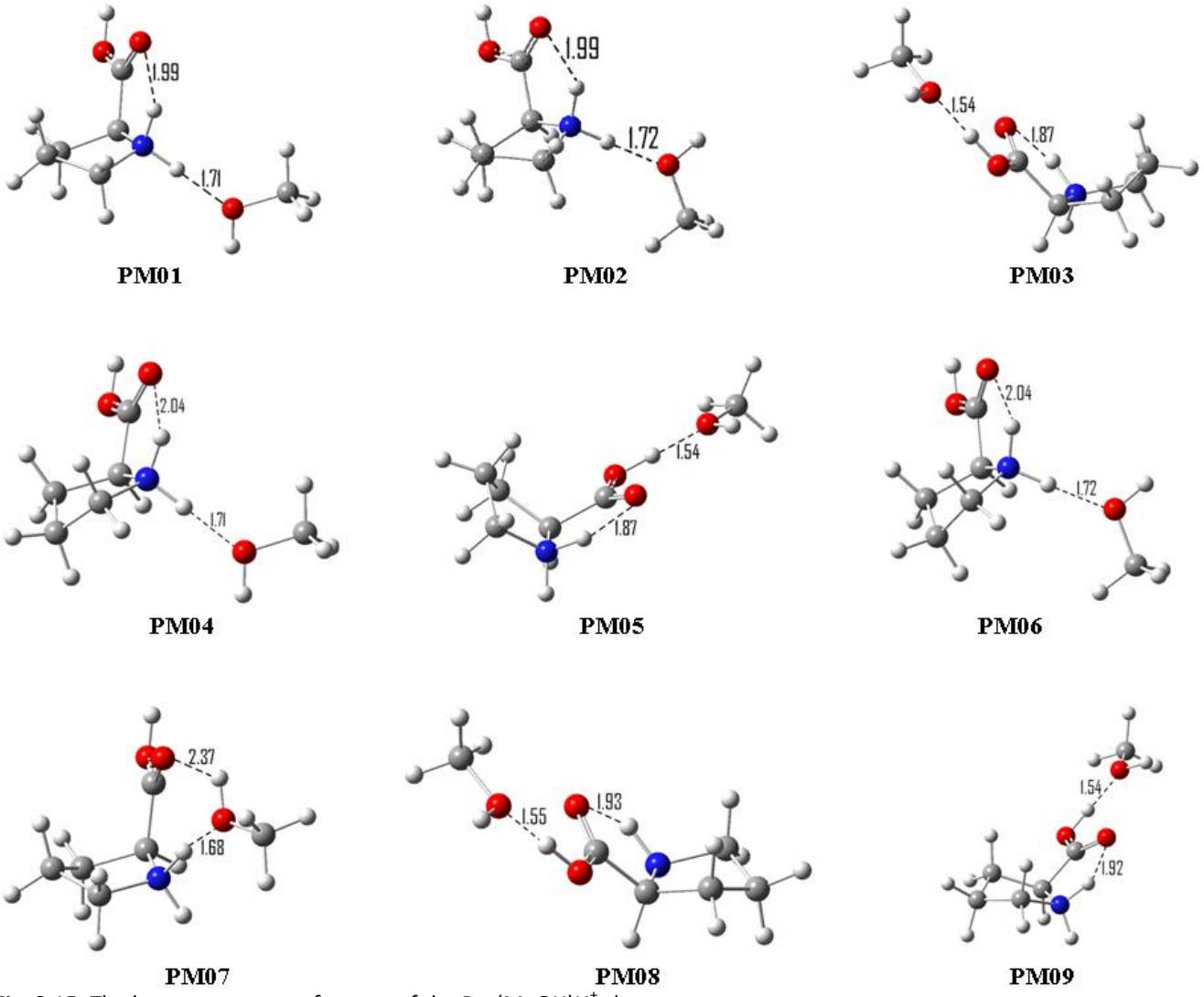

Fig. 3.15: The lowest energy conformers of the Pro(MeOH)H$^+$ cluster.

Table 3.12: A comparison of the ΔH^{o} for reaction 3.6between B3LYP and MP2(Full) methods for the nine lowest energy conformers. % abundance is calculated assuming a Boltzmann distribution of energies, all of which were calculated using the MP2(Full) method.

	B3LYP (kcalmol^{-1})	MP2 (kcalmol^{-1})	ΔS^{o} (calmol^{-1}K^{-1})	% abundance (400K)
PM01	-16.3	-17.5	-26.1	45.4
PM02	-16.2	-17.3	-28.4	11.7
PM03	-16.7	-17.2	-30.6	3.3
PM04	-16.2	-17.1	-27.6	13.0
PM05	-16.7	-17.0	-28.8	6.6
PM06	-16.0	-17.0	-27.0	15.5
PM07	-14.6	-16.4	-34.6	0.2
PM08	-16.3	-16.3	-29.4	2.0
PM09	-16.3	-16.1	-28.6	2.3

3.3 Addition of a Second Methanol Molecule to the Proton-Bound Cluster of Glycine and Methanol

One conclusion drawn from the study of the proton-bound cluster of glycine with methanol was that one methanol molecule is not sufficient to stabilize the zwitterion of glycine, rationalized because methanol is not a strong enough base for proton transfer from the glycine carboxyl group to the methanol oxygen atom to be a favourable process. However, if a second methanol molecule is introduced to the cluster, then it should perturb the interaction between the first methanol molecule and protonated glycine as described statistically by Zernike and Ornstein. This means that the second methanol molecule should weaken the bond between glycine and the proton bound to it, facilitating proton transfer to the first methanol molecule. Gas phase studies on the structure and energies of neutral and protonated glycine and alanine with multiple water molecules has also been undertaken.[11,12,14,16,18,19] An early Monte Carlo simulation of large hydrated clusters, $Gly(H_2O)_{18}$, revealed that the glycine zwitterion is trapped in the central cavity of the clathrate structure of water, in which the water molecules are hydrogen bonded in a hexagonal pattern.[11] This differs from the pentagonal clathrate structure observed by Holland and Castleman.[40]

With knowledge regarding the structure and energetics of the complexation of the first methanol molecule to protonated glycine, the reaction of interest at this junction is depicted in Eq. 3.8 below,

$$Gly\text{-}H^{+}\text{--}MeOH + MeOH \leftrightarrows Gly\text{-}H^{+}\text{--}(MeOH)_2 \qquad (3.8)$$

Studying this reaction in the gas phase poses several problems. HPMS can be a useful tool for studying the stepwise addition of relatively small solvent molecules such as ammonia or water to small ions such as Na^{+} or Mg^{2+}. These cluster ions are often very stable, with minimal loss in entropy. However, if the ion of interest is a molecular ion such as $GlyH^{+}$, the initial entropy loss for the addition of a small number of solvent molecules is normally large because the ion and solvent molecules lose several additional degrees of freedom. In an experiment, this results in a low abundance of higher order clusters, where even an order of two or three may be too high to give an appreciable abundance. To minimize the entropic contribution to the free energy of the second order cluster, the temperature range for the experiments should be and was maintained at lower temperatures, while simultaneously balancing a sufficient glycine vapour pressure. Another limitation arises because the partial pressure of glycine is controlled only by the temperature of the ion source and, since glycine has a low volatility, at any time we should expect a low pressure of glycine, giving low abundances of any species that contains glycine. To make matters more difficult, at the lower limit of temperatures used in the experiment, the cluster of protonated glycine with a neutral glycine molecule as depicted in Eq. 3.9, will be the most abundant adduct of glycine.

$$GlyH^{+} + Gly \leftrightarrows Gly\text{-}H^{+}\text{-}Gly \qquad (3.9)$$

The other parameter besides temperature that can be controlled in such an experiment to affect the cluster ion abundance is the quantity or partial pressure of the neutral (methanol) introduced into the ion source. This can be controlled by increasing the gas mixture flow rate,

however at the same time an increase in total pressure inside the source could tend to lead to a greater amount of collisional dissociation of the desired cluster ions just outside the ion source. Alternatively, the fraction of methanol in the reactant gas can be increased, so that the partial pressure of methanol in the ion source for a particular experiment would be in the range of 0.5 to 1.5 Torr. This would be an acceptable compromise because the methane bath gas still remains largely in excess. For pressures of methanol in this range, a relatively substantial number of methanol molecules will be protonated, even in the presence of glycine, even though it has a higher proton affinity. It is known that the dominant speciation of methanol in the gas phase in a chemical ionization process will be dependent upon the pressure and temperature in the ion source.[41] Past work which focused on the gas phase reactions of protonated methanol with neutral methanol in a CI experiment has confirmed the existence of two major products, $C_2H_7O^+$ and $C_2H_9O_2^+$.[42-45] The former has been confirmed through ^{18}O labelling of protonated methanol as the product of nucleophilic backside attack of neutral methanol on protonated methanol.[44,45] The electron rich oxygen atom on a neutral methanol molecule is free to attack the carbon atom of a protonated methanol ion through a second order nucleophilic substitution, expelling water and producing protonated dimethyl ether at m/z 47, as shown in Fig. 3.16.[43]

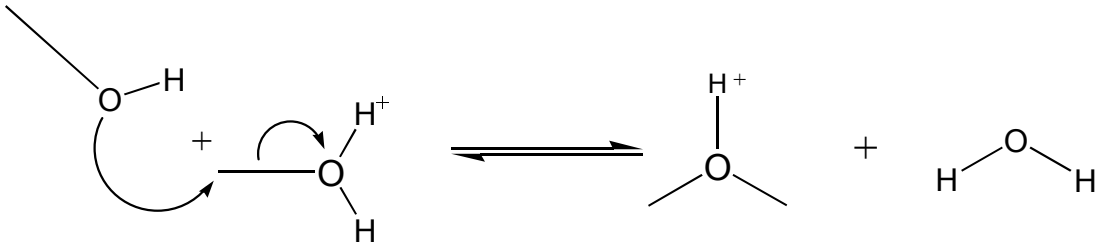

Fig. 3.16: Nucleophilic backside attack of inverted methanol on protonated methanol to produce protonated dimethyl ether.

The latter product results from the association reaction involving the formation of an ionic hydrogen bond between the protonated methanol ion and the neutral methanol oxygen atom. This

reaction is illustrated with molecular geometries optimized at the B3LYP/6-311+g(d,p) level in Fig. 3.17.

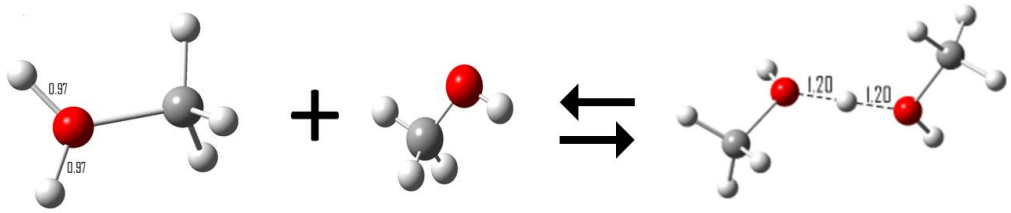

Fig. 3.17: Association reaction of the proton-bound cluster between two methanol molecules.

Of the two reactions, the former dominates at low pressure, while the latter prevails at high pressures above 1 Torr. The dehydration product is only observed at these high pressures at high temperatures.[46] Above 1 Torr, the formation of the proton-bound complex is favourable because it is collisionally stabilized, and highly exothermic, releasing over 35 kcal mol^{-1} of energy. Measurements of rate constants for both processes also support that the proton-bound cluster is almost exclusively produced if methanol is in its ground internal state,[47-51] although there are still conflicting results.[52] The conditions at which the experiment is performed therefore favour the latter product. Proton transfer is another important reaction in the chemical ionization of methanol,[53] but it should not affect the results of this work, because it occurs on such a fast time scale, that it is not observable in our experiments.

3.3.1 **Experimental and Computational Results for the Addition of the Second Methanol Molecule to the Proton-Bound Cluster of Glycine and Methanol**

The experimental and computational results of this work will be presented. However, a discussion of this subject at this point would be highly speculative. Therefore, the discussion will be omitted. The van't Hoff plot for the reaction given in Eq. 3.8 is displayed in Fig. 3.18.

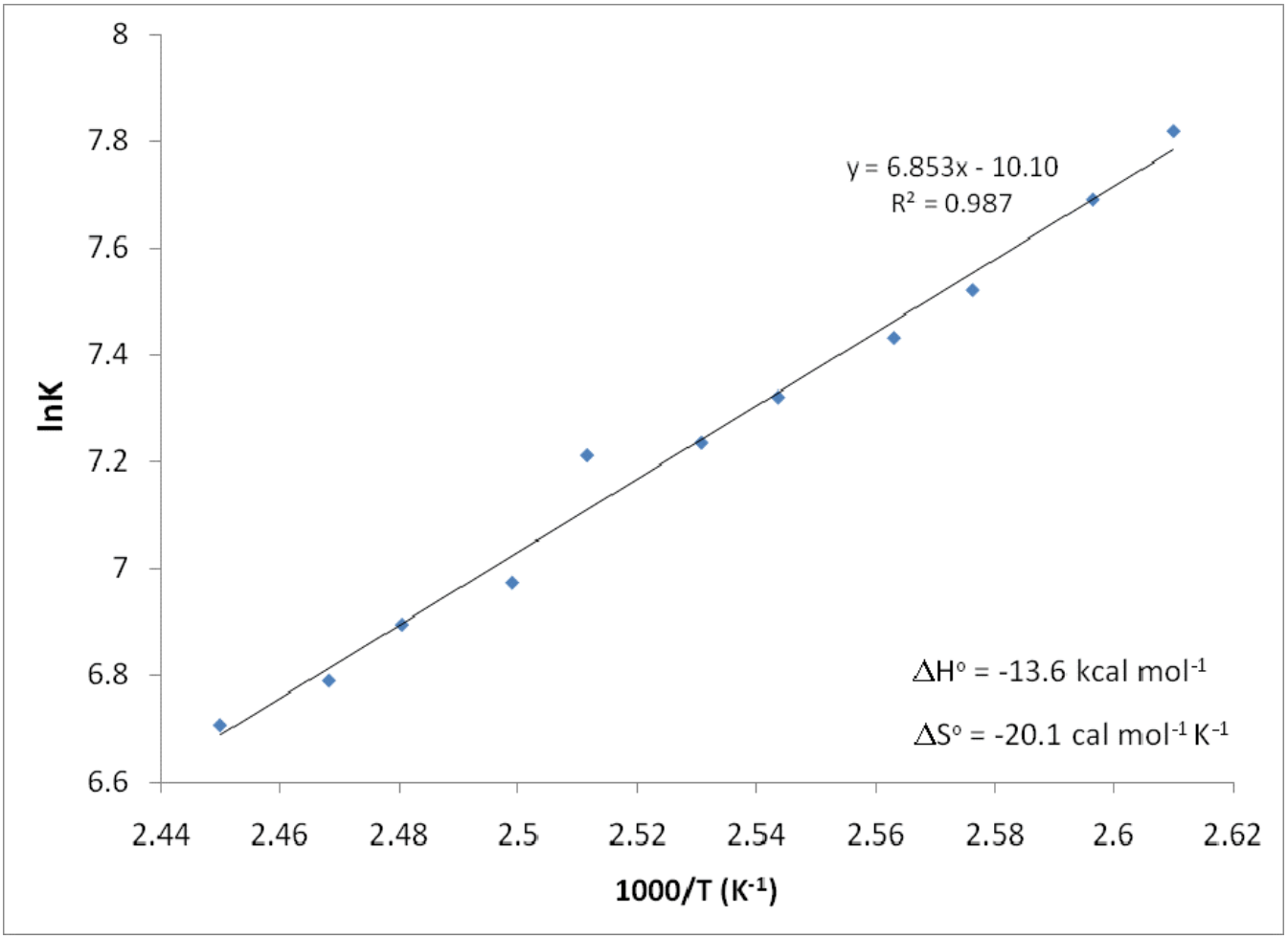

Fig. 3.18: van't Hoff plot for the reaction given in Eq. 4.1 recorded between the temperatures of 380 to 410 K.

The enthalpy change of the reaction is -13.6 kcal mol^{-1}, while the entropy change is -20.1 cal mol^{-1} K^{-1}. The second methanol therefore is bound approximately 7 kcal mol^{-1} less strongly to protonated glycine than the first. To produce thermochemical data describing the sequential addition of two methanol molecules to protonated glycine the results obtained here can be added to the previous results collected for the addition of the first methanol molecule to protonated

glycine, to give respective enthalpy and entropy changes for the overall reaction of -35.6 kcal mol^{-1} and -53.6 cal mol^{-1} K^{-1}

The second methanol molecule clearly does not bind as strongly as the first. However, at the same time, the loss of entropy is not as great upon the addition of the second methanol molecule, because the cluster continues to only lose 3 degrees of translational freedom, but gains more internal degrees of freedom. This tendency for the loss of entropy to approach zero as order or size of the cluster increases is well understood.[54]

The optimized structures of various conformers of the Gly-H^+--$(MeOH)_2$ cluster calculated at the B3LYP/6-311+g(d,p) level of theory are shown in Fig. 3.19, and their respective energies are given in Table 3.13.

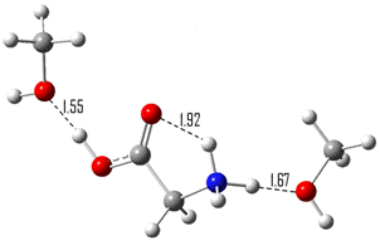

GMM01

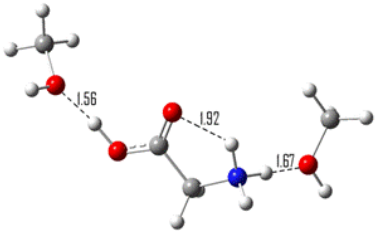

TS01

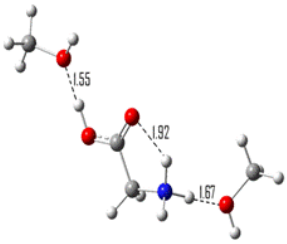

GMM02

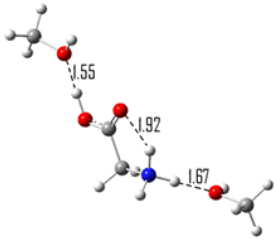

TS02

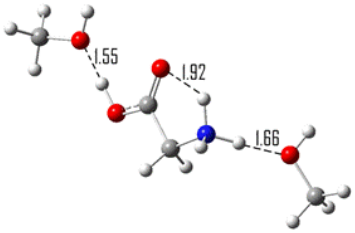

GMM03

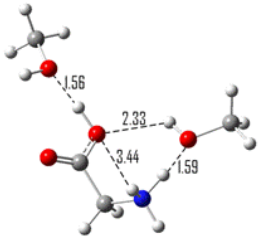

TS03

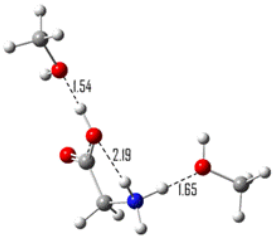

GMM04

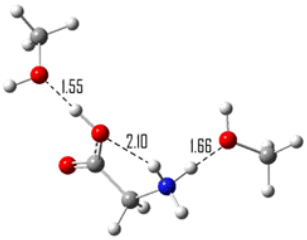

TS04

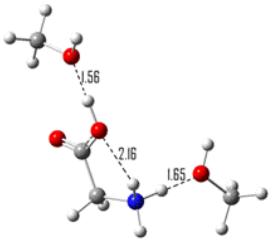

GMM05

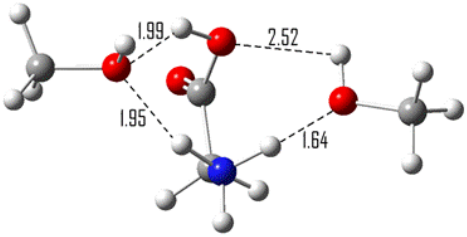

TS05

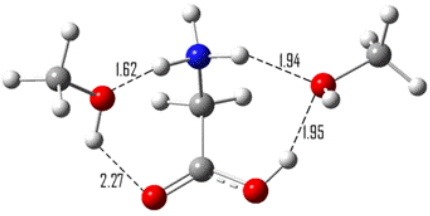

GMM06

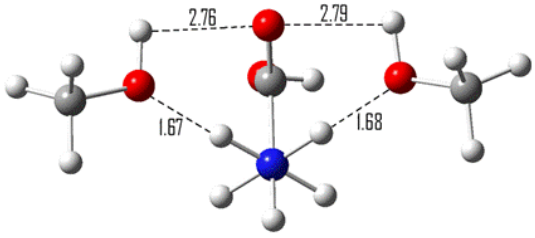

TS06

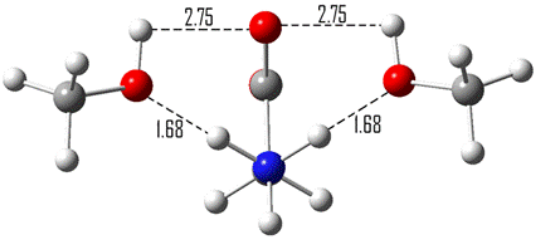

GMM07

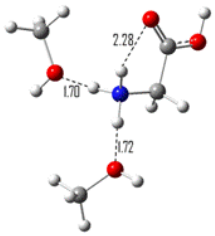

TS07

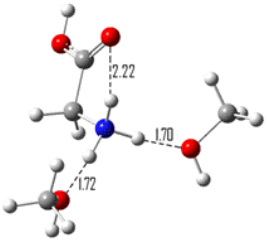

GMM08

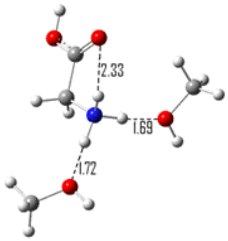

TS08

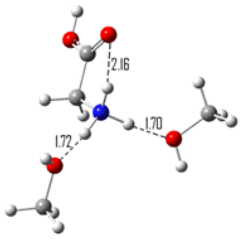

GMM09

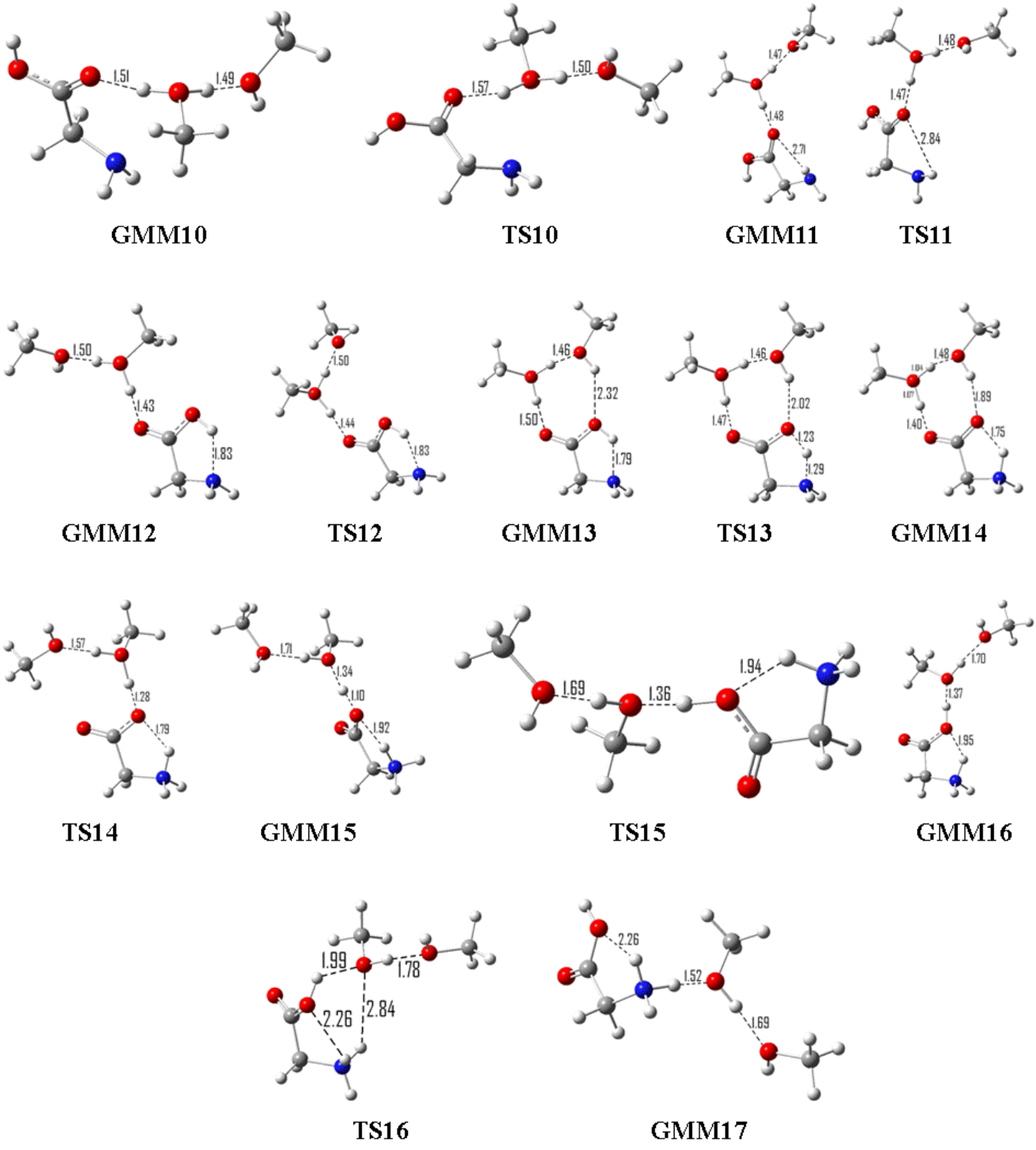

Fig. 3.19: Structures of various conformers of Gly-H^+--$(MeOH)_2$ optimized at the B3LYP/6-311+g(d,p) level of theory.

Table 3.13: Summary of enthalpies and entropies of association of all stationary points fitting in Fig. 3.19 calculated at the MP2(Full)/6-311++g(2d,2p)//B3LYP/6-311+g(d,p) level including zero-point and thermal energy corrections.

	ΔH (kcalmol^{-1})	ΔS (calmol^{-1}K^{-1})		ΔH (kcalmol^{-1})	ΔS (calmol^{-1}K^{-1})
GMM01	-36.5	-58.3	**GMM10**	-25.8	-59.7
TS01	-36.0	-59.8	**TS10**	-14.6	-61.4
GMM02	-36.3	-57.9	**GMM11**	-21.3	-57.8
TS02	-36.4	-62.6	**TS11**	-20.6	-62.1
GMM03	-36.2	-57.3	**GMM12**	-31.7	-62.2
TS03	-30.9	-67.2	**TS12**	-31.6	-67.8
GMM04	-32.9	-57.9	**GMM13**	-31.7	-66.4
TS04	-32.3	-63.7	**TS13**	-31.6	-71.8
GMM05	-32.8	-58.8	**GMM14**	-32.8	-70.6
TS05	-22.1	-66.2	**TS14**	-26.8	-64.8
GMM06	-25.9	-65.8	**GMM15**	-28.7	-63.6
TS06	-25.8	-62.1	**TS15**	-27.2	-65.9
GMM07	-38.0	-61.3	**GMM16**	-26.5	-58.9
TS07	-37.5	-63.3	**TS16**	-17.0	-63.8
GMM08	-37.0	-56.8	**GMM17**	-30.3	-59.5
TS08	-37.5	-64.4			
GMM09	-36.8	-54.5			

3.4 Conclusions

The results here confirm that one or two methanol molecules can not stabilize the zwitterion of the 5 protonated aliphatic amino acids. *ab initio* calculations illustrate that the first methanol molecule prefers binding to the ammonium group over the carboxyl group by roughly 2 kcal mol^{-1}, and hence will not remove a proton from the amino acid carboxyl group. HPMS experiments confirmed these calculations, showing that the first methanol molecule is either singly coordinated to the ammonium group, or doubly coordinated, acting as an electron donor to the ammonium group, and as a proton donor to the amino acid carbonyl group. The agreement between the experimental results and the calculated results suggest that the internal energy of the methanol molecule is large enough to give several low-lying conformers, separated by small

transition states when clustered to the amino acids under the experimental temperature. Although these conformers are similar in energy, the calculations showed that, with increasing side chain size the lowest-lying conformer changes structure between Val and Leu, likely due to steric hindrance which forces the cluster to adopt a loser structure, which maximizes the ΔG^{o} of the association reaction. This change in structure becomes especially evident in the case of proline, where due to its strained pyrrolidine ring, only single coordination between the ammonium group proton and the methanol oxygen atom seems thermodynamically plausible. The results of this work form the beginning stages towards a better understanding of how protic solvents stabilize both the canonical and zwitterionic forms of aliphatic side chain amino acids in the gas phase. Future studies will need to focus on the addition of multiple methanol molecules in order to gain a thorough appreciation of the solvation behaviour of these protonated amino acids in the gas phase.

Chapter 4
The Structures and Energies of the Methanol Stabilized Protonated Nucleic Acid Bases

4.1 Introduction

Nucleic acid bases serve as the building blocks of our genetic coding, DNA and RNA. They are highly functional molecules, each possessing a number of hydrogen bond donors and/or acceptors. However, they are also all cyclic molecules, so attachment of a solvent molecule onto either of them is limited by the fixed configuration of each atom and σ-bond within the molecule. The nucleic acids can be split into two groups based on their structure. The monocyclic molecules uracil, thymine and cytosine each possess a pyrimidine ring, and are appropriately named pyrimidine bases. The two others, adenine and guanine are bicyclic, and are named purine bases, since they are substituted purines.

An interesting feature of nucleic acid bases is their aromaticity. This causes a great degree of stabilization which in turn leads to difficulty for weaker Lewis bases to penetrate directly to the pyrimidine and purine rings, and interactions are more favourable on the outer subsituents, where the entropy of cluster formation is low. For the same reason, proton transport between tautomers of nucleic acids have such large energy barriers, often in excess of 35 kcal mol^{-1}, as the stable ring loses its aromaticity in the transfer process.

The protonation and hydration of neutral and protonated nucleic acids and bases in the gas phase has been of considerable interest as of late,[1-8] particularly the hydration and the tautomerism of cytosine.[1,3,8] Cytosine is interesting because it is identical to uracil, with one of the carbonyl groups replaced by an amino group, forcing the ring nitrogen beside the amino group to lose its proton to the amino group, becoming a weak hydrogen bond acceptor. Calculation shows that

protonation most favourably takes place at the carbonyl oxygen, resulting in the enol-amino tautomer of cytosine. However, the keto-amino form, in which the N3 site (see Fig. 4.1 for numbering conventions) is protonated, is also a low energy structure, and likely coexists with the enol-amino form.[1] In fact, this coexistence has been confirmed experimentally via UV-UV and UV-IR spectroscopic "hole-burning" schemes.[4] Previous low-level *ab initio* calculations have revealed two low-lying tautomers for both protonated uracil and protonated thymine.[7] The most dominant form is the enol-amino form, in which protonation takes place on O4, trans to N3. The other low-lying tautomer is the di-enol form, where N3 is left without a proton, but experimentally, only the enol-amino form was observed when no transport catalyst was introduced.[4] In the gas phase, the reported calculated tautomer is protonated at N6,[7] but in practice, will depend on the conditions of the experiment, since most of the nitrogen atoms have similar basicity. The calculated result agrees with the principally observed tautomer in aqueous solution.[6]

There has also been previous work done in our group towards an understanding of the solvation of nucleic acids by Lewis bases, as well as proton transport mechanisms within the nucleosides. Wu and McMahon have recently studied the dissociation energies and structures of clusters of the strong Lewis base ammonia with the protonated adducts of uracil, thymine, cytosine and adenine using HPMS.[7] They noted that the magnitude of the bond between ammonia and the protonated nucleic acids decrease in the order uracil, cytosine, thymine and adenine, with bond energies ranging from 27.9 kcal mol^{-1} for $U(NH_3)H^+$ to 17.5 kcal mol^{-1} for $A(NH_3)H^+$. In all four cases, the measured enthalpy and entropy matched very well with the enthalpy and entropy calculated at MP2(full)/6-311++g(2d,2p)//B3LYP//6-31+g(d,p), which inspired the same calculation to be used for the systems discussed here. The proton transfer problem discussed above was addressed here as well, for thymine. There exists an ambiguity for thymine because the di-keto amino form of the neutral species is by far the lowest energy tautomer, but for the protonated adducts, the di-enol

form is slightly lower in energy than the enol-keto amino form. The possibility that direct protonation of the neutral enol-keto form of thymine was eliminated, based on the idea that the natural abundance of this tautomer would be so low with respect to the abundance of the neutral di-keto amino form. However, for the pyrimidine nucleic acids, partial to complete proton transfer from the most acidic moiety to ammonia was shown to be a favourable process, and therefore a unimolecular proton transfer mechanism with an ammonia catalyst was proposed, having two sequential proton transfer steps, with transition state energies no more than 10 kcal mol^{-1} higher in energy than the local minima. This emphasizes that ammonia is a strong Lewis base in the gas phase, but weaker Lewis bases such as alcohols or water may not facilitate proton transfer as well in the role of a catalyst to proton transfer.

4.2 Experimental and Computational Results

4.2.1 **Tautomers of Protonated Pyrimidine Nucleic Acid Bases**

Like the amino acids, nucleic acid bases possess a number of functional groups that can serve as both hydrogen bond donors and acceptors. They are, as previously mentioned, cyclic and aromatic, so instead of envisioning permutations of various conformations, one must consider various tautomerism and proton migration processes that could potentially occur within the molecules. In the absence of a "solvent" molecule, an isolated gas phase nucleic acid is not likely to tautomerize, however, our own preliminary investigation using the B3LYP functional and the 6-31+g(d,p) basis set reveals that each nucleic acid does possess a number of low energy tautomers, the most stable of which are shown in Fig. 4.1, and their enthalpies and entropies relative to the most stable tautomer for each type of nucleic acid are listed in Table 4.1. The energies were calculated as single point energies at the MP2(Full)/6-311++g(2d,2p) level of theory.

From literature, the neutral form of uracil and thymine are similar, both adopting their canonical forms in solution and in the gas phase, which is the di-keto form, with N1 and N3 each bonded to a hydrogen atom.[4,9-11] The lowest energy tautomer of protonated uracil, UH01, maintains the same tautomerism as its neutral counterpart, but O4 is protonated, with the proton oriented trans from N3 to minimize charge repulsion from the O4 and N3 protons. UH02 is the di-enol form of protonated uracil, thus N3 is deprotonated to allow for the O2 and O4 atoms to each accept protons oriented cis to N3. The O-H bond length at the O4 site is unaffected by proton transfer from N3 to O2, and the O-H bond at O2 is equally strong as that at O4, both possessing bond lengths of 0.97 Å. At the MP2/6-311++g(2d,2p) level and including vibrational and thermal energy corrections, UH02 is only 0.7 kcal mol^{-1} higher in energy than UH01, but the relative energies for these two tautomers calculated at B3LYP/6-11+g(d,p) are reversed, with UH02 just 0.2 kcal mol^{-1} lower in energy than UH01. Likewise, they are reversed when the size of the basis set is increased.[12] A transition state calculation at this level for the transfer of the proton from N3 to O2 reveals an energy barrier of over 40 kcal mol^{-1}. This high energy barrier suggests that once protonated, the configuration is locked into place possibly until solvent is introduced. UH03 is a slightly higher energy configuration of the di-enol tautomer. It should be noted that protonation of N3, giving it a second proton, was highly destabilizing, because it forces N3 to adopt an sp^3 hybridization, generating ring strain in an otherwise planar molecule.

Neutral thymine is similar to neutral uracil in that going from N1 to O4, there is a pattern in terms of hydrogen bond donors and acceptors, going donor, acceptor, donor, acceptor. The only difference between the two molecules is the methyl substituent located on C5. It is a source of steric hindrance. For this reason in part, the di-enol tautomer is the lowest energy conformer, named TH01, followed by the protonated canonical di-keto amino form of thymine, TH02, which is

3.9 kcal mol^{-1} higher in energy than TH01, an analogous structure to UH01. Again, the O-H bond lengths are 0.97 Å, and this bond length is independent of which tautomer is being considered.

Only two low energy tautomers of protonated cytosine (CH^+) were optimized. Previous work has revealed that the most stable neutral form of cytosine in the gas phase is the keto-enol form, where a hydrogen atom is located at the N1 position, resulting in a secondary amine moiety.[4,7,13-17] It should be noted at this time that this configuration appears to be the most stable for all pyrimidine bases. Removal of the proton from N1 to another site in the molecule resulted in a large increase in energy, and was eliminated. As well, protonation at the amine site at C4 was roughly 30 kcal mol^{-1} higher in energy than CH01. This could be because the addition of the proton at this site restricts the N-C4 bond to σ-type, and the positive charge is localized at the ammonium moiety. CH01 is the enol-amino tautomer of CH^+. Therefore, the N1, O2 and N4 sites are all hydrogen bond donors, with N3 to be expected as being weakly hydrogen bond accepting. It was found to be the most stable CH^+ tautomer here by 1.5 kcal mol^{-1}, but previous experiments using diffraction data[18] and calculations using the HF/STO-3G level of theory[19] reveal that CH02, the keto-amino tautomer, is the most stable. In the keto-amino form (CH02), the N-H bonds at the N4 site are unaffected by movement of the proton from O2 to N3.

4.2.2 **Protonation of the Purine Base Adenine**

The most stable form of neutral adenine is the amino form, with a hydrogen atom bonded to N1, resulting in a secondary amine group in this position.[2,4,6] Protonation can therefore occur at the N3, N6, or N8 sites. The most favourable of these is the N6 site, which agrees with previous literature.[2,6,7] This generates AH01, in which the localized positive charge is the furthest removed from the N1 secondary amine moiety. The adjacent amino group in position 5 is also electron-donating, and therefore stabilizes the positive charge Protonation at N8 to give AH02 is only 1.9 kcal

mol^{-1} less stable than AH01. The loss of entropy upon protonation to give AH01 or AH02 are equal, and therefore the free energy difference between both tautomers will only differ by 1.9 kcal mol^{-1}. It is likely that at any temperature in the limit of thermal dissociation of the purine base, both tautomers should exist. AH03, in which the N3 site is protonated is 8.8 kcal mol^{-1} higher in energy than AH01, considerably less favourable than the tautomers in which protonation occurred in the six-membered ring.

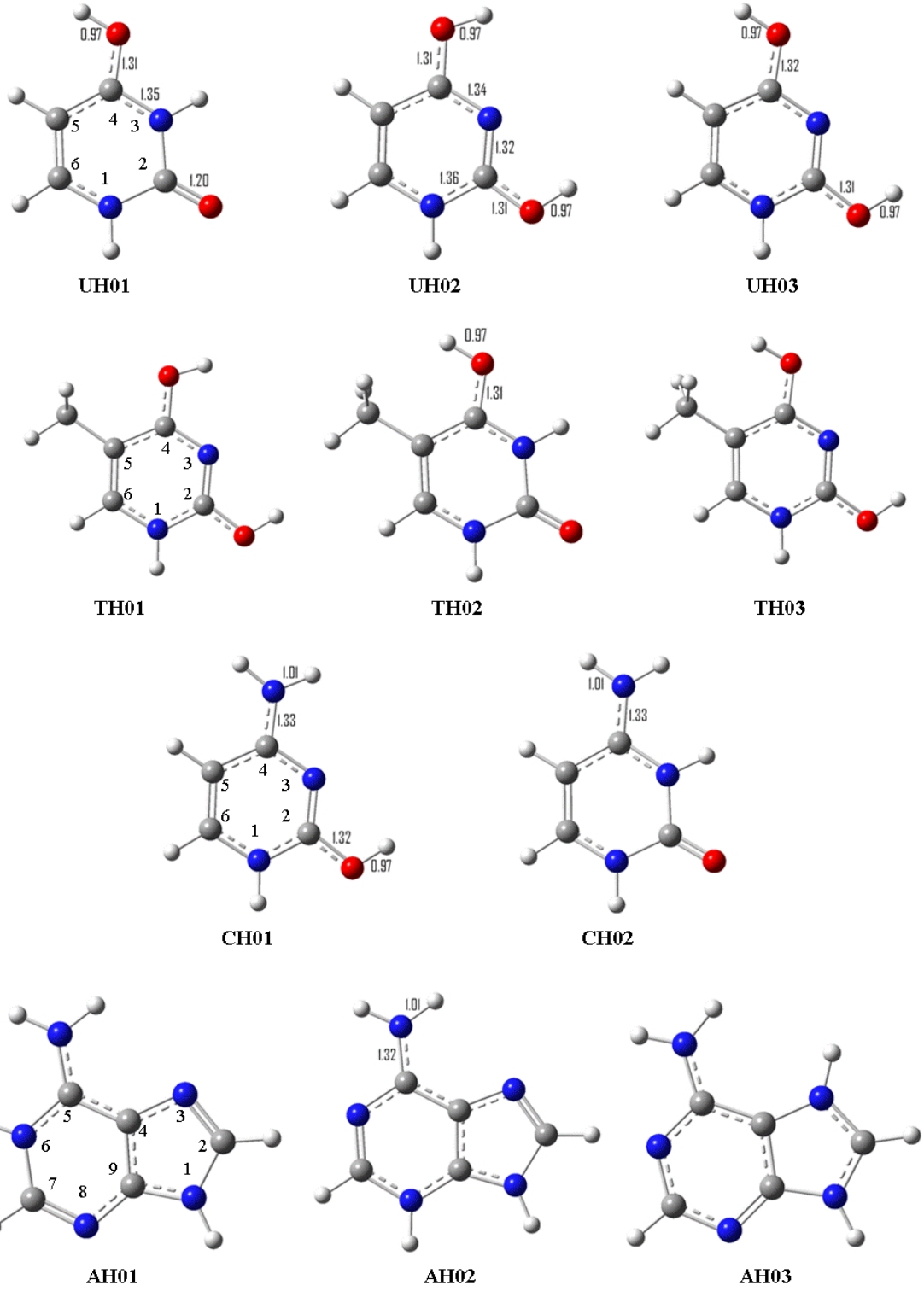

Fig. 4.1: The low-lying tautomers of the protonated nucleic acid bases uracil, thymine, cytosine and adenine optimized at B3LYP/6-31+g(d,p)

Table 4.1: Relative enthalpies and entropies of the lowest-lying tautomers of the protonated nucleic acid bases uracil, thymine, cytosine and adenine calculated at MP2(Full)/6-311++g(2d,2p)//B3LYP/6-31+g(d,p)

	$\Delta\Delta H^o$ (kcalmol^{-1})	$\Delta\Delta S^o$ (calmol^{-1}K^{-1})
UH01	0.0	0.0
UH02	0.7	-0.7
UH03	1.4	-0.5
TH01	0.0	0.0
TH02	3.9	0.8
TH03	4.4	-0.1
CH01	0.0	0.0
CH02	1.5	0.7
AH01	0.0	0.0
AH02	1.9	0.0
AH03	8.8	1.3

4.2.3 **Experimental Results**

The van't Hoff plots for the association reactions 4.1 through 4.4 were all obtained between the temperatures of 393 K and 443 K, and are presented in Figs. 4.2 through 4.5. The thermochemical results are listed in Table 4.2.

$$UracilH^+ + MeOH \leftrightarrows Uracil\text{-}H^+\text{--}MeOH \quad (4.1)$$

$$ThymineH^+ + MeOH \leftrightarrows Thymine\text{-}H^+\text{--}MeOH \quad (4.2)$$

$$AdenineH^+ + MeOH \leftrightarrows Adenine\text{-}H^+\text{--}MeOH \quad (4.3)$$

$$CytosineH^+ + MeOH \leftrightarrows Cytosine\text{-}H^+\text{--}MeOH \quad (4.4)$$

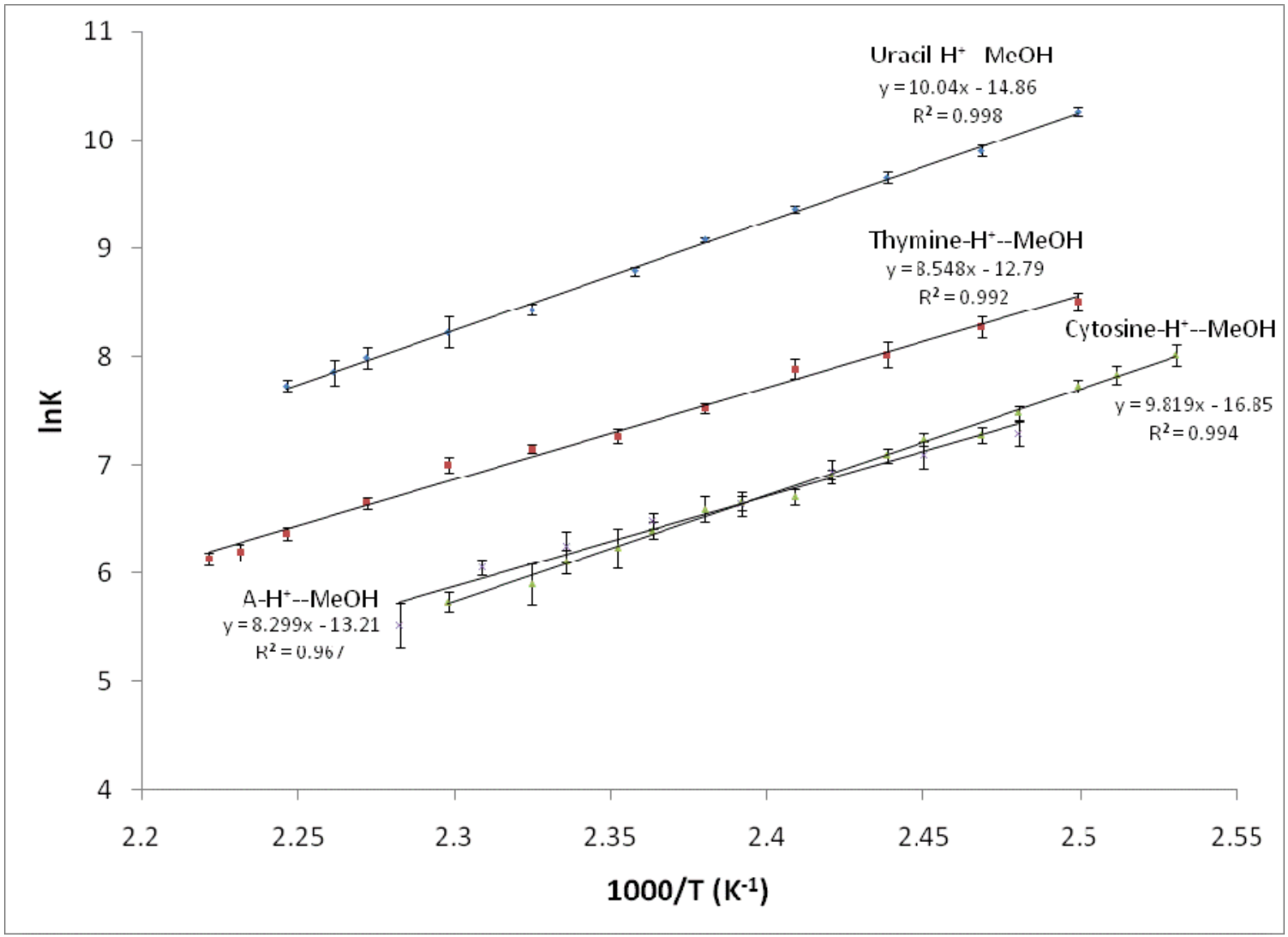

Fig. 4.2: van't Hoff plots for the reactions depicted in Eqs. 4.1-4.4

Table 4.2: Enthalpy and entropy changes for the reactions 4.1 to 4.4

	ΔH^o (kcalmol^{-1})	ΔS^o (calmol^{-1}K^{-1})
Uracil-H$^+$--MeOH	-20.1±1.0	-29.5±3.0
Thymine-H$^+$--MeOH	-17.0±1.0	-25.4±3.0
Adenine-H$^+$--MeOH	-14.5±1.0	-21.4±3.0
Cytosine-H$^+$--MeOH	-19.5±1.0	-33.5±3.0

The experimentally measured enthalpy for the formation of U-H$^+$--MeOH was -20.1 kcal mol^{-1}, and its entropy was -29.5 kcal mol^{-1}. The measured enthalpy falls 2-3 kcal mol^{-1} lower in energy than the calculated values for the most stable conformer UM01-01 (Fig. 4.3) at MP2(full)/6-311++g(2d,2p)//B3LYP/6-31+g(d,p), but is within 1.5 kcal mol^{-1} of the enthalpy of several conformers slightly higher in energy, namely UM01-02, which was derived from the lowest energy conformer for the protonated form of uracil, UH01.

The experimental enthalpy and entropy changes accompanying the formation of clusters of T-H$^+$--MeOH are -17.0 kcal mol^{-1} and -25.4 cal mol^{-1} K^{-1} respectively. Both the enthalpy and entropy changes are slightly lower than for the proton-bound clusters of uracil with methanol. The enthalpy change measured experimentally is just over 1 kcal mol^{-1} lower than that calculated for the most stable conformer of T(MeOH)H$^+$ calculated at MP2(Full)/6-311++g(2d,2p)//B3LYP/6-31+g(d,p) from Fig. 4.5. It matches closely with the enthalpy calculated for various conformers in which methanol is directly proton-bound to TH01, which is the lowest energy conformer of protonated thymine, in which thymine adopts its di-enol form.

The experimentally determined enthalpy for the formation of C-H$^+$--MeOH was -19.5 kcal mol^{-1}, and its entropy was -33.5 cal mol^{-1} K^{-1}. Both the enthalpy and entropy changes are slightly

higher than those for the most stable structure, CM03-01, calculated at MP2(full)/6-311++g(2d,2p) with thermal and vibrational corrections, shown in Fig. 4.6.

The measured enthalpy and entropy of A-H^+--MeOH are lower still, being -14.5 kcal mol^{-1} and -21.4 cal mol^{-1} K^{-1} respectively. The enthalpy change of the most stable calculated conformer, AM01-01 from Fig. 4.7 is 4.4 kcal mol^{-1} higher than that measured experimentally, falling outside of experimental error. There is likely extensive tautomerism taking place within the timescale of ion formation and detection which lead to the formation of a higher energy AH^+ tautomer.

4.2.4 **Computed Energies and Structures of the U-H^+--MeOH Cluster**

The geometries of all tautomers and methanol stabilized tautomers of the protonated nucleic acids were optimized using the B3LYP DFT functional and the 6-31+g(d,p) basis set. The B3LYP functional has produced precise energies in the past, however, single-point energy calculations were still performed using the MP2(Full) electron-correlation theory with the 6-311++g(2d,2p) basis set.[20-26] The proton-bound clusters of uracil and methanol have been calculated by considering the addition of a methanol molecule to the two low-lying conformers of protonated uracil seen in Fig. 4.1, UH01 and UH02. All enthalpy and entropy changes of the association of protonated uracil with methanol are with reference to UH01, and are summarized in Table 4.3.

The lowest energy conformer for the cluster of U-H^+--MeOH was UM01-01, derived from UH01, having an enthalpy and entropy of -23.7 kcal mol^{-1} and -31.5 cal mol^{-1} K^{-1} respectively. Methanol accepts a hydrogen bond from the proton on O4, elongating the hydroxyl group bond length from 0.97 to 1.04 Å. UM01-02 and UM01-03 are conformers in which methanol is bound to the amine group. The hydrogen bond lengths in these two conformers are both 0.12 Å longer than the one formed in UM01-01, giving evidence that the proton on O4 is more acidic than the one on N3. Many adducts derived from UH02 and UH03 were found to have energies and entropies within

1 kcal mol^{-1} and 1 cal mol^{-1} K^{-1} from the above values. The experimental enthalpy is lower than that for UM01-01 by 3.6 kcal mol^{-1}. This phenomenon cannot be explained from a thermodynamic standpoint, because the free energy change using the experimentally obtained values, at the average experimental temperature of 400 K is -8.3 kcal mol^{-1} whereas under the same conditions, the free energy change of formation of UM01-01 is -11.1 kcal mol^{-1}, i.e. significantly more favourable. Since experiment matches closely with the calculated values obtained for UM01-02, the kinetics of the transfer of a methanol molecule from the N3 hydrogen atom to the adjacent hydrogen on O4 were investigated computationally. The transition between UM01-01 and UM02-02 would likely involve 180^{o} rotation of the C4 hydroxyl group, followed by the formation of a hydrogen bond between the methanol oxygen atom and the proton on N3. Calculation at the B3LYP/6-31+g(d,p) level of theory reveals a rotational barrier of only 4 kcal mol^{-1} for rotation of the O4 hydroxyl group. Once rotated, formation of the hydrogen bond between methanol and the N3 proton is highly stabilizing, bringing the energy of the cluster back down to within 1 kcal mol^{-1} from the energy of UM01-01. Loss of the O4-H-O hydrogen bond is the most energy costly process in the methanol transfer, bringing the cluster energy up to that of UM01-02, while simultaneously increasing the entropy of the cluster.

The di-enol form of UH^{+} is also greatly stabilized by methanol. The most acidic proton is on O2 and methanol prefers to bind at this site, giving UM02-01. The covalent O-H bond at this site is elongated to 1.04 Å as opposed to 1.03 Å when methanol is attached to the proton on O4 in UM02-03, and the cluster is 1.6 kcal mol^{-1} more stable in this configuration. Methanol binding at the N1 hydrogen site is also favourable for this tautomer, giving UM02-01. This conformer is more stable than UM01-02, even though the N1-H bond for the former is shorter than the N3-H bond in the latter.

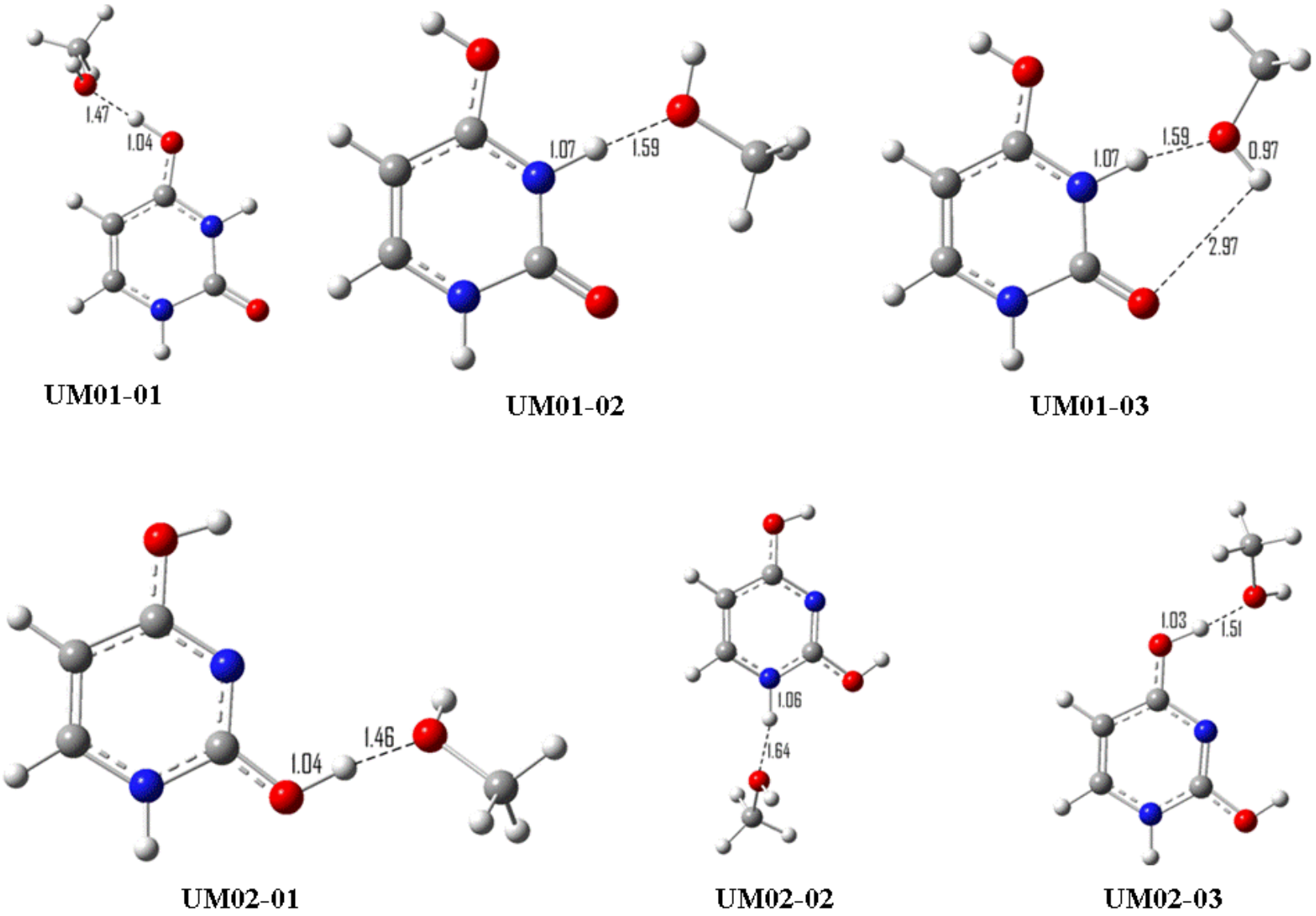

Fig. 4.3: Structures of the U-H$^+$--MeOH cluster derived from UH01 and UH02 optimized at the B3LYP/6-31+g(d,p) level of theory.

Table 4.3: Enthalpy, entropy and free energy of association of the low-lying U-H^+--MeOH tautomers calculated at MP2(Full)/6-311++g(2d,2p)/6-31+g(d,p)

	ΔH^o (kcalmol^{-1})	ΔS^o (calmol^{-1}K^{-1})	ΔG^o(400) (kcalmol^{-1})
UM01-01	-23.0	-32.2	-10.1
UM01-02	-18.6	-29.9	-6.6
UM01-03	-18.4	-27.9	-7.2
UM02-01	-22.0	-31.1	-9.6
UM02-02	-21.1	-30.0	-9.1
UM02-03	-20.4	-30.6	-8.2

Due to the stability of the UM02 conformers, an investigation into how methanol aids the proton transfer from N3 to O2 was undertaken. The secondary intermolecular hydrogen bond in UM01-03 is weak, and almost non-existent, but if it were strengthened, it could stabilize the cluster enough to allow direct proton transfer from N3 to the methanol oxygen atom. A transition state for this proton transfer was found. The distance between N3 and the proton was 1.55 A, which is out of the range of a covalent interaction. The proton was in fact closer to the oxygen atom on methanol than to uracil. The secondary hydrogen bond was shortened from 2.97 to 1.70 Å. However, a stable minimum could not be located where protonated methanol existed with neutral uracil. This suggests that the proton transfer is concerted, and as one proton approaches methanol, the other proton breaks away towards O2, more similar to an S_N1 substitution. In fact, no stationary minimum could be optimized in which methanol was protonated, leading to the conclusion that the transition state upon methanol catalysis for the proton transfer from N3 to O2 within UH^+ involves the formation of the methoxyl anion bound by two protons to an enol tautomer of neutral uracil. This transition is shown in Fig. 4.4, and is only 6.0 kcal mol^{-1} higher in energy than the UM01-03 methanol stabilized tautomer calculated at the B3LYP/6-31+g(d,p) level of theory with no thermal or vibrational correction. When the single-point energy using the MP2(full) method is used, and the thermal and zero-point energy corrections are included, then the energy barrier decreases to

roughly 4 kcal mol^{-1}. This is a significant improvement over the case with the methanol catalyst absent.

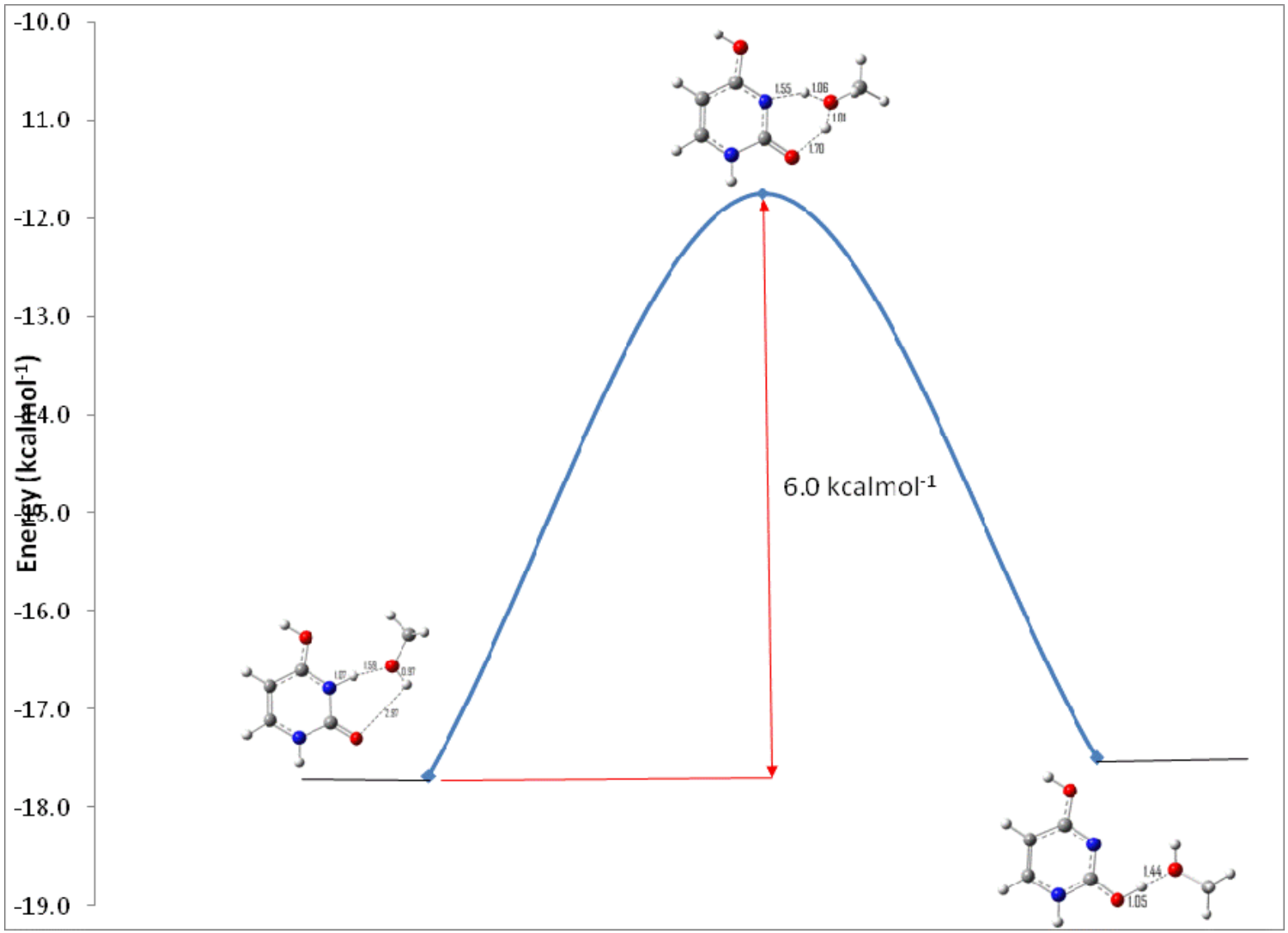

Fig. 4.4: Methanol-catalyzed proton transfer in protonated uracil between the enol-amino tautomer and the di-enol tautomer. The transition is a concerted double-proton transfer generating neutral uracil and the methoxyl anion. Energies were calculated at the B3LYP/6-31+g(d,p) level of theory.

4.2.5 **Computed Energies and Structures of the T-H$^+$--MeOH Cluster**

Since the di-enol tautomer of TH$^+$ in which the protons on O2 and O4 are trans to N3 is the lowest in energy of the tautomers calculated, the enthalpies and entropies of complexation with one methanol molecule were determined using TH01 as a reference. The structures of the lowest energy methanol-stabilized tautomers are illustrated in Fig. 4.5, and their corresponding enthalpies and entropies of association are listed in Table 4.4. As previously mentioned, thymine possesses the same pattern of hydrogen bond donors and acceptors as uracil, and therefore most of the low-lying conformers of the T(MeOH)H$^+$ cluster are analogous with those of U(MeOH)H$^+$. The difference between the two nucleic acids is the presence of a methyl group located on C5. The methyl group hinders protonation on O4 cis to the N3 atom, as well as methanol coordination to this location. TM02-01 is the thymine analog to UM01-01, but is 6.4 kcal mol^{-1} higher in energy than that conformer.

The lowest energy conformer of the T-H$^+$--MeOH cluster is TM01-01, derived from TH01, with an enthalpy and entropy of formation of -18.6 kcal mol^{-1} and -29.9 cal mol^{-1} K^{-1}. In this conformation, methanol accepts a strong hydrogen bond from the hydroxyl group on C2. The intermolecular hydrogen bond length is only 1.48 Å and, similar to that seen with UM02-01, this site is the most preferable region for hydrogen bond formation because the N1 and N3 atoms tend to draw electron density into the ring, leaving a significant positive charge on the proton on O2. This region of the molecule is also not hindered sterically. Between the hydrogen sites on N1 and O4, the N1 site is slightly more favourable for hydrogen bonding with methanol. Upon attachment of methanol, the covalent N1-H and O4-H bonds are shortened by only 0.01 Å less than in their uracil counterparts, likely as a result of electron density being donated into the ring by the methyl group.

Conformers derived from TH02 are generally 2-4 kcal mol^{-1} higher in energy than those derived from TH01. This is a comparable energy difference to that of the isolated protonated nucleic acids, TH01 and TH02. This suggests that methanol does not stabilize one tautomer with respect to the other. This is not too surprising considering the effect of the methyl group on the conformation of TH^+. It is neither a hydrogen bond donor or an acceptor and may introduce a source of steric hindrance to the resulting complex with methanol. The weak electron donating characteristics of the methyl group can be neglected since it likely has roughly the same effect on both tautomers. The conformer TM02-01 is enthalpically less stable than any conformer from the TM01 series of tautomers. Although the hydrogen bond formed in this complex is comparable in strength to that formed in TM01-01, the proton on methanol is repelled by the methyl group, likely forcing the cluster to adopt a more entropically favourable geometry. In addition, the entropy loss of 30.3 cal mol^{-1} K^{-1} is the largest of all conformers because rotation about the hydrogen bond is hindered by the presence of the methyl substituent. Since the O4 proton is the most acidic proton within the TH02 tautomer, all other conformers in which methanol is not positioned near the C5 methyl group are less stable than TM02-01. TM02-02 and TM02-03 are analogous to UM01-02 and UM01-03 respectively, and again, the N3-H covalent bonds are shortened by only 0.01 Å less than in the uracil counterparts, while the primary hydrogen bond with methanol is 0.01 Å longer than in their uracil counterparts, perhaps a reflection of the respective proton affinities of uracil and thymine.

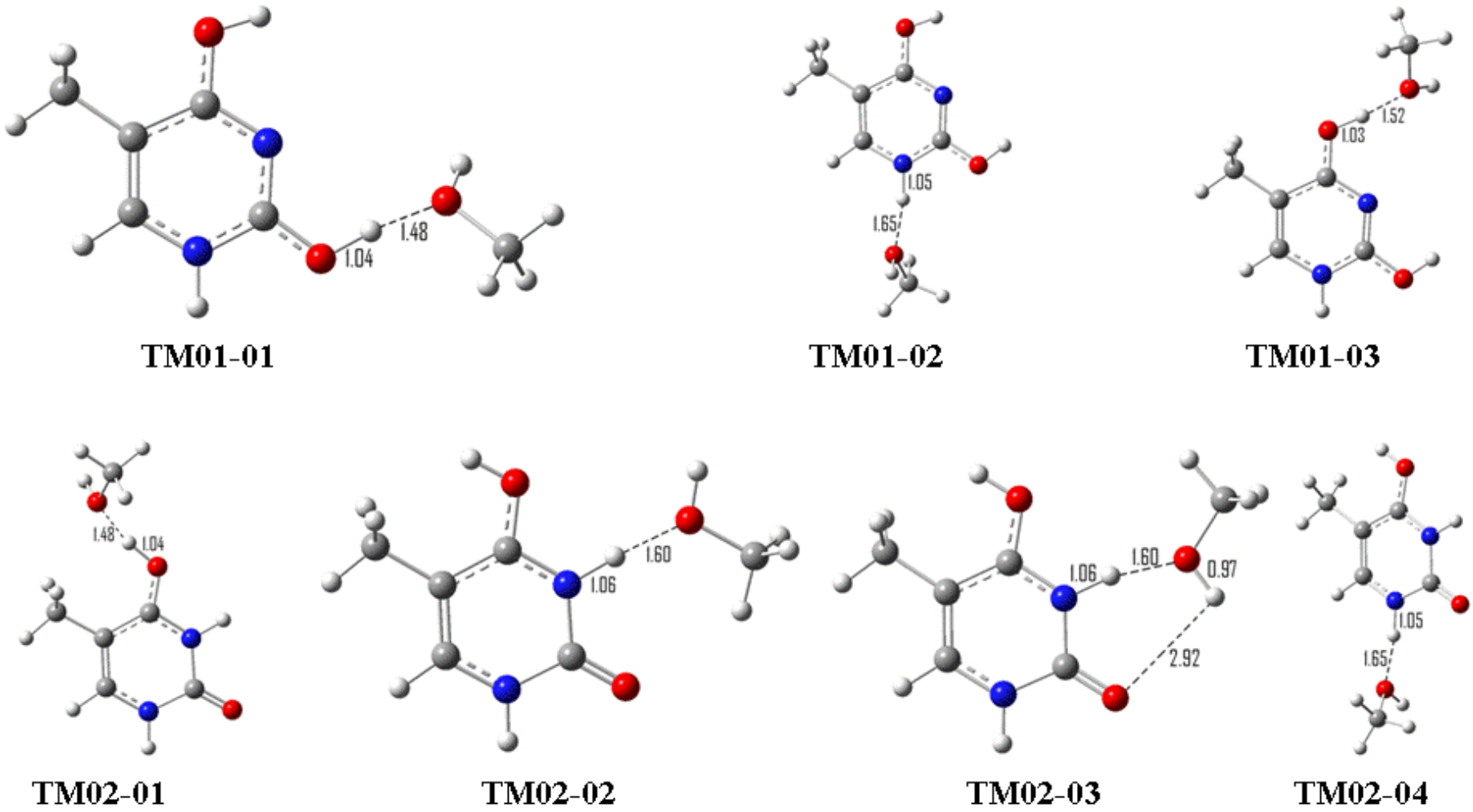

Fig. 4.5: Structures of the T-H$^+$--MeOH cluster derived from TH01 and TH02 optimized at the B3LYP/6-31+g(d,p) level of theory.

Table 4.4: Enthalpy, entropy and free energy of association of the low-lying T-H^+--MeOH tautomers calculated at MP2(Full)/6-311++g(2d,2p)/6-31+g(d,p)

	ΔH^o (kcalmol^{-1})	ΔS^o (calmol^{-1}K^{-1})	ΔG^o(400) (kcalmol^{-1})
TM01-01	-18.6	-29.9	-6.7
TM01-02	-17.9	-29.2	-6.2
TM01-03	-17.2	-29.2	-5.5
TM02-01	-16.6	-30.3	-4.4
TM02-02	-14.2	-29.0	-2.6
TM02-03	-14.0	-25.2	-3.9
TM02-04	-13.1	-28.2	-1.9

4.2.6 **Computed Energies and Structures of the C-H^+--MeOH Cluster**

Methanol stabilizes the various tautomers of CH^+ differently than for uracil and thymine because the carbonyl group in the four position is replaced by an amino group, so that the pattern of hydrogen bond donors and acceptors for cytosine becomes unique. The various tautomers clustered to methanol are shown in Fig. 4.6. The enthalpies and entropies of association for these clusters are given in Table 4.5. It has already been explained that protonation at the amino group to produce an ammonium substituent is unfavourable. The two lowest energy tautomers of CH^+, CH01 and CH02, can be stabilized by methanol accepting a hydrogen bond at the protonated site. The most stable conformer, CM02-01 is derived from CH02. The energies of the CH01 and CH02 tautomers are therefore reversed by introduction of the methanol molecule, and hence methanol plays a significant stabilizing role for the protonated cytosine keto-amino tautomer. Methanol stabilizes the localized positive charge on N3 by accepting a hydrogen bond from the proton on N3. In addition, it forms a hydrogen bond with the amino group hydrogen atom on N4. It is therefore tightly bound upon the formation of two hydrogen bonds, but loses more rotational degrees of freedom than a singly bound conformer. The enthalpy and entropy changes associated with its

formation are -18.3 kcal mol^{-1} and -31.9 cal mol^{-1} K^{-1} respectively. However, the free energy change for this conformer at 400°C is comparable to those of CM01-01 and CM01-02, two conformers derived from CH01, in which only a single hydrogen bond is formed between methanol and protonated cytosine. For this tautomer, methanol is bound only 0.3 kcal mol^{-1} stronger to the proton on O2 than the hydrogen atom bound to N1 because the proton affinity of nitrogen is higher than that of oxygen. In the case of CM01-03 and CM01-04, methanol is singly bound to the amino group on both sides respectively. Both of these conformers are between 5 and 7 kcal mol^{-1} less stable than CM01-01, and at the experimental temperature, will make up only an insignificant percentage of the conformer population. The hydrogen bond lengths in these conformers are 1.80 and 1.77 Å respectively, which are relatively long hydrogen bond lengths when compared to that in CM01-01. As observed with thymine, there is a decrease in the perturbation in the bond lengths of the hydrogen bond donating sites, but this time more significant, being 0.04 Å shorter. As a result, the intermolecular hydrogen bonds formed with methanol are between 0.02 to 0.03 Å longer, which may destabilize the cluster significantly when ionic hydrogen bonds are involved. Likewise, in the cases of CM02-03 and CM02-04, when methanol is only loosely bound to the CH02 tautomer, it is not significantly stabilized, and the free energy changes are only -3.8 and -2.9 kcal mol^{-1} respectively. Therefore the enthalpically favourable conformer should be the dominant species in the case of the C-H^+--MeOH cluster ion. However, for tautomers in which tightly bound conformers can not be formed, such as CH01, the methanol stabilized tautomer is almost as abundant as CM02-01 when hydrogen bonds are formed at the N1 and O2 positions, but are much less stable when methanol is bound to the amino group.

Based on the thermodynamic free energy change at 400°C, the most abundant conformer would be CM02-02. The energy of this conformer is 2.4 kcal mol^{-1} higher than that of the most stable conformer, yet entropically it is much more favourable. This is likely because the amino

group is free to rotate in this configuration, giving the cluster more means of internal energy distribution. The ring amino group at N3 and the carbonyl group at C2 are already fixed in position to maintain sp^2 hybridization within the ring, and suffer minimal loss of entropy by attachment to methanol. Again, the higher energy arises because the methanol proton is very weakly acidic. This secondary hydrogen bond likely is only allowed to form because the methanol oxygen is already slightly deshielded after accepting a hydrogen bond from the N3 amine group, which increases the electrophilicity, or acid strength of the methanol proton attached to it.

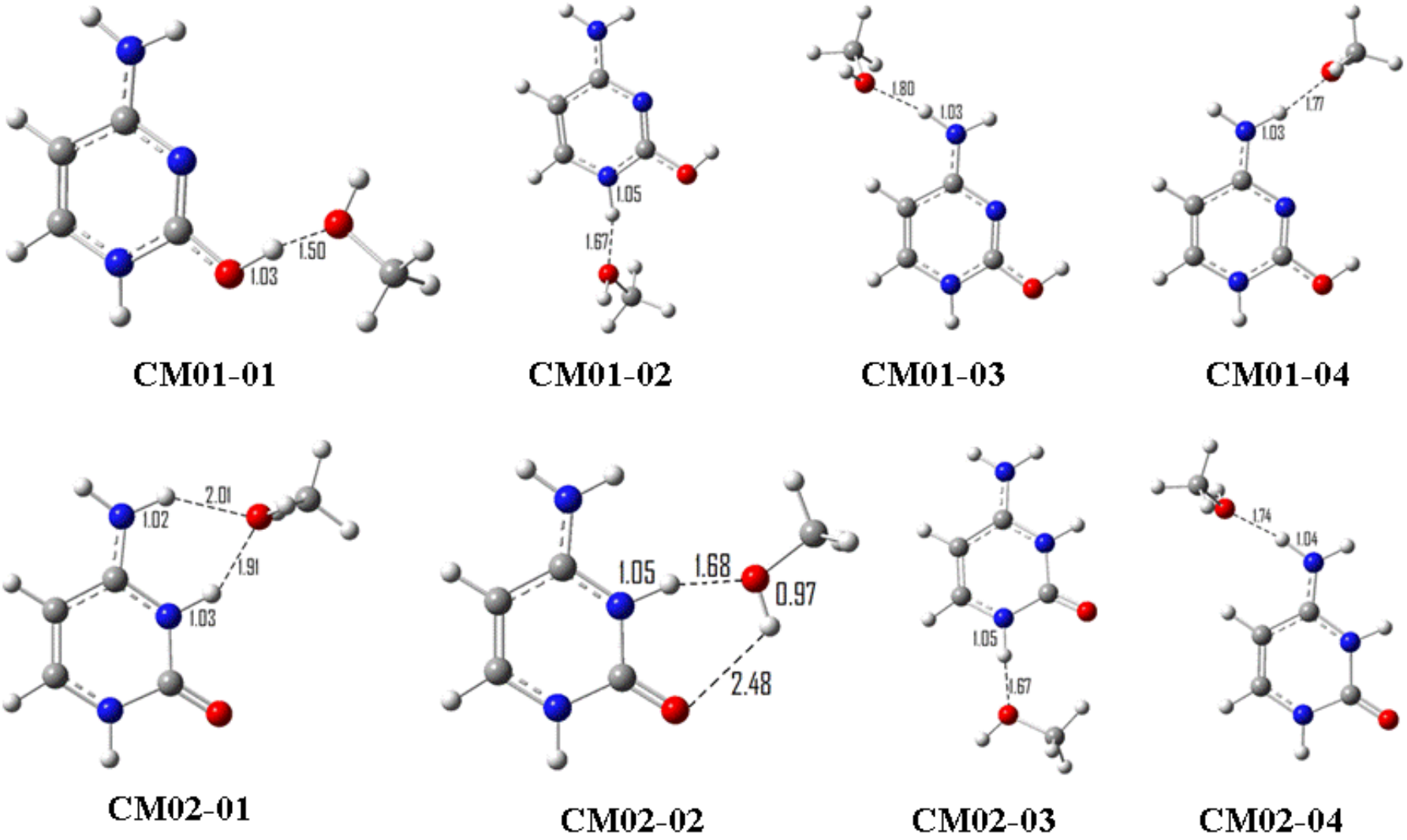

Fig. 4.6: Structures of the C-H^{+}--MeOH cluster derived from CH01 and CH02 optimized at the B3LYP/6-31+g(d,p) level of theory.

Table 4.5: Enthalpy, entropy and free energy of association of the low-lying C-H^+--MeOH tautomers calculated at MP2(Full)/6-311++g(2d,2p)/6-31+g(d,p)

	ΔH^o (kcalmol^{-1})	ΔS^o (calmol^{-1}K^{-1})	ΔG^o(400) (kcalmol^{-1})
CM01-01	-17.2	-29.4	-5.4
CM01-02	-16.9	-28.8	-5.4
CM01-03	-14.3	-29.2	-2.6
CM01-04	-12.3	-26.8	-1.6
CM02-01	-18.3	-31.9	-5.5
CM02-02	-15.9	-25.3	-5.7
CM02-03	-14.7	-27.4	-3.8
CM02-04	-14.6	-29.2	-2.9

4.2.7 **Computed Energies and Structures of the A-H^+--MeOH Cluster**

Protonated adenine, AH^+ has several hydrogen bond donating sites, but lacks any oxygen atoms, and is therefore limited in its hydrogen bond accepting ability. Because of this, up to three tautomers of AH^+ are stabilized by one methanol molecule. These clusters are shown in Fig. 4.7, and the corresponding enthalpy and entropy of association for each configuration is given in Table 4.6. The most stable tautomer is that in which both N1 and N6 carry a proton. The most stable cluster, AM01-01, is observed when both the protons on N6 and the N5 amino group donate hydrogen bonds to the methanol oxygen atom. The same conformer has been calculated as the lowest energy cluster of water attached to protonated adenine.[6] In fact, the energy orderings for all clusters of methanol with the AH01 tautomer are analogous to the clusters with water. This configuration is over 4 kcal mol^{-1} more stable than when methanol is coordinated to the proton localized on N1 in AM01-03. The hydrogen bond length in this conformer is large, being 1.71 Å, because N1 is highly basic. AM01-01 is also 3.5 kcal mol^{-1} lower in energy than AM01-02, where methanol is accepting a hydrogen bond from the proton on N5 cis to C4, and simultaneously donates a hydrogen bond to

N3. Methanol is a weak hydrogen bond donor, and the amino group in the fifth position on adenine is also only weakly hydrogen bond donating. From the determination of the free energies of both conformers in Table 4.6, the tighter structure of AM01-01 should dominate at the average experimental temperature 400^{o}C even though it is accompanied by a larger loss in entropy.

The conformers derived from AH02 are overall less stabilized by complexing with methanol relative to those derived from AH03. From AH02, the most stable conformer of A-H^{+}--MeOH is again that in which two hydrogen bonds are formed between AH^{+} and methanol, as is the case in AM02-01, in which protons on N1 and N8 are hydrogen bond donors, and the binding energy of the cluster is 16.2 kcal mol^{-1}. AM02-02 is a looser conformer than AM02-01 in which methanol is bound to the hydrogen on N8. This destabilizes the cluster by 0.3 kcal mol^{-1}, but the entropy loss is only -29.4 kcal mol^{-1}, so that the free energy of this conformer is 0.3 kcal mol^{-1} more favourable at the average experimental temperature. This tautomer can not be stabilized by methanol if it binds to the amino group, as AM02-03 and AM02-04 are both weakly bound clusters with positive free energy changes at 400^{o}C.

The most stable conformer derived from AH03 is AM03-01. Again, it is a tightly bound conformer accompanied by a large decrease in entropy due to the loss of rotational degrees of freedom. When the overall free energies of the conformers are considered, then AM03-01 and AM03-02 would exist in almost equal amounts, despite AM03-02 being 2.6 kcal mol^{-1} less stable than AM03-01.

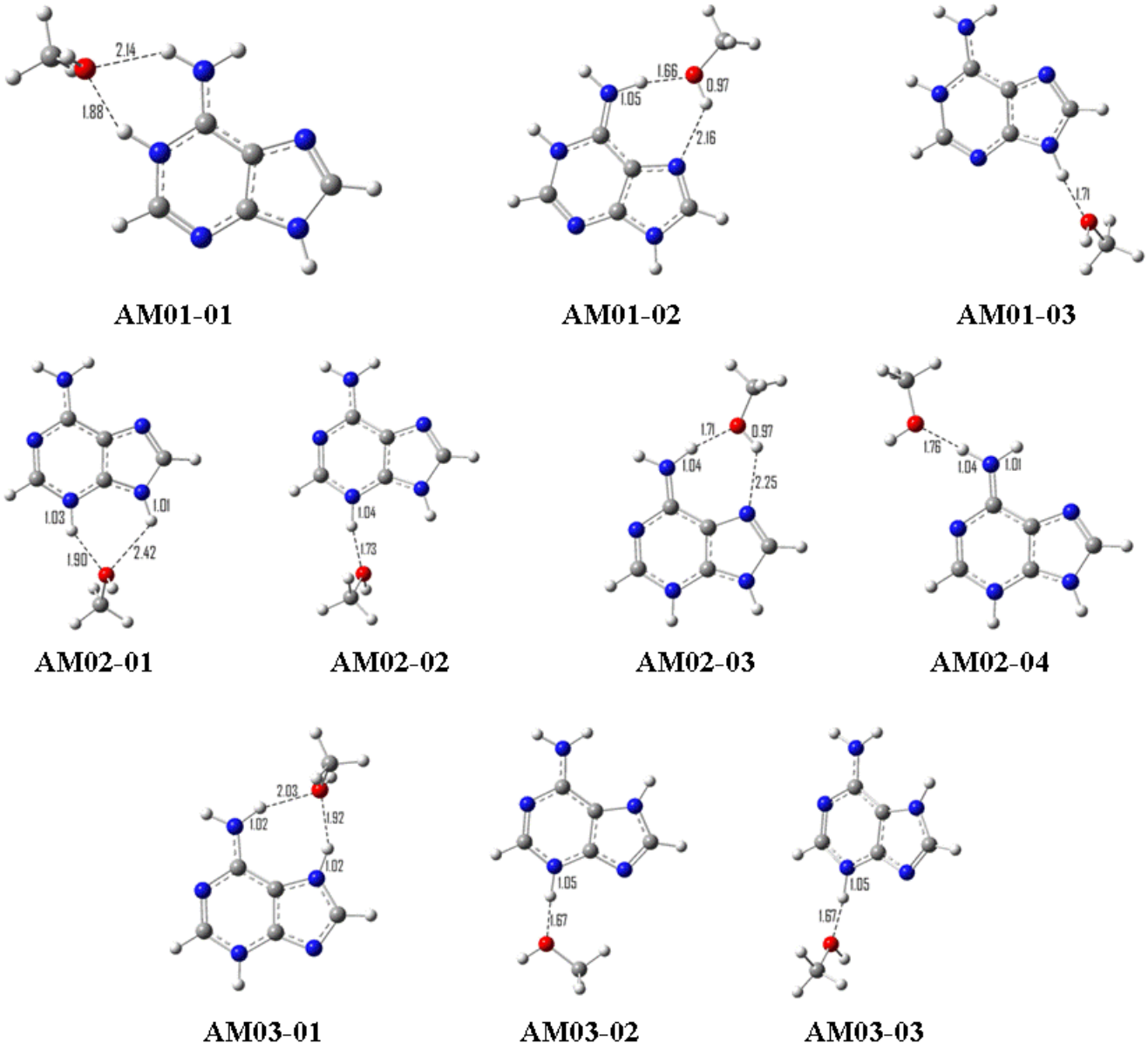

Fig. 4.7: Structures of the A-H$^+$--MeOH cluster derived from AH01 and AH02 optimized at the B3LYP/6-31+g(d,p) level of theory.

Table 4.6: Enthalpy, entropy and free energy of association of the low-lying A-H^+--MeOH tautomers calculated at MP2(Full)/6-311++g(2d,2p)/6-31+g(d,p)

	ΔH^o (kcalmol^{-1})	ΔS^o (calmol^{-1}K^{-1})	ΔG^o(400) (kcalmol^{-1})
AM01-01	-18.9	-32.3	-6.0
AM01-02	-15.4	-32.5	-2.4
AM01-03	-14.8	-27.3	-3.9
AM02-01	-16.2	-30.4	-4.0
AM02-02	-15.9	-29.2	-4.3
AM02-03	-11.6	-30.6	0.6
AM02-04	-9.8	-24.8	0.1
AM03-01	-18.3	-33.1	-5.0
AM03-02	-15.7	-27.1	-4.9
AM03-03	-15.5	-28.0	-4.3

4.3 Discussion and Conclusions

The experimentally measured enthalpy change of the U-H^+--MeOH cluster as recorded in Table 4.2 is -20.1 kcal mol^{-1}, making it the most strongly bound protonated cluster with methanol in the series of nucleic acid bases studied. The entropy of association was deduced from the intercept of the van't Hoff plot as being -29.5 kcal mol^{-1}. Comparing energies from Tables 6.2 and 6.3, it can be seen that the enthalpy matches most closely with the computed single point energy of UM02-03, which is derived from the second most stable protonated adduct of uracil, UH02, the di-enol form of uracil, in which the hydroxyl hydrogen atoms on O2 and O4 are oriented trans from the central nitrogen atom. The relationship between the experimental data and the computed energies for this conformer suggest that the UH02 tautomer is likely the most abundant tautomer present under the experimental conditions. Since our calculation would predict that UH01 is a more stable tautomer than UH02, a low energy pathway involving proton transfer from N3 to O2 must exist when protonated uracil forms a gas phase complex with methanol. As has been mentioned, in the

absence of a solvent molecule, the conversion between UH01 and UH02 is hindered by a 40 kcal mol^{-1} barrier. The high energy of the transition state can be attributed to a combination of two factors. The first is the high degree of separation between the hydrogen atom on N3 and the proton acceptor, O2 from UH01. In addition, the basicity of the bare N3 atom relative to that of O2 is much greater. The introduction of one methanol molecule selectively localized near the N3 proton opens a bridging path for the transferrable proton, which results in a significantly lower energy barrier for the transfer process.

To generalize the effect of the methyl substituent in protonated cytosine on the binding energy and entropy of the T-H^+--MeOH cluster, the structure and energies of this cluster and the U-H^+--MeOH cluster can be compared. The experimental enthalpy and entropy changes for the formation of the T-H^+--MeOH cluster from Table 4.2 match most closely with TM01-03. Again, from this data, we would expect that the di-enol tautomer, TH01, would be mostly stabilized by complex formation with methanol. Methanol will bind to the most acidic proton in the tautomer, on the opposite side of the methyl group to minimize steric repulsion between the proton on methanol and the methyl group. However, this conformation is analoguous to UM02-03, in which methanol accepts a hydrogen bond from the O4 hydrogen atom. Since experiment matches the calculation for these analogous conformers, it is likely that the methyl group plays no role in methanol selectivity towards a binding site on the protonated nucleic acid base, and that the methanol regioselectivity is only dependent on the acid strength of the proton that it binds to.

If methanol always prefers to bind to the most acidic proton, then the binding energy should be a linear function of the proton affinity difference between the nucleic acid base and methanol. The NIST database reports the proton affinities of neutral uracil, thymine, adenine, cytosine and methanol to be 208.6, 210.5, 225.3, 227.0 and 180.3 kcal mol^{-1} respectively. Relative to methanol,

all four nucleic acids are proton acceptors, which means their protonated analogues will be proton donors in complexes with methanol. One would therefore anticipate that the binding energies of clusters of the type discussed here where a proton is shared between two bases, should be directly related to the difference in proton affinity between the two bases. Specifically, the binding energies of U-H^+--MeOH and T-H^+--MeOH should be similar, with U-H^+--MeOH being only slightly more stable, while A-H^+--MeOH and C-H^+--MeOH should both be more weakly bound, with C-H^+--MeOH being the weakest. According to experiment, this is not the case, as illustrated graphically in Fig. 4.8. The relationship between the binding energy with proton affinity is consistent with previous experimental binding energies obtained for the same protonated nucleic acid bases clustered with ammonia.[7] It should be noted that the relative entropies did not follow similar trends. The results suggest a more thorough explanation of how methanol binds to adenine and cytosine, since these two nucleic acid bases do not possess an O4 atom as uracil and thymine do. The conformers of A-H^+--MeOH and C-H^+--MeOH which are likely the most abundant in a mixture of conformers when the experimental data is considered are AM01-03 and CM02-01. AM01-03 is a loose structure relative to the other conformers in Fig. 4.6, and its formation is less enthalpically because only one hydrogen bond is formed in the cluster. However, the ability for methanol to rotate freely about this hydrogen bond allows for full rotational and vibrational freedom, making it an entropically favourable configuration, and therefore more favourable at high temperature. The less favourable calculated free energy change of AM01-03 relative to AM01-01 could be caused by errors in calculating the entropies of the clusters, since these values are based on frequencies determined using a harmonic oscillator approximation. CM02-01 on the other hand exemplifies how the absence of the O4 binding site forces methanol to bind tightly and form two hydrogen bonds with CH^+. The structure of adenine permits the formation of two hydrogen bonds with methanol, but the experimental data does not reflect the computed enthalpies and entropies for those conformers.

Since many of the amine sites of adenine have similar basicities, it is also likely that this system possesses the most diverse distribution of conformers, because the experimentally measured enthalpy is a weighted average of the enthalpies of each conformer in the mixture, and only reflects the value of the most abundant isomer if the isomer distribution strongly favours a single species.

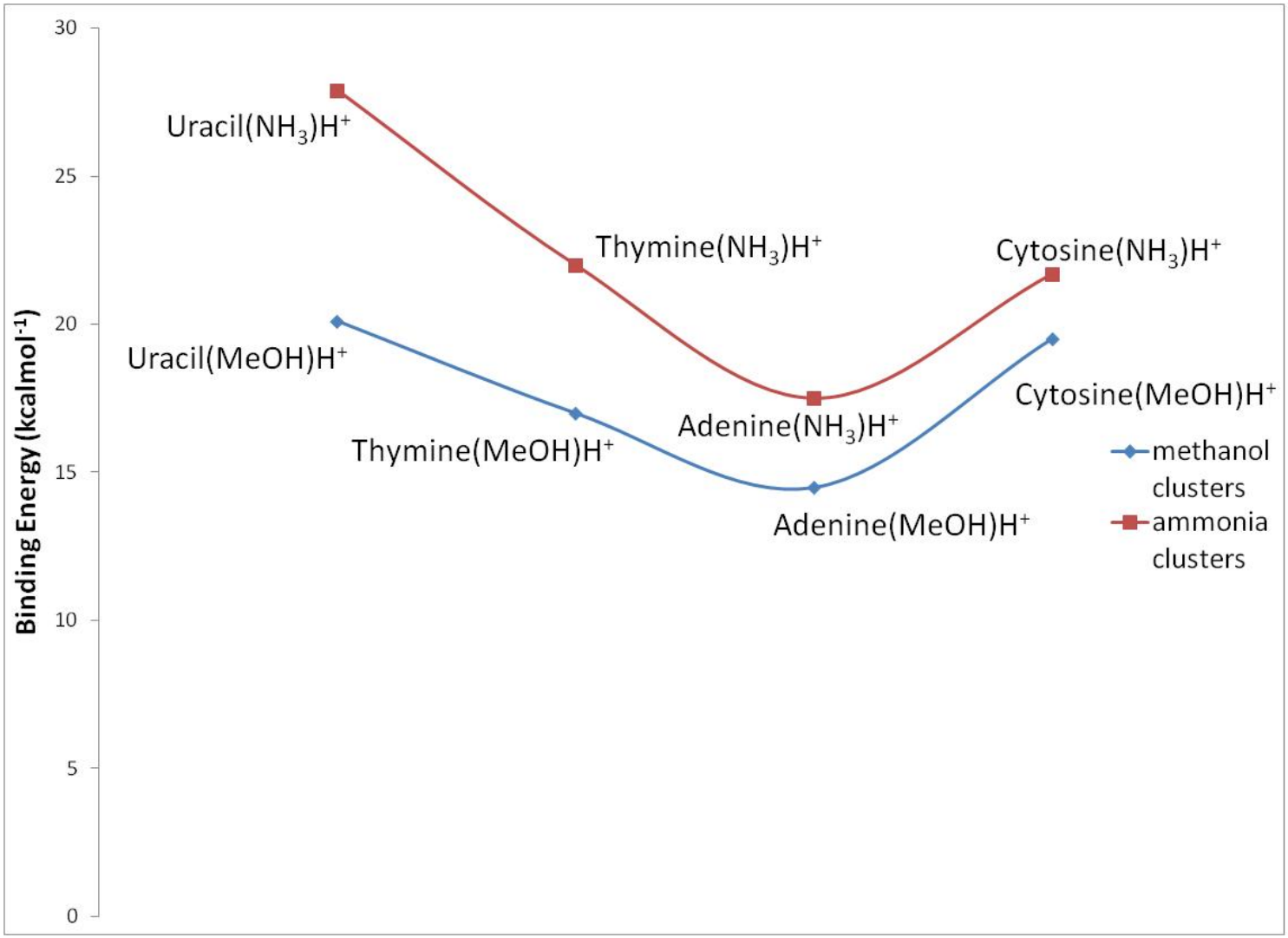

Fig. 4.8: Approximate relationship between binding energies of NA-H^+--MeOH clusters with the proton affinity of NA (Blue), compared to the experimental results from a study of NA-H^+--NH_3 (Red). Horizontal axis represents ordering of proton affinities for each nucleic acid base.

Chapter 5
Proposed Method For Indirect Measurement of Biomolecular Cation-π Interactions in the Gas Phase

5.1 Introduction

The cation-π interaction plays an important role in the secondary structure of proteins. Peptides with basic amino acid residues with cationic side chains such as arginine and lysine can be stabilized by interactions with the aromatic side chains of phenylalanine, tyrosine and tryptophan, if these three residues are present. Due to the numerous other interactions a protein may undergo both with itself and adjacent molecules, most experimental work in this area has attempted only to establish upper and lower limits to the magnitude of the cation-π interaction. Systems which form an upper boundary may be those in which the interaction is not thermodynamically restricted by large losses in entropy. An example of this type is the binding of group 1 ions Li^+, Na^+ and K^+ with the aromatic amino acids mentioned above.[1-4] A comparison of binding energies of Na^+ and K^+ to 6 aromatic molecules measured by Rodgers et al. by threshold collision-induced dissociation with guided ion beam tandem mass spectrometry, as well as Dunbar et al. using ligand-exchange equilibrium measurements in a Fourier transform ion cyclotron mass spectrometer, is listed in Table 5.1. The theoretical results calculated by Rodgers used the B3LYP/6-311++g(3df,3pd)//B3LYP/6-31+g(d) level of theory, while those of Dunbar were the energies obtained from the optimization at the B3LYP/6-31+g(d) level of theory. Both used vibrational and thermal energy corrections, as well as a basis set superposition error correction to reflect an overestimation in orbital overlap in the energy calculation of the complex.

Table 5.1: Comparison of experimental and theoretical binding energies of Na^+ and K^+ with aromatic molecules and amino acids. Rodgers' energies were calculated using the B3LYP functional and a 6-311++g(3df,3pd) basis set. Dunbar's were calculated using B3LYP and a 6-31+g(d) basis set, and give slightly higher binding energies.

	Experimental		*Theoretical*	
Na^+ / kcalmol^{-1}	**Rodgers**	**Dunbar**	**Rodgers**	**Dunbar**
Benzene	22.8			
Phenol	24.0			
Indole	29.1			
Phe	49.1	41.5	46.8	48.0
Tyr	50.0	41.8	47.4	48.3
Trp	51.9	43.0	50.4	52.0
K^+ / kcalmol^{-1}				
Benzene	17.5			
Phenol	17.7			
Indole	23.8			
Phe	36.0	24.9	33.7	34.7
Tyr	37.1	24.7	34.1	34.7
Trp	39.4	25.2	36.7	36.8

The experimental data obtained by Dunbar are noticeably lower than the data obtained by Rodgers, and the theoretical results reflect the experimental error in Dunbar's method, since both authors calculated energies that are much more consistent with Rodger's data. Both Na^+ and K^+ are calculated to bind to Phe and Tyr with roughly equal energies, but bind to Trp roughly 0.5 to 1.0 kcal mol^{-1} more strongly. The difference in binding energies remain virtually unchanged from the bond energy with the isolated benzene, phenol and indole rings, suggesting that other ion-molecule interactions taking place between ion and amino acid do not perturb the cation-π interaction to a large extent, they simply enhance the total binding energy. The binding energies of Na^+ to benzene and phenol collected by Rodgers also agree with those obtained by Armentrout, which are 21.1 kcal mol^{-1} and 23.5 kcal mol^{-1} respectively.[5] The larger binding energy to phenol is the result of an electrostatic interaction between the ion and the phenol hydroxyl group oxygen atom. McMahon et al. also observed a larger free energy change for the complex formation of Na^+ with phenol, being 16.7 kcal mol^{-1} versus Na^+ and benzene, which was only 15.7 kcal mol^{-1}.[6] These free energies were

obtained by single temperature measurements in a Fourier Transform Ion Cyclotron Mass Spectrometer (FT-ICR).

Research related to the cation-π interaction has been extended to larger biological cations as well.[7] Dougherty and Stauffer have confirmed that even hydrophobic host molecules containing a cavity surrounded by aromatic groups are capable of recognizing cationic quaternary amines, such as acetylcholine, by a stabilizing cation-π interaction. This was to confirm their previous similar observations.[8-10] The stabilization and structure of proteins by cation-π interactions have also been studied.[11-14] Computational simulation using the CAPTURE algorithm[15] on DNA and RNA binding proteins reveals the presence of one cation-π interaction for every 70 to 80 residues.[15,16] Estimates of the magnitude of the cation-π interaction ranged from 6 to 15 kcal mol^{-1} depending on the cation-π pair, with the Arg-Trp pair being the most strongly bound.[11] The magnitude of the cation-π interaction tends to play a significant role in secondary structure of these proteins as well. For example, in RNA binding proteins, 50% of the Lys residues formed the helix structure, while the Arg residues formed roughly equal amounts of helix and strand.[11]

In an acidic aqueous solution of a bio-organism, a basic amino acid such as arginine (Arg) or lysine (Lys) will exist as a protonated species, thus having a substantial positive charge on its side chain. If the positive charge on the side chain of Arg or Lys comes in close proximity with the negative quadrupole moment of an aromatic substituent of Phe, Tyr or Trp, a cation-π interaction between the two may occur. Since these interactions are generally much weaker than ionic hydrogen bonds, it is difficult to study them using conventional methods, and it often becomes necessary to achieve mere estimates of the magnitude of the interaction by an indirect approach. In addition, proteins are virtually involatile, so it becomes necessary to use smaller clusters to perform measurements in the gas phase to model their interactions. However, attempting to model exactly

the cation-π interactions occurring within proteins containing aromatic residues using small molecules is a rather impossible task on a thermodynamic basis. The difference between the two scales lies in where the entropy loss upon formation of the cation-π interaction originates. Within proteins, the cation-π interaction may be formed between two residues located on the same protein, or two residues present on two closely positioned proteins. Although there may be some loss in entropy associated with the loss of translational degrees of freedom, most of the entropy loss is due to the formation of a tightly packed and folded protein structure, which hinders both the vibrational and rotational degrees of freedom of the cluster, and potentially introduces steric hindrance between bulky side groups. Between two smaller molecules that form a cation-π pair, such as protonated diglycine ($GlyGlyH^+$) and benzene, there is a significant loss of entropy associated with the loss in translational degrees of freedom upon association. In the gas phase, it is not generally possible to study proteins because they are relatively involatile. Therefore, if one wants to get an estimate of the strength of the cation-π interaction between two proteins, it is necessary to introduce some form of rotational and vibrational hindrance to the cluster, in an attempt to induce a conformation change that approaches the local structure of a protein.

An additivity scheme referred to as the double-mutant approach has been suggested which minimizes the entropy of the system, and can therefore fairly reliably estimate the magnitude of even weak cation-π or arene-arene interactions.[17] The double-mutant approach uses tightly bound complexes of two amide oligomers possessing aryl subunits, referred to as molecular zippers. The free energy of formation of the molecular zipper can be compared to the free energy of formation of another cluster, where one of the oligomers has an aryl end group replaced by a bulky alkyl group. The authors believed that this mutation would also eliminate a secondary interaction between an amide moiety and the terminal aryl group that was removed, and so used a second

mutation to estimate that secondary interaction, by removing any terminal π-π interaction. The concept of double-mutation was inspiration for the approach attempted in this work, to be described below.

Consider the formation of the cluster of protonated diglycine ($GlyGlyH^+$) with the aromatic alchohol, phenol. A number of possible interactions could potentially stabilize the cluster. $GlyGlyH^+$ may donate an ionic hydrogen bond from its terminal ammonium group (the terminal amino group is most likely protonated) to the phenol hydroxyl group oxygen atom. In the most desirable configuration for the purpose of this project, phenol may also bind to the carboxyl moiety in an alternative configuration, but this would be considered less likely since the interaction would be void of ionic character, and the ammonium group is more acidic than the carboxyl group. However, this configuration could be stabilized by the formation of a secondary cation-π interaction between the negative quadrupole moment of the phenol phenyl ring, and the cationic ammonium group. This configuration meets the criteria of a rotationally and vibrationally hindered cation-π interaction. Unfortunately, several problems have been introduced that require resolution. The first is that several conformers may exist for this cluster, and it is not possible to isolate specific conformations using conventional mass spectrometry, since it is a mass indiscriminant technique. However, if the particular conformer of interest has a more favourable free energy relative to other conformers, it is likely the only conformer present in significant abundance, and the measured binding energy will reflect the binding energy of that conformer.

A peptide is an oligomer built out of amino acid units joined together through amide linkages. Diglycine is the simplest peptide, being the condensation product of two glycine molecules. Peptides are of particular interest in this context due to their innate flexibility. Proton migration and tautomerism of peptides in the gas phase have been the focus of previous studies.[18-23]

This past work has demonstrated that protonation of diglycine takes place most favourably at the terminal amino group, and two low-lying conformations exist.[20] Firstly, an extended form, in which an intramolecular hydrogen bond is formed between the ammonium group and the amide carbonyl oxygen in the plane of the peptide backbone. The second has a rotated backbone, or an L-conformation, in which that mentioned hydrogen-bond is 90^{o} out of the plane of the terminal carboxyl group. This conformation is 0.3 kJ mol^{-1} higher in energy than the extended geometry if the energy calculation is performed using the MP2 method, or 6.5 $kJmol^{-1}$ higher in energy if the B3LYP Density Functional Theory hybrid functional is used. As a reference geometry for the optimizations and energies calculated here, the extended form, protonated at the amino group was used. This being said, computational studies of water attachment on protonated GlyGly have revealed that a U-conformation is stabilized by 8-17 kJ mol^{-1} over the extended conformation as water forms two hydrogen bonds with protonated GlyGly, one as an acceptor to the ammonium moiety, and another as a donor to the carboxyl moiety.[20] Hydrogen/Deuterium exchange experiments between deuterated methanol and protonated peptides have also demonstrated that the principle exchange site is the terminal carboxyl group, even though the amine site is the most favourable protonated site.[18] This can be rationalized by the similar gas phase basicities of the acid moiety and the methanol hydroxyl group. It is however an interesting result because the same functional groups undergo no hydrogen/deuterium exchange if they are isolated (the only functional group present). This has been demonstrated in the case of 4-aminobenzoic acid and its dimethyl derivative by Gard et al., and provides evidence towards multiple interactions and therefore isomerisation between methanol and protonated peptides and amino acids, and establishes a spatial relationship between the two functionalities.[24]

5.1.1 **Modeling Lys-Phe/Tyr Cation-π Pairing Using Protonated Diglycine and Phenol**

Fig. 5.1 summarizes the eight geometries of the GlyGly-H^+--Phenol cluster calculated as a preliminary exercise for this work. This system incorporates small molecules that would be representative of the pairing of Lys with Phe or Tyr. DP01-DP04 are conformers that possess a cation-π interaction at the ammonium group. DP05-DP08 are missing the cation-π interaction, though it may be substituted by a second hydrogen bond. The energies calculated at the MP2(full)/6-311++g(2d,2p)//B3LYP/6-311+g(d,p) level of theory with vibrational and thermal energy corrections relative to the extended geometry of $GlyGlyH^+$ (seen in DP04, DP06 and DP07) are given in Table 5.2. Based on these results, it is apparent that a U and L-conformation of $GlyGlyH^+$ is greatly stabilized by the introduction of the cation-π interaction at the ammonium site. This is evidenced by the energies of conformers DP01 and DP02 respectively, relative to DP05, which replaces the cation-π interaction with an ionic hydrogen bond. Analysis of the relative abundances of each of the eight conformers using a Boltzmann distribution based on the free energies of each conformer at 423 K reveals that DP01 comprises approximately 85% of the product mixture. DP02 is predicted to have a 10% abundance. The complete analysis for the remaining conformers is shown in the curve in Fig. 5.2 as well. This is evidence that the binding energy that would be measured for the GlyGly-H^+--Phenol cluster should be representative of the energies of DP01 and DP02.

The estimate of the magnitude of the cation-π interaction in DP01 or DP02 can be obtained by subtracting the magnitude of the hydrogen bond from the net binding energy. Experimentally, to determine an approximate magnitude of the hydrogen bond, a calibration curve must be prepared, by measuring the binding energies of a number of alcohols with protonated diglycine. It is assumed that these alcohols will bind to the ammonium group of $GlyGlyH^+$ forming an ionic hydrogen bond, which unfortunately is unlike the nonionic hydrogen bonds present in DP01 and DP02, but this

shortcoming is offset by the gain in intramolecular stability of $GlyGlyH^+$ when only one intermolecular ionic hydrogen bond is formed, as demonstrated in the clusters of $Gly\text{-}H^+$--MeOH.

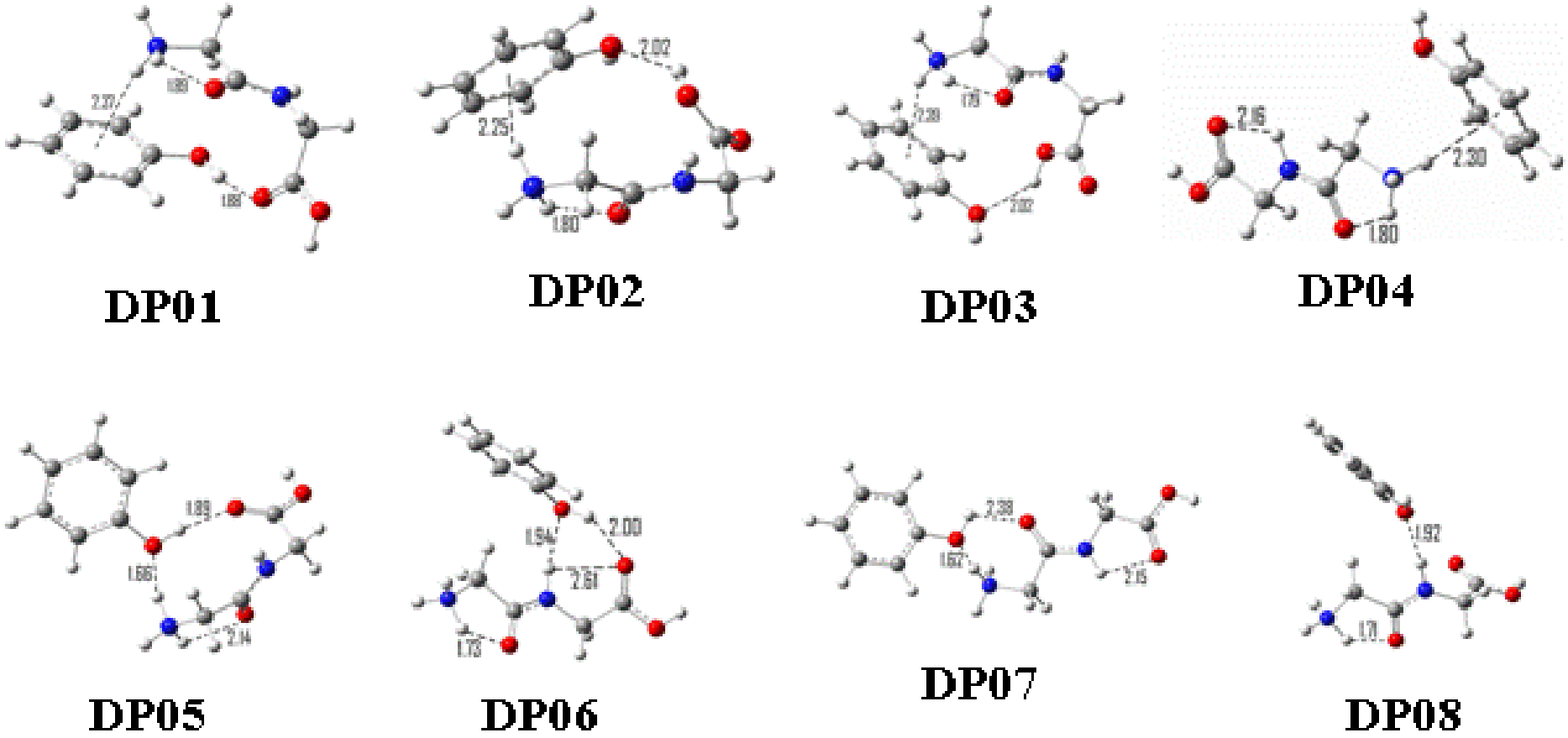

Fig. 5.1: Eight lowest energy conformers of the GlyGly-H^+--Phenol proton-bound cluster optimized at the B3LYP/6-311+g(d,p) level of theory. DP01 through DP03 simultaneously possess hydrogen bonding and a cation-π interaction.

Table 5.2: Enthalpy and entropy changes of cluster association for the eight conformers in Fig. 5.1. Energies were calculated as single-point energies using the MP2 Perturbation model with a 6-311++g(2d,2p) basis set.

	ΔH^o (kcal/mol)	ΔS^o (cal/molK)		ΔH^o (kcal/mol)	ΔS^o (cal/molK)
DP01	-23.7	-38.0	**DP05**	-20.9	-36.9
DP02	-21.2	-36.8	**DP06**	-16.3	-32.7
DP03	-15.3	-36.8	**DP07**	-15.4	-29.6
DP04	-16.6	-29.8	**DP08**	-15.4	-29.6

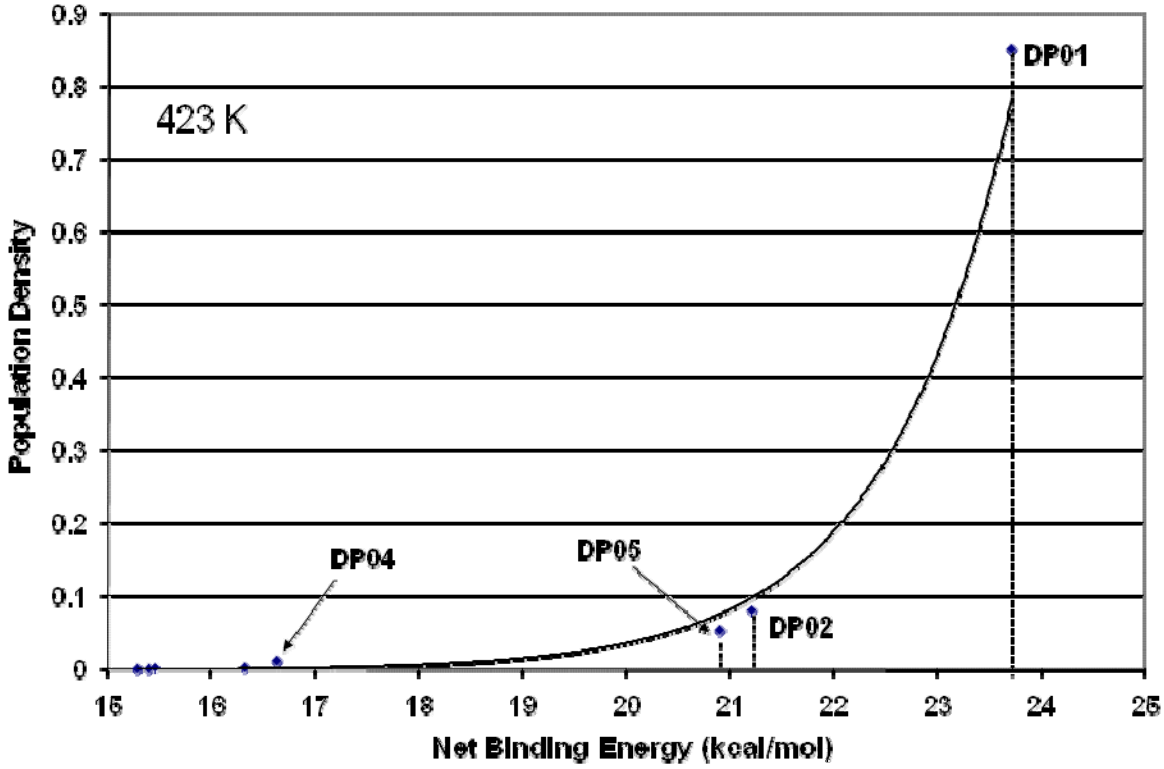

Fig. 5.2: Relative abundances of DP01 through DP08 determined from fitting their free energies to a Boltzmann distribution at 423 K.

Accompanying these two interactions is a probable conformational change of the peptide, likely promoted by steric hindrance between the peptide and the bulky 6-membered phenolic ring. This would destabilize the cluster, increasing the energy of $GlyGlyH^+$ relative to its extended conformation. This loss of enthalpy must be accounted for to properly estimate the cation-π binding energy. Overall, the cation-π interaction can be determined by subtracting the energetic contribution of the hydrogen bond from the net binding energy, followed by the addition of the

enthalpy that was lost from the conformation change caused by steric hindrance as represented in Eq. 5.1,

$$\Delta H_{cation\text{-}\pi} = \Delta H_{total} - \Delta H_{H\text{-}bond} + \Delta H_{steric} \quad (5.1)$$

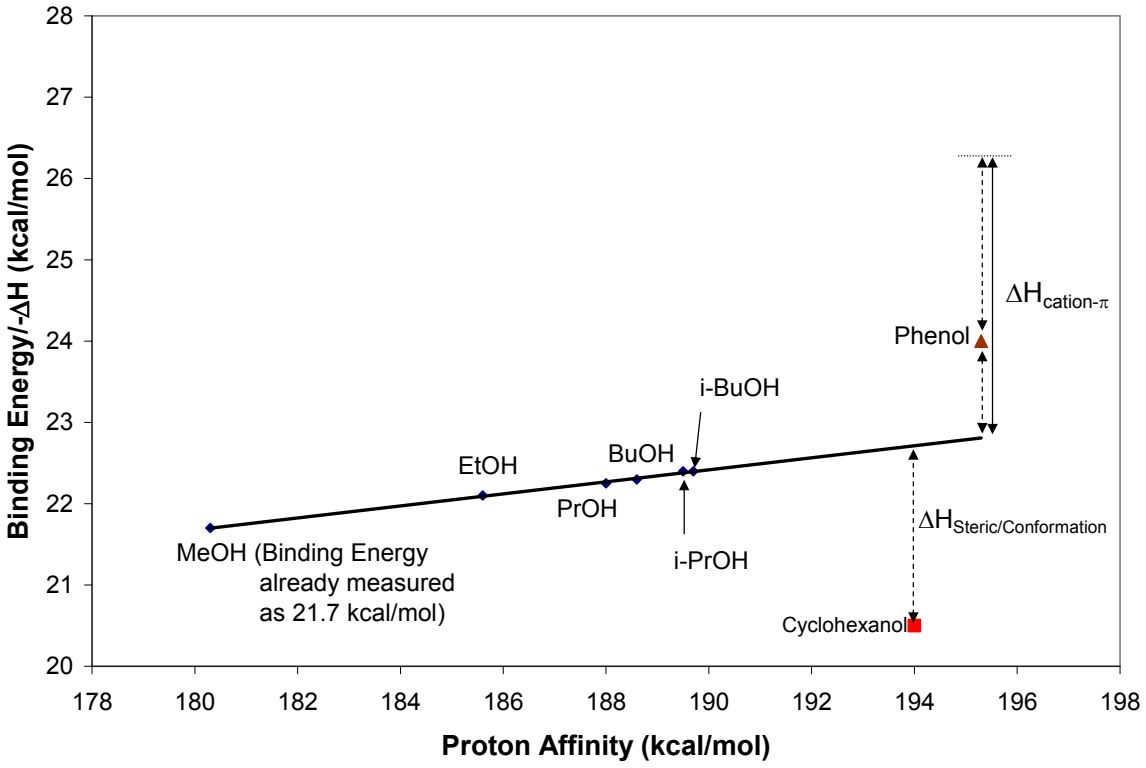

Figure 5.3: Anticipated linear correlation between GlyGly-H^+--Alcohol binding energy and alcohol proton affinity. The cation-π interaction between phenol and $GlyGlyH^+$ can be determined by subtracting an estimate of a hydrogen bond energy and adding in loss of binding energy due to steric effects caused by ring bulk.

Eq. 5.1 is represented graphically in Fig. 5.3, with the five alcohols to be used to produce the calibration curve present on a line. Note that Fig. 5.3 serves only as an illustration, and does not represent actual experimental results. These will be given and discussed below. To account experimentally for the mentioned peptide conformation change, a reference species may be used experimentally to "provoke" it. With the assumption that any conformation change is to compensate for steric hindrance caused by the bulky phenolic ring, another alcohol such as

cyclohexanol might promote these conformational changes without exhibiting cation-π interactions. Hence cyclohexanol was used here.

5.2 Results

The results section will be divided into several independent sections to describe the relevant data for the overall study.

5.2.1 **The Proton Affinity of Cyclohexanol**

The proton affinity (PA) of cyclohexanol (CH) has not been previously reported in the NIST database or any other database investigated. It was calculated and measured experimentally using acetone as a reference compound. Although this value could be calculated directly using the reaction depicted in Eq. 5.2,

$$CH + H^+ \leftrightarrows (CH)H^+ \qquad (\Delta H = -PA_{CH}) \qquad (5.2)$$

it could not be measured directly because the binding energy of H^+ to cyclohexanol is very high, and the isolated proton can not be observed, due to its high reactivity, and tendency to speciate with the CI products of methane. The proton affinity of acetone is well known,[25] and can serve as a reliable reference compound for the charge transfer reaction given by Eq. 5.3. Measurements were performed through a proton exchange (PE) reaction, where the proton is reversibly transferred from acetone to cyclohexanol,

$$AcH^+ + CH \leftrightarrows (CH)H^+ + Ac \qquad (\Delta H_{PE} = PA_{AC} - PA_{CH}) \qquad (5.3)$$

and therefore,

$$PA_{CH} = PA_{Ac} - \Delta H_{PE} \qquad (5.4)$$

Optimization and energy calculations were performed for both the protonated and non-protonated boat and chair conformations of cyclohexanol, and the enthalpies of the proton-exchange reaction with three compounds of well known proton affinity (methanol, ethanol, and acetone) were calculated. The computational results suggest that the cyclohexanol proton affinity is very similar to that of acetone (~194 kcal/mol). See Table 5.3 for the results, and Fig. 5.4 for the van't Hoff plot of the proton exchange reaction.

Table 5.3: Calculated proton affinity of cyclohexanol using methanol, ethanol and acetone as references

Reference	PA of Reference (kcal/mol)	ΔH (kcal/mol)	PA of Cyclohexanol (Chair) (kcal/mol)
Methanol	180.3	- 15.290	195.59
Ethanol	185.6	- 9.280	194.88
Acetone	194.0	+0.372	193.63

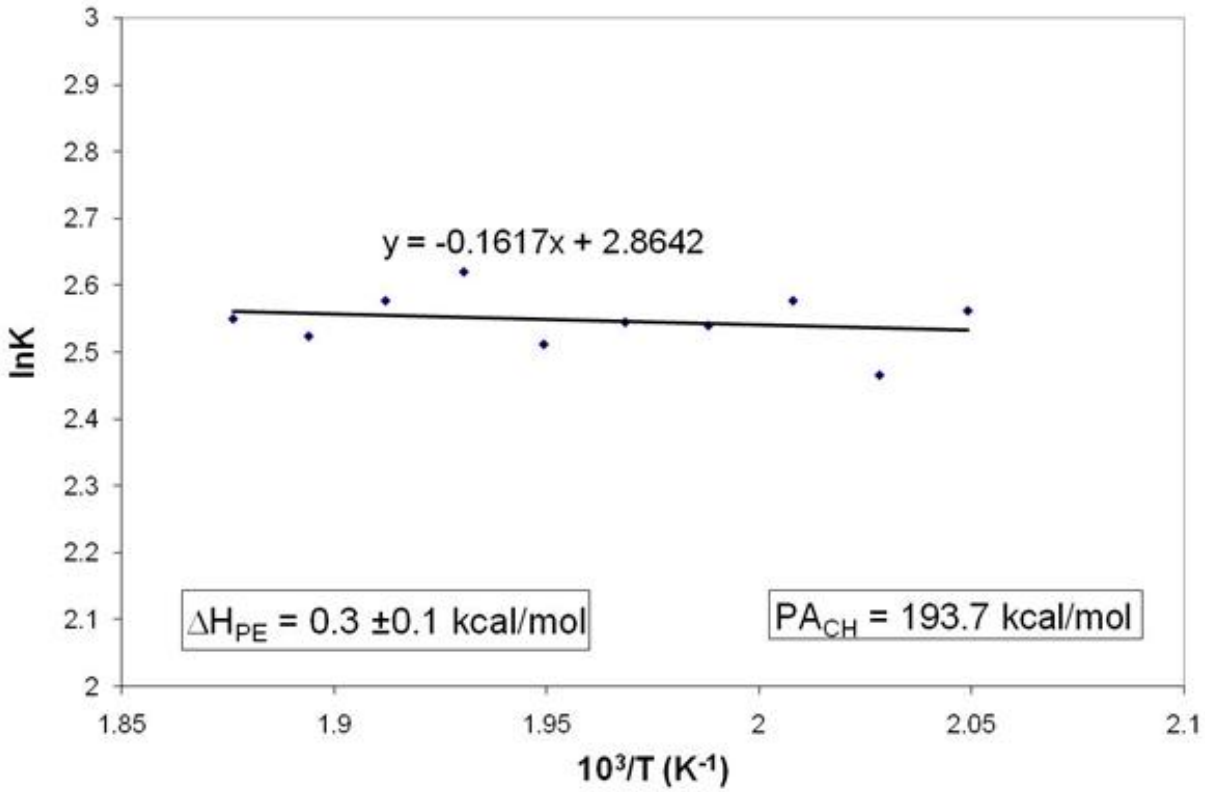

Fig. 5.4: van't Hoff plot for the proton exchange reaction $(CH)H^+$ + Acetone ⇆ CH + AcH^+

The van't Hoff plot above indicates that ΔH^o for the proton exchange reaction was +0.3 ±0.1 kcal/mol. Using the relationship in Eq. 5.4, this means that the proton affinity of cyclohexanol is experimentally measured to be approximately 193.7 kcal/mol, which is very similar to the value obtained theoretically in Table 5.3, when acetone was used as a reference.

5.2.2 **The Cation-π Interaction in the Cluster of GlyGly-H^+--Bz**

As a preliminary estimate of the magnitude of the cation-π interaction between $GlyGlyH^+$ and a phenyl ring, the enthalpy and entropy of the formation of a GlyGly--H^+--Bz cluster was measured. Benzene was chosen because it is a liquid at room temperature, thermodynamically stable and the dominant interaction with $GlyGlyH^+$ should be the cation-π interaction formed between the benzene negative quadrupole moment and the cationic ammonium moiety of $GlyGlyH^+$. Experiments were performed using a partial pressure of benzene roughly ten-fold higher than the methanol pressure in a typical experiment that would form the proton-bound cluster of methanol with an amino acid to increase the intensity of the GlyGly--H^+--Bz cluster relative to the diglycine proton-bound dimer. The relative abundances of the $GlyGlyH^+$ species and its cluster with benzene were measured between 130 and 160^{o}C, and the van't Hoff plot between these temperatures is illustrated in Fig. 5.5.

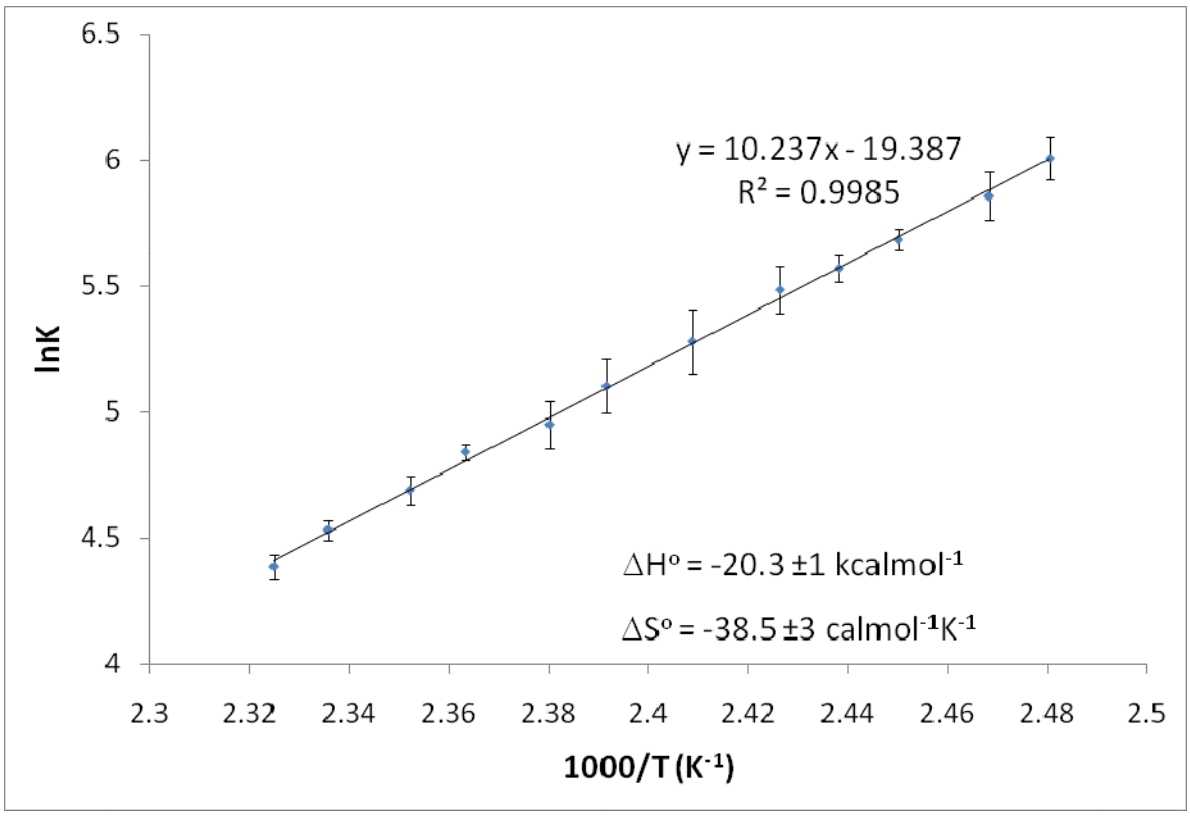

Fig. 5.5: van't Hoff plot for cluster formation of benzene and protonated diglycine

From the slope and intercept of this plot, the enthalpy and entropy of the formation of the GlyGly-H^+--Bz cluster are -20.3 kcal mol^{-1} and -38.5 cal mol^{-1} K^{-1} respectively. The cation-π interaction is of approximately the same magnitude as an ionic hydrogen bond formed by an ammonium group to an alcohol moiety. This value forms the upper limit of the cation-π interaction strength for biological systems because neither component of the complex must change conformation, and thus the interaction is unhindered. Surprisingly, the entropy change is higher than expected. Since the interaction is unhindered, one would expect that the only contribution to the loss in entropy be in the translational component, and the vibrational component of entropy should increase due to the vibrational degrees of freedom gained by formation of the cation-π bond.

Two possible conformers of the GlyGly--H^+--Bz cluster were optimized using the B3LYP functional with the 6-311+g(d,p) basis set, and a single-point energy calculation for each optimized geometry was computed by applying the MP2/6-311++g(2d,2p) level of theory. These two conformers are presented below in Fig. 5.6

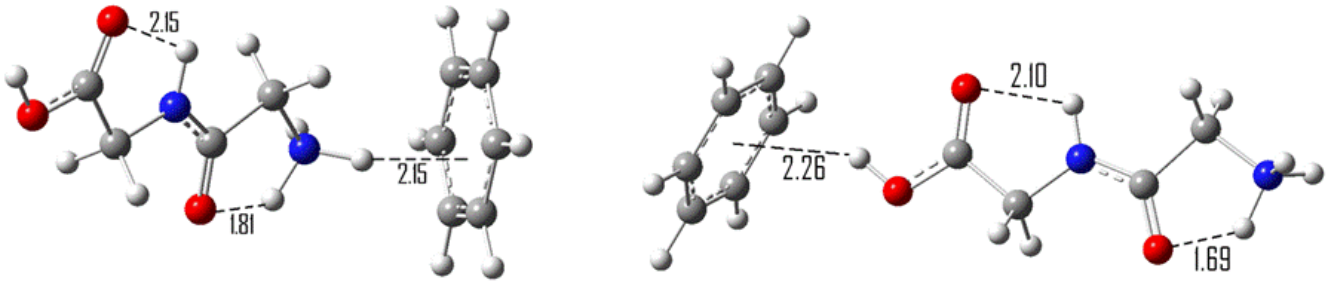

ΔH = -15.6 kcal/mol

ΔS = -23.0 cal/molK

ΔH = -8.6 kcal/mol

ΔS = -32.6 cal/molK

Fig. 5.6: Two possible geometries for the coordination of benzene with $GlyGlyH^+$. The interaction on the left represents a cation-π interaction. The right is a π-hydrogen bond.

The ammonium-coordinated conformer (left) is evidently the most strongly bound configuration of the cluster, having a cation-π interaction length just over 0.1 Å shorter than the carboxyl-coordinated form, in which a π-hydrogen bond is the only intermolecular interaction. There are three likely reasons why this is the case. First, the protons on the ammonium group are generally more acidic than the proton on the carboxyl end. This results in the ammonium group being a better hydrogen bond donor than the carboxyl group. Secondly, going in hand with the first idea, is that the ammonium group is charged, and hence the cation-π interaction occurring in the stronger is indeed truly a cation-π interaction, dominated by electrostatic attraction, whereas the interaction in the carboxyl-centred conformer could be classified as a π-hydrogen bond, because the ionic character is lacking. The third difference between the two groups is that the carboxyl group has an excess of electron density centred around the carbonyl oxygen atom. This introduces an unfavourable interaction with the benzene quadrupole moment so that it is not actually aligned in

the direction of the bond, but distorted, leaving only a small amount of overlap between the benzene quadrupole moment and the proton. The repulsive effect is likely minimized by the intramolecular hydrogen bond formed between the carbonyl oxygen and amide hydrogen atoms, which draws some electron density away from the carbonyl group. In contrast, the interaction seen in the ammonium-coordinated conformer occurs in a very electropositive region of $GlyGlyH^+$. The ammonium moiety almost adopts a bidentate coordination with benzene, but this effect will be discussed below.

5.2.3 **Attachment of Alcohols to Protonated Diglcyine**

The equilibrium constants for the association reactions of protonated diglycine with several aliphatic alcohols of varying proton affinities were recorded as a function of temperature. Specifically, the reactions conducted are shown in Eqs. 5.5 to 5.9

$$GlyGlyH^+ + MeOH \leftrightarrows GlyGly\text{-}H^+\text{--}MeOH \quad (5.5)$$

$$GlyGlyH^+ + EtOH \leftrightarrows GlyGly\text{-}H^+\text{--}EtOH \quad (5.6)$$

$$GlyGlyH^+ + n\text{-}PrOH \leftrightarrows GlyGly\text{-}H^+\text{--}(n\text{-}PrOH) \quad (5.7)$$

$$GlyGlyH^+ + i\text{-}PrOH \leftrightarrows GlyGly\text{-}H^+\text{--}(i\text{-}PrOH) \quad (5.8)$$

$$GlyGlyH^+ + n\text{-}BuOH \leftrightarrows GlyGly\text{-}H^+\text{--}(n\text{-}BuOH) \quad (5.9)$$

where MeOH = methanol, EtOH = ethanol, n/i-PrOH = n/i-propanol and n-BuOH = n-butanol.

The van't Hoff plots for Eqs. 5.5 to 5.9 are presented in Fig. 5.7, and the enthalpy, entropy and free energy change at 400 K of each reaction is listed in Table 5.4 along with the computed data for the alcohol-stabilized extended and U conformations of $GlyGlyH^+$.

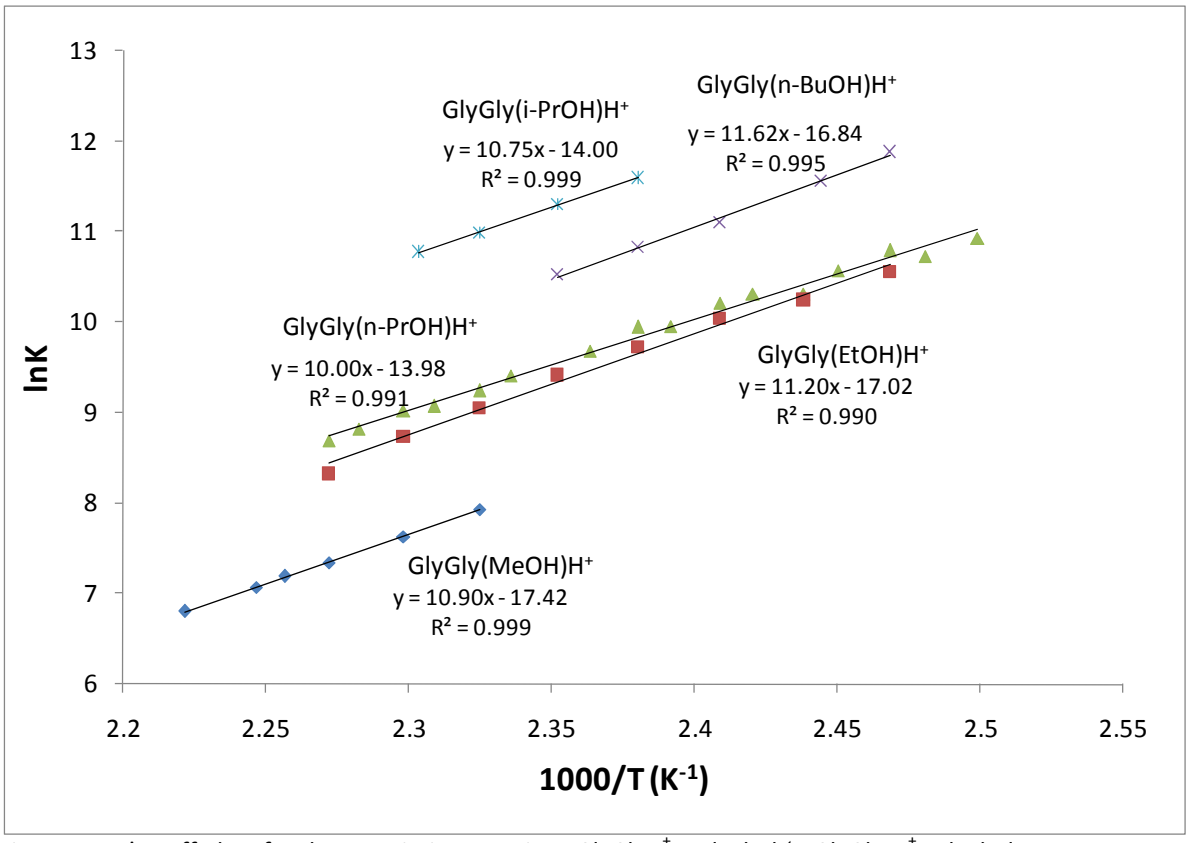

Fig. 5.7: van't Hoff plots for the association reactions $GlyGlyH^+$ + Alcohol ⇆ $GlyGly\text{-}H^+$--Alcohol

To be sure the results were reproducible, all systems were investigated again, yielding similar results. Taking the opposite sign of the enthalpy change gives the total binding energy of the clusters. To establish whether a direct relationship exists between the proton affinity difference between GlyGly and the alcohol, and the binding energy, the binding energy of the cluster was plotted against the proton affinity of the alcohol. This plot is shown in Fig. 5.8.

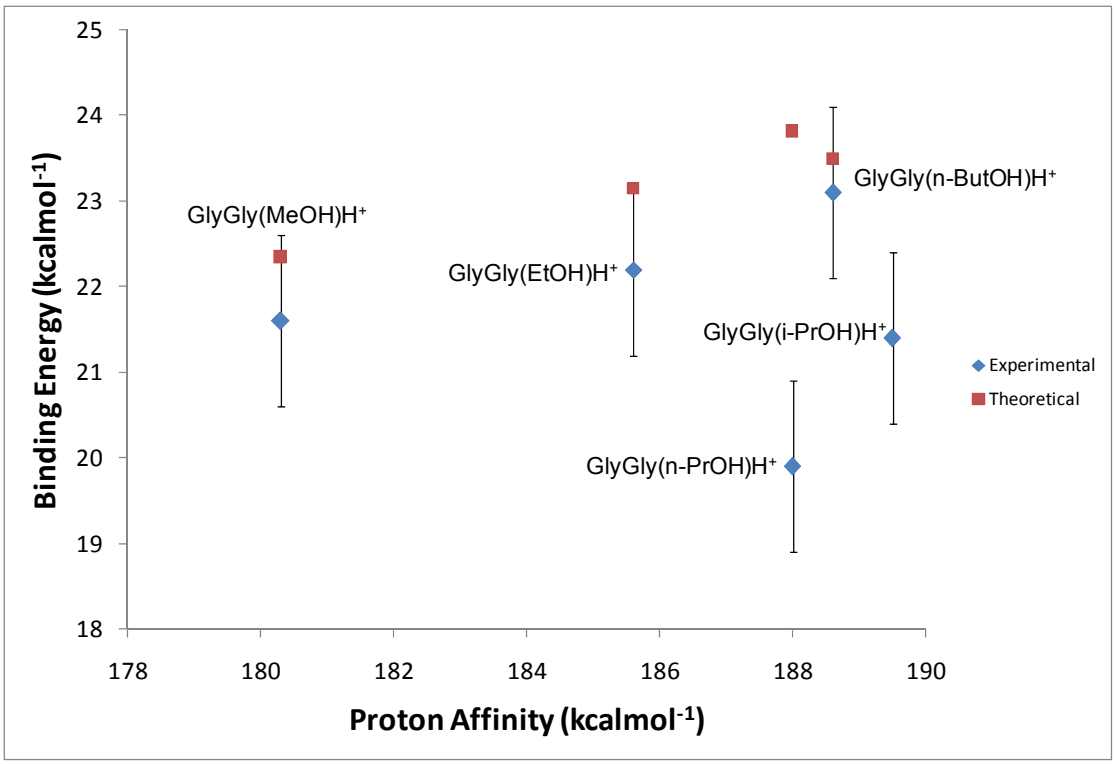

Fig. 5.8: Experimental and Calculated Binding Energies versus the respective alcohol proton affinities. The cluster of i-PrOH with $GlyGlyH^+$ was not optimized. Theoretical energies calculated at MP2/6-311++g(2d,2p) level of theory.

The error bars in Fig. 5.8 span ±1 kcal mol^{-1}, where the biggest source in the uncertainty of the experimental results stem from indeterminate errors in the temperature of the reaction. The energies of the most stable conformers in the case of the association of methanol, ethanol and butanol with $GlyGlyH^+$ falls within this experimental error, and show a linear correlation with their respective alcohol proton affinities. There is however a slight positive curvature in the correlation for their experimentally measured binding energies, going from methanol to butanol, but it is not exceeding the experimental error. No calculation was performed with i-propanol and experiments with it proved to be difficult, as only four equilibrium constants were measured for its cluster with $GlyGlyH^+$. However, the calculated value for the GlyGly-H^+--n-PrOH cluster is several kcal mol^{-1} higher in energy than the upper limit achieved experimentally. The discrepancy is likely not caused by an error in the calculation, and the van't Hoff plot gives no evidence of much deviation. It is

possible that n-propanol forms an entropy favoured cluster with $GlyGlyH^+$. To verify this idea, the free energies of the clusters using the experimental data and theoretical data were plotted against the gas phase basicities of each alcohol, shown in Fig. 5.9. The experimental results reveal a clearer relationship between free energy and gas phase basicity, indicating that the conformation of the cluster is based on the gas phase basicity difference between GlyGly and the alcohol, and not on the proton affinity difference. A poor correlation is observed from the theoretical results, likely because of large errors in the calculated entropy, which becomes a dominant term at higher temperatures.

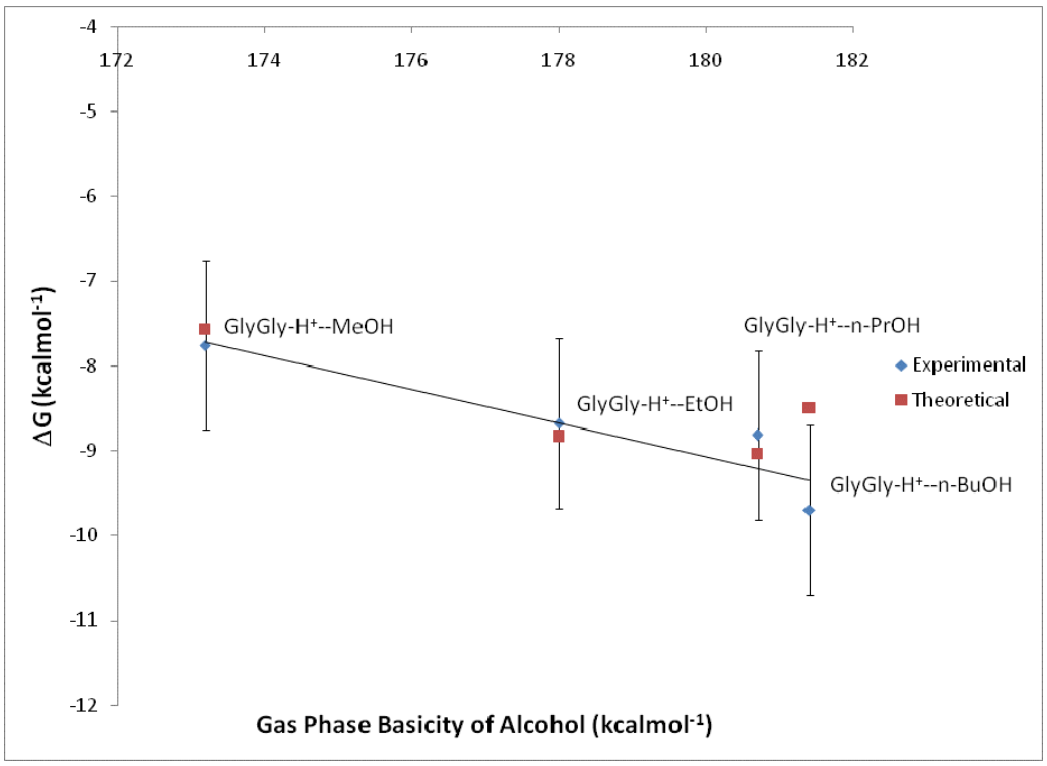

Fig. 5.9: Correlation between free energy of cluster formation and alcohol gas phase basicity for the reactions $GlyGlyH^+$ + Alcohol ⇆ GlyGly-H^+--Alcohol.

5.2.3.1 Conformers of the GlyGly-H^+--Alcohol Clusters

Several low-lying conformations of protonated diglycine that have been reported in the literature[20] were optimized along with their alcohol adducts at the B3LYP/6-311+g(d,p) level of

theory. Frequencies were also calculated unscaled. The energies reported here are from the single-point calculation at MP2(Full)/6-311++g(2d,2p) based on the geometries obtained from the optimization. Only clusters in which $GlyGlyH^+$ is in its extended or U conformation will be discussed here, as they were the lowest energy conformers. These are presented in Fig. 5.10, and their enthalpies, entropies and free energies at the average experimental temperature of 400 K are given in Table 5.4 along with the experimental data.

GlyGly-H^+—MeOH

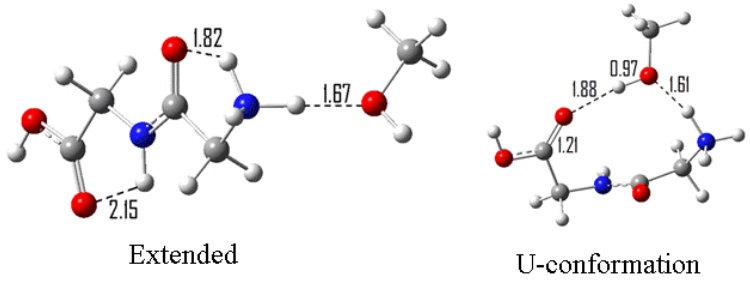

Extended U-conformation

GlyGly-H^+—EtOH

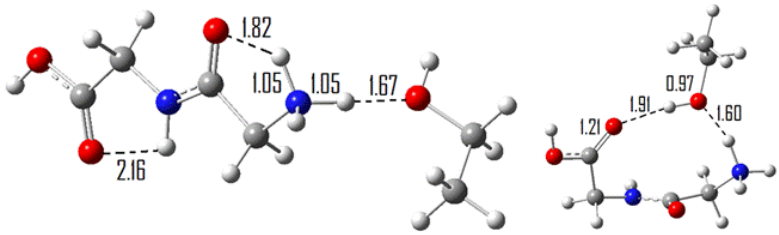

Extended U-conformation

GlyGly-H^+—PrOH

Extended U-conformation

GlyGly-H^+—BuOH

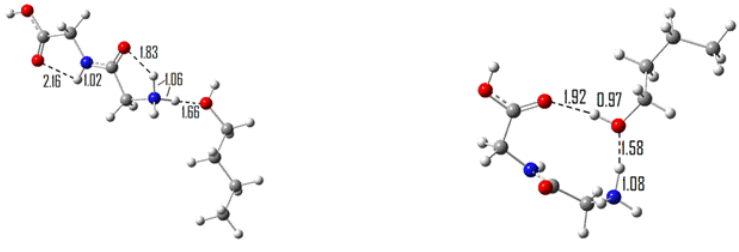

Extended U-conformation

Fig. 5.10: The optimized alcohol-stabilized extended and U conformations of $GlyGlyH^+$ for the alcohols MeOH, EtOH, n-PrOH and n-BuOH.

Table 5.4: Experimental enthalpy, entropy and free energy changes for the attachment of an alcohol molecule onto $GlyGlyH^+$ compared to the computed values for stabilization of the extended and U conformations of $GlyGly^+$.

	ΔH^o (kcalmol^{-1})	ΔS^o (calmol^{-1}K^{-1})	ΔG^o(400)
GlyGly-H$^+$--MeOH	**±1 kcalmol^{-1}**	**±3 calmol^{-1}K^{-1}**	
Experimental	-21.6	-34.6	-7.8
Extended	-17.8	-27.6	-6.8
U Conformation	-22.3	-36.9	-7.6
GlyGly-H$^+$--EtOH			
Experimental	-22.2	-33.8	-8.7
Extended	-18.8	-28.7	-7.3
U Conformation	-23.2	-35.8	-8.8
GlyGly-H$^+$--n-PrOH			
Experimental	-19.9	-27.7	-8.8
Extended	-19.2	-29.1	-7.6
U Conformation	-23.8	-36.9	-9.0
GlyGly-H$^+$--n-BuOH			
Experimental	-23.1	-33.5	-9.7
Extended	-19.9	-30.2	-7.8
U Conformation	-23.5	-37.5	-8.5
GlyGly-H$^+$--i-PrOH			
Experimental	-21.4	-27.8	-10.3

Calculation shows that the U-Conformation of $GlyGlyH^+$ is highly stabilized by attachment of an alcohol molecule. It is always more stable than the extended conformation in which the alcohol is bound at the ammonium group by 3-4 kcal mol^{-1} in each case. Typically, the enthalpy change of the U conformation matches closely with experiment, falling well within the experimental error of ±1 kcal mol^{-1}. The exception to this is the cluster with n-propanol which, judging by the computed energy, prefers to adopt an extended conformation even upon the first methanol attachment. However, the free energy change at 400 K based on the computed energies and enthalpies of the U conformation match closest with experiment for every cluster except in the case of the cluster with ethanol. The calculated entropy change for the formation of this cluster is noticeably more favourable than for the other clusters, but differs from the experimentally measured entropy change by 6.2 cal mol^{-1} K^{-1}.

The effect of chain length on conformer geometry is negligible in going from the cluster with methanol to that with butanol, for both the extended and the U conformation. The extended conformation is internally stabilized by two intramolecular hydrogen bonds between the ammonium group and the amide oxygen, and the amide nitrogen and the terminal carbonyl group. The magnitude of the former is predicted to be equal to the magnitude of the intermolecular ionic hydrogen bond with methanol, since the N-H donating bonds are lengthened by the same amount. For example, in the extended geometry of GlyGly-H^+--MeOH, both N-H donating bonds are extended to 1.05 Å. The length of the sole intermolecular hydrogen bond formed with the alcohol remains virtually constant through the series of alcohols, at 1.66-1.67 Å.

The general structure of the U conformation as well is negligibly affected by the length of the alcohol chain. In each case, the ammonium group is rotated along a 34.8^o dihedral angle from the amide carbonyl group. This is not too surprising, since the ionic hydrogen bond that forms here originates as an electrostatic attraction, with a well defined directionality defined by the lone pair of electrons on the methanol oxygen atom accepting the hydrogen bond. The rotation of the ammonium group is simply a direct consequence of that directionality. Likewise, the terminal carboxyl group is generally rotated at a dihedral angle of 87-88^o out of plane from the amide hydrogen atom. This angle decreases only slightly in going from methanol through to butanol. Interestingly, the ionic hydrogen bond formed between the methanol oxygen atom and the cationic ammonium moiety decreases in length by 0.01 A in each case, from methanol, to ethanol, to propanol and finally butanol. This is counterintuitive to what would be predicted based on the increasing order of proton affinity along this series of alcohols. As the proton affinity of the alcohol increases, the proton should reside closer to its hydroxyl oxygen atom, resulting in a stronger hydrogen bond. Although the relative binding energies of the GlyGly-H^+--Alcohol clusters increase from methanol to butanol, this is not represented in the structure.

The structural data therefore suggest that the chain length plays no entropic role in the formation of these clusters, as it is well removed from any binding site in both conformations.

5.2.4 **The GlyGly-H^+--Phenol Cluster**

Sample introduction

In its standard state, phenol is a solid. In order to be certain of the pressure of neutral phenol in the ion source, it was necessary to introduce it along with the bath gas through a flow control valve, similarly to all other experiments discussed thus far. To accomplish this, 0.5 M solutions of phenol in deionized water were prepared and introduced at an appropriate volume into an 80^{o}C 2.54 L reservoir where the entire solution would be vaporized instantaneously.

Results

Although several reasons may be advanced, the proton-bound cluster of diglycine with phenol was not observable in the experiment. One reason could be due to the abundance of water and several hydrates of the cluster were formed, leaving negligible amounts of the non hydrated cluster.

5.3 Discussion and Conclusions

Although up until now, the overall goal of this series of experiments has not been achieved, the three experiments described in this chapter that worked successfully are important in their own respects. The proton affinity of cyclohexanol was previously not recorded, but theory and a charge transfer experiment conducted here both confirmed it to be 194.3 ±1 kcal mol^{-1}. The NIST database lists the proton affinity of phenol as being only 1.0 kcal mol^{-1} greater than this, an interesting feature since phenol is aromatic. The π system apparently has very little effect in stabilizing an inherent

positive charge in the gas phase, and the ability of a molecule to be a good proton acceptor in the gas phase relies on inductive stabilization. The proton affinity of hexanol was not obtained, but based on the previous idea, is likely within ±1 kcal mol^{-1} from either that of phenol or cyclohexanol.

The binding of $GlyGlyH^+$ to benzene is simply an extension of a simpler model, that with the ammonium ion with benzene. This simplified system has been studied in the past[26,27] giving a binding energy of 15.7 kcal mol^{-1} at the highest reported level of theory, MP2/6-31+G*. Our own calculation for this system produces a value of 19.4 kcal mol^{-1} using the MP2(full)/6-311++g(2d,2p) level of theory. The literature value is very similar to the binding energy calculated for the cation-π interaction in the GlyGly-H^+--Bz, the structure of which is shown in Fig. 5.6, along with an enthalpy change of -15.6 kcal mol^{-1}. Our calculated value for the binding energy of the NH_4^+--Bz cluster is consistent with the measured binding energy for the GlyGly-H^+--Bz cluster presented here. Considering some of the geometry in the region of the interaction, it is remarkable that these values are so similar. The optimized structure of NH_4^+ and $GlyGlyH^+$ bound to benzene shows the nitrogen atom in line with the benzene C_6 axis. However, the N-H bond is skewed by 30 to 40^o with respect to the C_6 axis, and approaches a bidentate coordination. The ammonium ion has a T_d symmetry point group, and is considered an ion of high symmetry. Several arguments can be made for the skewed interaction angle between NH_4^+ and benzene. Firstly, the electrostatic component of the cation-π interaction will give directionality to the interaction along the sp^3 hybridized orbitals that bond each hydrogen atom to the nitrogen atom. This means that near the outer region of the ion, there is significant s-character which was allowed to penetrate upon hybridization. Since an s orbital is spherically symmetric and has no angular nodes, there is equal probability that it will interact with a region of electron density, such as a lobe of a quadrupole moment, at any internal orientation. This translates to the NH_4^+ ion simply not "deciding" on a directionality. This argument quickly falls apart when carefully comparing the geometry of the NH_4^+-benzene interaction through

several different optimizations, because one would see that the skew angle is consistently the same, and not just randomly out of place. An explanation using thermodynamic arguments would also not be feasible, because although one could apply it to the GlyGly-H^+--Bz cluster, no rationization would make sense for the ammonium ion. The only likely reasoning behind the skewed angle is that the electronic structure of one of the two, or possibly both contributors is changing upon interaction. As stated previously, the origin of the interaction is a dispersion force. The N-H bond is strongly polarized, as evidenced by the large measured binding energy between $GlyGlyH^+$ and benzene. At the same time, benzene can freely rotate about its C_6 axis, and therefore a relatively small entropy change is observed upon association. As the cation-π interaction forms, reaching a minimum potential energy, a repulsion between the nitrogen atom and the negative quadrupole moment of benzene approaches a maximum, until an alternate configuration is established. As a result, the negative quadrupole lobe may become distorted, and offset from its axis. This is the most likely change in electronic structure, because the N-H bond has mostly covalent character.

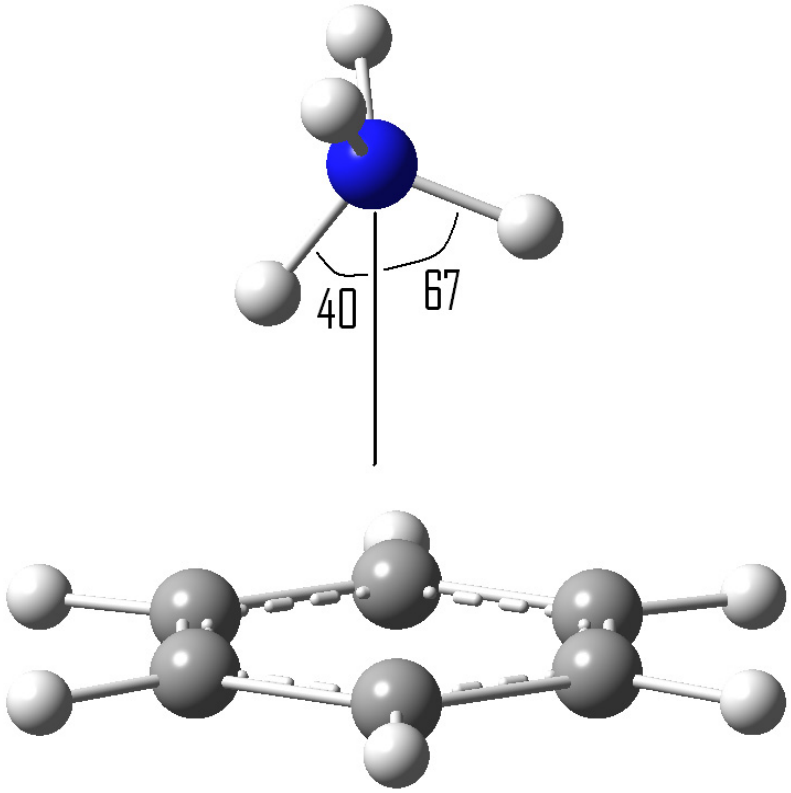

Fig. 5.11: Optimized geometry of the NH_4^+--Bz cation-π interaction, calculated at the B3LYP/6-311+g(d,p) level of theory.

This study also demonstrates that there is no question that linear chain alcohols also serve the same function to protein secondary structure as water, illustrated by the relative stability of the solvated U conformation of $GlyGlyH^+$ relative to the extended geometry. It was shown that with increasing chain length and proton affinity of the alcohol, the binding energy increases linearly with increasing proton affinity. However, the optimized geometries of the alcohol stabilized U conformation do not show significant differences in bond length and dihedral angles in proximity to the interaction, nor the hydrogen bond lengths themselves. Although we were not able to find peptide data specifically for the $GlyGlyH^+$ conformer, one paper[20] reported that a single water molecule could stabilize the U conformation of $AlaGlyH^+$ by 2.7 kcal mol^{-1} with respect to the extended conformation. Our calculations (shown in Table 5.4) show that the linear chain alcohols can stabilize the former with respect to the latter by 3.5 to 4.5 kcal mol^{-1}. These results again place

emphasis on the hydrogen bond accepting ability of the solvent, when it has a lower proton affinity than the amino acid or peptide, in stabilizing the cluster. This particular structure is not reliant on highly protic solvents. This idea remains consistent in solution as well, where solvent-assisted proton transport becomes a dominant process. Transition state calculations have demonstrated that methanol is a better proton transport catalyst than water,[28] as it facilitates a 3,4 proton shift from the amide oxygen atom to the amide nitrogen atom in peptides, moreso relative to water.

With regards to the GlyGly-H^+--Phenol cluster, it is acknowledged that the hydrogen bond formed in the dominant conformers DP01 and DP02 are different in character than the strong ionic hydrogen bond formed in DP05. Using the additivity method proposed here, this would result in a slight underestimate of the magnitude of the cation-π interaction. However, subtracting the loss of cluster stability due to steric effects is anticipated to give a much more reliable estimate than that previously reported in gas phase and computational literature.

Conclusions and Future Work

The goal of this thesis was to demonstrate the usefulness of HPMS for its ability to accurately measure absolute binding energies of gas-phase ions generated through ion-molecule reactions. The focus was the solvation of ionic (protonated) biomolecules by alcohols. The results obtained here demonstrate that in their simplest forms (between small molecules in the gas phase), ionic hydrogen bonds and cation-π interactions have similar magnitudes, providing further evidence of their electrostatic origins. What differentiates them within the biological molecules that they may stabilize is their frequency of occurrence, and an unfavourable entropic loss for cation-π interactions. Calculation of the optimized structure of benzene coordinated to protonated diglycine suggests that the directionality of the cation-π interaction in this system is not well-defined, unlike ionic hydrogen bonds, however the ammonium group of $GlyGlyH^+$ tends to be stabilized by adopting a bidentate attachment to the benzene molecule.

The pyrimidine nucleic acid bases gave measured enthalpies and entropies similar to some calculated conformers, but not as favourable as those with the lowest energy. A possible reason for this could be due to the presence of a large number of tautomers of varying gas phase acidity present in the reaction mixture, where some are less reactive than others. Ring stiffness could also contribute. Calculation has shown that the presence of methanol catalyzes proton transport from N3 to O2 in these nucleic acid bases, decreasing the transport barrier by roughly 35 kcal mol^{-1}, making tautomerization a favourable process. The keto-amino and di-enol tautomers of the protonated nucleic acid bases are nearly equal in energy, and the energy ordering depends on what level of theory at which the calculation is being performed. The purine base adenine is stabilized if methanol binds to any one of its amine sites. Adenine possesses many favourable protonation sites.

The clustering of methanol to the protonated amino acids Gly, Ala, Val, Leu, Ile and Pro also provided interesting results. The measured binding energies for these clusters correlates linearly with the proton affinity of the neutral amino acid, suggesting that attachment of methanol to protonated amino acids can always form a cluster of favourable free energy, and that no structure is limited kinetically. The ammonium moiety on each amino acid has been confirmed to be the most preferable site of attachment for the methanol molecule, and in each case, save the proline cluster, there is roughly equal probability of methanol forming a monodentate complex with the protonated amino acid, as a bidentate, the second interaction between the amino acid carbonyl oxygen, and the methanol OH proton. Protonated proline differs, in that bidentate coordination destabilizes the complex by adding ring strain. The monodentate conformation of the Pro-H^+--MeOH cluster remains analogous to that of the other five amino acids, and its binding energy correlates with its proton affinity. A correlation between clusters of $GlyGlyH^+$ with the alcohols MeOH, EtOH, n-PrOH and n-BuOH was seen through calculation. However, it is a weaker correlation than that observed with the amino acids, likely because the flexible dipeptides can adopt several conformations, and are not easily locked into one, as are the amino acids. Experimentally, the correlation was weak, but this could also be due to low collisional stabilities of the larger alcohols, breaking down into smaller fragments either before or after clustering with $GlyGlyH^+$. The alcohol size appeared to have no direct effect on the relative free energies of each cluster. These energies are primarily determined by the conformation of the peptide, since the alcohol chain is removed from the centre of the complex. Generally, the U-conformation of GlyGlyH+ benefitted most from clustering

Experiments on the addition of a second methanol molecule to the Gly-H^+--MeOH cluster show that the cluster is stabilized to a lesser extent than from the addition of the first methanol molecule. This is likely because the second methanol molecule has to either bind to the carboxyl moiety, which is 2-3 kcal mol^{-1} less favourable than the ammonium group, or it will attach to the ammonium group, but

the binding of the first methanol molecule has depolarized the other N-H bonds, hence weakening any additional hydrogen bond that may be formed there. Sequential addition of methanol molecules to $GlyH^+$ will not stabilize the glycine zwitterion. However, the current experimental setup makes it difficult to monitor whether the sequential addition mode is actually occurring. To flesh out a more thorough understanding of the methanol stabilized zwitterion, IRMPD spectra using an FEL for glycine solvated in methanol would be helpful. Similarly, IRMPD would be useful to elucidate the dominant tautomers of nucleic acid bases stabilized by methanol. Further work in measuring binding energies using HPMS of high order clusters of $Gly\text{-}H^+\text{--}(MeOH)_n$, (n being an integer greater than 2) are crucial in paving a path between gas phase and bulk solution properties. Finally, a realization in measuring the cation-π interaction using the method outlined in the last chapter should be carried out, to confirm or correct previously measured values of the cation-π interaction in biological systems.

References:

Chapter 1

(1) Legon, A. C.; Millen, D. J. *Acc.Chem. Res.* **1987**, *20*, 39.

(2) Cazzoli, G.; Favero, P. G.; Lister, D. G.; Legon, A. C.; Millen, D. J.; Kisiel, Z. *Chem. Phys. Lett.* **1985**, *117*.

(3) Legon, A. C.; Soper, P. D.; Flygare, W. H. *J. Chem. Phys.* **1981**, *74*.

(4) Legon, A. C.; Willoughby, L. C. *Chem. Phys. Lett.* **1983**, *95*.

(5) Soper, P. D.; Legon, A. C.; Flygare, W. H. *J. Chem. Phys.* **1981**, *74*.

(6) Couprie, M. E.; Ortega, J. M. *Analusis* **2000**, *28*, 725.

(7) Maitre, P.; Caer, S. L.; Simon, A.; Jones, W.; Lemaire, J.; Mestdagh, H.; Heninger, M.; Mauclaire, G.; Boissel, P.; Prazeres, R.; Glotin, F.; Ortega, J. M. *Nuclear Instruments and Methods in Physics Research A* **2003**, *507*, 541.

(8) Wu, R.; McMahon, T. B. *Angew. Chem. Int. Ed.* **2007**, *46*, 3668.

(9) Quinonero, D.; Garau, C.; Frontera, A.; Ballester, P.; Costa, A.; Deya, P. M. *Chemical Physics Letters* **2002**, *359*, 486.

(10) Schwabacher, A. W.; Zhang, S.; Davy, W. *J. Am. Chem. Soc.* **1993**, *115*, 6995.

(11) Clark, T. E.; Makha, M.; Sobolev, A. N.; Dalgarno, S. J.; Atwood, J. L.; Raston, C. L. *Cryst. Growth Des.* **2007**, *7*.

(12) Lakshminarayanan, P. S.; Kumar, D. K.; Ghosh, P. *J. Am. Chem. Soc.* **2006**, *128*.

(13) Matsumoto, A.; Tanaka, T.; Tsubouchi, T.; Tashiro, K.; Saragai, S.; Nakamoto, S. *J. Am. Chem. Soc.* **2002**, *124*.

(14) Nagahama, S.; Inoue, K.; Sada, K.; Miyata, M.; Matsumoto, A. *Cryst. Growth Des.* **2003**, *3*.

(15) Saigo, K.; Kobayashi, Y. *Chem. Res.* **2007**, *7*.

(16) Tatko, C. D.; Waters, M. L. *J. Am. chem. Soc.* **2004**, *126*.

(17) Toth, G.; Kover, K. E.; Murphy, R. F.; Lovas, S. *J. Phys. Chem.* **2004**, *108*.

(18) Yamamoto, Y.; Yamamoto, A.; Furuta, S.; Horie, M.; Kodama, M.; Sato, W.; Akiba, K. Y.; Tsuzuki, S.; Uchimaru, T.; Hashizume, D.; Iwasaki, F. *J. Am. Chem. Soc.* **2005**, *127*.

(19) Tsuzuki, S.; Fujii, A. *Phys. Chem. Chem. Phys.* **2008**, *10*.

(20) Shibasaki, K.; Fujii, A.; Mikami, N.; Tsuzuki, S. *J. Phys. Chem. A* **2007**, *111*.

(21) Takagi, T.; Tanaka, A.; Matsuo, S.; Maezaki, H.; Tani, M.; Fujiwara, H.; Sasaki, Y. *1987* **J. Chem. Soc., Perkin Trans. 2**, *89*.

(22) Tsuzuki, S.; Honda, K.; Uchimaru, T.; Mikami, M.; Tanabe, K. *J. Am. Chem. Soc.* **2000**, *122*.

(23) Courty, A.; Mons, M.; Dimicoli, I.; Piuzzi, F.; Gaigeot, M. P.; Brenner, V.; Pujo, P. d.; Millie, P. *J. Phys. Chem. A* **1998**, *102*.

(24) Mons, M.; Dimicoli, I.; Tardivel, B.; Piuzzi, F.; Brenner, V.; Millie, P. *Phys. Chem. Chem. Phys.* **2002**, *4*.

(25) Cozzi, F.; Ponzini, F.; Annunziata, R.; Cinquini, M.; Siegel, J. S. *Angew. Chem. Int. Ed. Engl.* **1995**, *34*, 1019.

(26) Gallivan, J. P.; Dougherty, D. A. *Proc. Natl. Acad. Sci.* **1999**, *96*, 9459.

(27) Mecozzi, S.; Jr., A. P. W.; Dougherty, D. A. *Proc. Natl. Acad. Sci.* **1996**, *93*, 10566.

(28) Dougherty, D. A. *Science* **1996**, *271*.

(29) Meot-Ner, M.; Sieck, L. W. International Journal of Mass Spectrometry and Ion Processes **1991**, 109, 187.

(30) Wincel, H. *Int. J. Mass Spectrom.* **2006**, *251*, 23.

(31) Kohtani, M.; Breaux, G. A.; Jarrold, M. F. *J. Am. Chem. Soc.* **2004**, *126*, 1206.

(32) Grigorean, G.; Gronert, S.; Lebrilla, C. B. *Int. J. Mass Spectrom.* **2002**, *219*, 79.

(33) Jockusch, R. A.; Lemoff, A. S.; Williams, E. R. *J. Am. Chem. Soc.* **2001**, *123*, 12255.

(34) Jockusch, R. A.; Price, W. D.; Williams, E. R. *J. Phys. Chem. A* **1999**, *103*, 9266.

(35) Lemoff, A. S.; Bush, M. F.; Williams, E. R. *J. Am. Chem. Soc.* **2003**, *125*, 13576.

(36) Rogalewicz, F.; Hoppilliard, Y.; Ohanessian, G. *International Journal of Mass Spectrometry* **2003**, *227*, 439.

(37) Strittmatter, E. F.; Lemoff, A. S.; Williams, E. R. *J. Phys. Chem. A* **2000**, *104*, 9793.

Chapter 2

(1) McMahon, T. B. High Pressure Mass Spectrometry. In *Energetics of Stable Molecules and Reactive Intermediates*; Piedade, M. E. M. d., Ed.; Kluwer Academic Publishers, 1999; pp 259.

(2) Wu, R.; McMahon, T. B. *Angew. Chem. Int. Ed.* **2007**, *46*, 3668.

(3) Raspopov, S. A.; McMahon, T. B. *J. Mass Spectrom.* **2005**, *40*, 1536.

(4) Wu, R.; McMahon, T. B. *J. Am. Chem. Soc.* **2006**, *129*, 569.

(5) Gaussian 03, Revision C.02,
M. J. Frisch, G. W. Trucks, H. B. Schlegel, G. E. Scuseria, M. A. Robb, J. R. Cheeseman, J. A. Montgomery, Jr., T. Vreven, K. N. Kudin, J. C. Burant, J. M. Millam, S. S. Iyengar, J. Tomasi, V. Barone, B. Mennucci, M. Cossi, G. Scalmani, N. Rega,
G. A. Petersson, H. Nakatsuji, M. Hada, M. Ehara, K. Toyota, R. Fukuda, J. Hasegawa, M. Ishida, T. Nakajima, Y. Honda, O. Kitao, H. Nakai, M. Klene, X. Li, J. E. Knox, H. P. Hratchian, J. B. Cross, C. Adamo, J. Jaramillo, R. Gomperts, R. E. Stratmann, O. Yazyev, A. J. Austin, R. Cammi, C. Pomelli, J. W. Ochterski, P. Y. Ayala, K. Morokuma, G. A. Voth, P. Salvador, J. J. Dannenberg, V. G. Zakrzewski, S. Dapprich, A. D. Daniels, M. C. Strain, O. Farkas, D. K. Malick, A. D. Rabuck, K. Raghavachari, J. B. Foresman, J. V. Ortiz, Q. Cui, A. G. Baboul, S. Clifford, J. Cioslowski, B. B. Stefanov, G. Liu, A. Liashenko, P. Piskorz, I. Komaromi, R. L. Martin, D. J. Fox, T. Keith, M. A. Al-Laham, C. Y. Peng, A. Nanayakkara, M. Challacombe, P. M. W. Gill, B. Johnson, W. Chen, M. W. Wong, C. Gonzalez, and J. A. Pople, Gaussian, Inc., Wallingford CT, 2004.

(6) Peng, C.; Ayala, P. Y.; Schlegel, H. B.; Frisch, M. J. *J. Comp. Chem.* **1996**, *17*, 49.

(7) Clark, T.; Chandrasekhar, J.; Spitznagel, G. W.; Schleyer, P. R. *J. Comp. Chem.* **1982**, *4*, 294.

(8) Frisch, M. J.; Pople, J. A.; Binkley, J. S. *J. Chem. Phys.* **1983**, *80*, 3265.

(9) Woon, D. E.; Jr., T. H. D. *J. Chem. Phys.* **1993**, *99*, 1914.

Chapter 3

(1) Chakkaravarthi, S.; Gromiha, M. M. *Polymer* **2005**, *47*, 709.

(2) Dougherty, D. A. *Science* **1996**, *271*, 163.

(3) Gromiha, M. M.; Suwa, M. *International Journal of Biological Macromolecules* **2004**, *35*, 55.

(4) Prajapati, R. S.; Sirajuddin, M. S.; Durani, V.; Sreeramulu, S.; Varadarajan, R. *J. Am. Chem. Soc.* **2006**.

(5) Kim, K.; Friesner, R. A. *J. Am. Chem. Soc.* **1997**, *119*, 12952.

(6) Beranova, S.; Cai, J.; Wesdemoitis, C. *J. Am. Chem. Soc.* **1995**, *117*, 9492.

(7) Ding, Y.; Krogh-Jespersen, K. *Journal of Computational Chemistry* **1996**, *17*, 338.

(8) Wang, W.; Pu, X.; Zheng, W.; Wong, N.; Tian, A. *Journal of Molecular Structure (Theochem)* **2003**, *626*, 127.

(9) Ding, Y.; Krogh-Jesperson, K. *Chemical Physics Letters* **1992**, *199*, 261.

(10) Ding, Y.; Krogh-Jespersen, K. *Chemical Physics Letters* **1992**, *199*, 261.

(11) David, C. W. *Chemical Physics Letters* **1981**, *78*, 337.

(12) Jensen, J. H.; Gordon, M. S. *J. Am. Chem. Soc.* **1995**, *117*, 8159.

(13) Jockusch, R. A.; Price, W. D.; Williams, E. R. *J. Phys. Chem. A* **1999**, *103*, 9266.

(14) Kassab, E.; Langlet, J.; Evleth, E.; Akacem, Y. *Journal of Molecular Structure (Theochem)* **2000**, *531*, 267.

(15) Strittmatter, E. F.; Lemoff, A. S.; Williams, E. R. *J. Phys. Chem. A* **2000**, *104*, 9793.

(16) Jockusch, R. A.; Lemoff, A. S.; Williams, E. R. *J. Am. Chem. Soc.* **2001**, *123*, 12255.

(17) Lemoff, A. S.; Bush, M. F.; Williams, E. R. *J. Am. Chem. Soc.* **2003**, *125*, 13576.

(18) Park, S.; Ahn, D.; Lee, S. *Chemical Physics Letters* **2003**, *371*, 74.

(19) Xu, S.; Nilles, J. M.; Jr., K. H. B. *J. Chem. Phys.* **2003**, *119*, 10696.

(20) Ai, H.; Bu, Y.; Li, P.; Chen, Z.; Hu, X. *Journal of Molecular Structure* **2004**, *678*, 91.

(21) Wu, R.; McMahon, T. B. *Can. J. Chem.* **2005**, *83*, 1978.

(22) Cong, X.; Czerwieniec, G.; McJimpsey, E.; Ahn, S.; Troy, F. A.; Lebrilla, C. B. **2006**.

(23) Remko, M.; Rode, B. M. *J. Phys. Chem. A* **2006**, *110*, 1960.

(24) Bush, M. F.; Forbes, M. W.; Jockusch, R. A.; Oomens, J.; Polfer, N. C.; Saykally, R. J.; Williams, E. R. *J. Phys. Chem. A* **2007**, *111*, 7753.

(25) Wu, R.; McMahon, T. B. *Angew. Chem. Int. Ed.* **2007**, *46*, 3668.

(26) Ai, H.; Bu, Y. *J. Chem. Phys.* **2004**, *120*, 2208.

(27) Wincel, H. *Int. J. Mass Spectrom.* **2006**, *251*, 23.

(28) Tsang, C. W.; Harrison, A. G. *J. Am. Chem. Soc.* **1976**, *98*.

(29) Dookeran, N. N.; Yalcin, T.; Harrison, G. *Journal of Mass Spectrometry* **1996**, *31*, 500.

(30) Klassen, J. S.; Kebarle, P. *J. Am. Chem. Soc.* **1997**, *119*, 6552.

(31) Rogalewicz, F.; Hoppilliard, Y.; Ohanessian, G. *International Journal of Mass Spectrometry* **2003**, *227*, 439.

(32) Gard, E.; Green, M. K.; Bregar, J.; Lebrilla, C. B. *J. Am. Soc. Mass Spectrom.* **1994**, *94*, 623.

(33) Meot-Ner, M.; Field, F. H. *J. Am. Chem. Soc.* **1974**, *96*, 3168.

(34) Meot-Ner, M.; Sieck, L. W. *International Journal of Mass Spectrometry and Ion Processes* **1991**, *109*, 187.

(35) Kohtani, M.; Breaux, G. A.; Jarrold, M. F. *J. Am. Chem. Soc.* **2004**, *126*, 1206.

(36) Grimsrud, E. P.; Kebarle, P. *J. Am. Chem. Soc.* **1973**, *95*, 7939.

(37) Czinki, E.; Csaszar, A. G. *Chem. Eur. J.* **2003**, *9*, 1008.

(38) Lee, K.; Park, S.; Jeon, I.; Lee, B.; Ahn, D.; Lee, S. *Bull. Korean Chem. Soc.* **2005**, *26*, 909.

(39) Woon, D. E.; T.H. Dunning, J. *J. Chem. Phys.* **1993**, *99*, 1914.

(40) Holland, P. M.; Casteman, A. W. *J. Chem. Phys.* **1980**, *72*.

(41) Dang, T. T.; Bierbaum, V. M. *J. Mass Spectrom. Ion Processes* **1991**, *117*, 65.

(42) Munsen, M. S. B. *J. Am. Chem. Soc.* **1965**, *87*.

(43) Henis, J. M. S. *J. Am. Chem. Soc.* **1968**, *90*.

(44) Kleingeld, J. C.; Nibbering, N. M. M. *Org. Mass Spectrom.* **1982**, *17*.

(45) Graul, S. T.; Squires, R. R. *Int. J. Mass Spectrom. Ion Processes* **1987**, *81*.

(46) Grimsrud, E. P.; Kebarle, P. *J. Am. Chem. Soc.* **1973**, *95*.

(47) Vogt, J.; Beauchamp, J. L. *J. Am. Chem. Soc.* **1975**, *97*.

(48) Harrison, A. G.; Lin, P. H.; Tsang, C. W. *Int. J. Mass Spectrom. Ion Phys.* **1976**, *19*.

(49) McMahon, T. B.; Beauchamp, J. L. *J. Phys. Chem.* **1977**, *81*.

(50) Thomas, R.; Barassin, J.; Barassin, A. *J. Mass Spectrom. Ion Phys.* **1981**, *41*.

(51) Bass, L. M.; Cates, R. D.; Jarrold, M. F.; Kirchner, N. J.; Bowers, M. T. *J. Am. Chem. Soc.* **1983**, *105*.

(52) Morris, R. A.; Viggiano, A. A.; Paulson, J. F.; Henchman, M. J. *J. Am. Chem. Soc.* **1991**, *113*.

(53) Sieck, L. W.; Abramson, F. P.; Futrell, J. H. *J. Chem. Phys.* **1966**, *45*.

(54) Tissandier, M. D.; Cowen, K. A.; Feng, W. Y.; Gundlach, E.; Cohen, M. H.; Earhart, A. D.; Coe, J. V.; Jr., T. R. T. *J. Phys. Chem. A* **1998**, *102*, 7787.

Chapter 4

(1) Colominas, C.; Luque, F. J.; Orozco, M. *J. Am. Chem. Soc.* **1996**, *118*, 6811.

(2) Forde, G. K.; Forde, A. E.; Hill, G.; Ford, A.; Nazario, A.; Leszczynski, J. *J. Phys. Chem. B* **2006**, *110*, 15564.

(3) Hunter, K. C.; Rutledge, L. R.; Wetmore, S. D. *J. Phys. Chem. A* **2005**, *109*, 9554.

(4) Robertson, E. G.; Simons, J. P. *Phys. Chem. Chem. Phys.* **2000**, *3*, 1.

(5) Sukhodub, L. F. *Chem. Rev.* **1986**, *87*, 589.

(6) Turecek, F.; Chen, X. *Am. Soc. Mass Spec.* **2005**, *16*, 1713.

(7) Wu, R.; McMahon, T. B. *J. Am. Chem. Soc.* **2006**, *129*, 569.

(8) Florian, J.; Baumruk, V.; Leszczynski, J. *J. Phys. Chem.* **1996**, *100*.

(9) Podolyan, Y.; Gorb, L.; Leszczynski, J. *J. Phys. Chem.* **2000**, *104*.

(10) Russo, N.; Toscana, M.; Grand, A.; Jolibois, F. *J. Comput. Chem.* **1998**, *19*.

(11) Wolken, J. K.; Turecek, F. *J. Am. Soc. Mass Spectrom.* **2000**, *11*.

(12) Wolken, J. K.; Turecek, F. *J. Am. Soc. Mass Spectrom.* **2000**, *11*, 1065.

(13) Brown, R. D.; Godfrey, P. D.; Mcnaughton, D.; Pierlot, A. P. *J. Am. Chem. Soc.* **1989**, *111*.

(14) Fogarasi, G. *J. Phys. Chem.* **2002**, *106*.

(15) Kobayashi, R. *J. Phys. Chem.* **1998**, *102*.

(16) Piacenza, M.; Grimme, S. *J. Comput. Chem.* **2004**, *25*.

(17) Szczesniak, M.; Szczepaniak, K.; Kwiatkowski, J. S.; Kubulat, K.; Person, W. B. *J. Am. Chem. Soc.* **1988**, *110*.

(18) Taylor, R.; Kennard, O. *J. Mol. Struct.* **1982**, *78*, 1.

(19) Delbene, J. E. *J. Phys. Chem.* **1983**, *87*.

(20) Jasien, P. G.; Fitzgerald, G. *J. Chem. Phys.* **1990**, *93*.

(21) Leszczynski, J. *J. Phys. Chem.* **1992**, *96*.

(22) Estrin, D. A.; Paglieri, L.; Corongiu, G. *J. Phys. Chem.* **1994**, *98*.

(23) Gould, I. R.; Burton, N. A.; Hall, R. J.; Hillier, I. H. J. *J. Mol. Struct.* **1995**, *331*.

(24) Nguyen, M. T.; Chandra, A. T.; Zeegers-Huyskens, T. *J. Chem. Soc., Faraday trans.* **1998**, *94*.

(25) Tian, S. X.; Zhang, C. F.; Zhang, Z. J.; Chen, X. J.; Xu, K. Z. *Chem. Phys.* **1999**, *242*, 217.

(26) Kryachko, E. S.; Nguyen, M. T.; Zeegers-Huyskens, T. *J. Phys. Chem. A* **2001**, *105*, 1288.

Chapter 5

(1) Dunbar, R. C. *J. Phys. Chem. A* **2000**, *104*, 8067.

(2) Gapeev, A.; Dunbar, R. C. *J. Am. Chem. Soc.* **2001**, *123*, 8360.

(3) Ruan, C.; Rodgers, M. T. *J. Am. Chem. Soc.* **2004**, *126*, 14600.

(4) Ryzhov, V.; Dunbar, R. C.; Cerda, B.; Wesdemiotis, C. *Am. Soc. Mass Spec.* **2000**, *11*, 1037.

(5) Armentrout, P.; Rodgers, M. *J. Phys. Chem. A* **2000**, *126*, 14600.

(6) McMahon, T. B.; Ohanessian, G. *Chem. Eur. J.* **2000**, *6*, 2931.

(7) Dougherty, D. A. *Science* **1996**, *271*.

(8) Shepodd, T. J.; Petti, M. A.; Dougherty, D. A. *J. Am. Chem. Soc.* **1986**, *108*.

(9) Stauffer, D. A.; Dougherty, D. A. *Tetrahedron Lett.* **1988**, *29*.

(10) Stauffer, D. A.; Jr., R. E. B.; Dougherty, D. A. *Angew. Chem. Int. Ed. Engl.* **1990**, *29*.

(11) Chakkaravarthi, S.; Gromiha, M. M. *Polymer* **2006**, *47*, 709.

(12) Gromiha, M. M.; Suwa, M. *International Journal of Biological Macromolecules* **2005**, *35*, 55.

(13) Prajapati, R. S.; Sirajuddin, M.; Durani, V.; Sreeramulu, S.; Varadarajan, R. *Biochemistry* **2006**.

(14) Gilis, D.; Biot, C.; Buisine, E.; Dehouck, Y.; Rooman, M. *J. Chem. Inf. Model.* **2006**, *46*, 884.

(15) Gallivan, J. P.; Dougherty, D. A. *Proc. Natl. Acad. Sci.* **1999**, *96*, 9459.

(16) Gromiha, M. M.; Santhosh, C.; Ahmad, S. *Int. J. Mass Spectrom.* **2004**, *34*.

(17) Adams, H.; Carver, F. J.; Hunter, C. A.; Morales, J. C.; Seward, E. M. *Angew. Chem. Int. Ed. Engl.* **1996**, *35*, 1542.

(18) Gard, E.; Green, M. K.; Bregar, J.; Lebrilla, C. B. *J. Am. Soc. Mass Spectrom.* **1994**, *5*.

(19) Klassen, J. S.; Kebarle, P. *J. Am. Chem. Soc.* **1997**, *119*, 6552.

(20) Kohtani, M.; Breaux, G. A.; Jarrold, M. F. *J. Am. Chem. Soc.* **2004**, *126*, 1206.

(21) Rodriquez, C. F.; Cunje, A.; Shoeib, T.; Chu, I. K.; Hopkinson, A. C.; Siu, K. W. M. *J. Am. Chem. Soc.* **2001**, *123*.

(22) Wincel, H. *Int. J. Mass Spectrom.* **2006**, *251*, 23.

(23) Zhu, C.; Balta, B.; Aviyente, V.; Lifshitz, C. *J. Phys. Chem. A* **2000**, *104*, 7061.

(24) Ranasinghe, A.; Cooks, R. G.; Sethi, S. K. *Org. Mass Spectrom.* **1992**, *27*.

(25) Hunter, E. P.; Lias, S. G. *J. Phys. Chem. Ref. Data* **1998**, *27*, 413.

(26) Deakyne, C. A.; Meot-Ner, M. *J. Am. Chem. Soc.* **1985**, *107*.

(27) Kim, D.; Lee, E. C.; Kim, K. S.; Tarakeshwar, P. *J. Phys. Chem. A* **2007**, *111*, 7980.

(28) Rodriquez, C. F.; Cunje, A.; Shoeib, T.; Chu, I. K.; Hopkinson, A. C.; Siu, K. W. M. *J. Phys. Chem. A* **2000**, *104*, 5023.